Institute of Physics Polish Academy of Sciences

Interactions between small molecules and amyloid beta peptides: Implications for Alzheimer's disease

Doctor of Philosophy thesis

Son Tung Ngo

Advisor:

Prof. dr. hab Mai Suan Li

Submission Date: 2015

Warsaw, 2015

Abstract

Currently, five drugs and many potential inhibitors for Alzheimer's disease (AD) have been discovered, but the completed treatment is still unavailable. Therefore, finding efficient drugs for AD is of great interest. Drug candidates have been identified based mainly on three hypotheses including cholinergic, tau, and amyloid cascade hypotheses. A lot of recent experimental evidences support the last hypothesis positing that AD is caused by aggregation of intracellular Aβ peptides which mainly have two forms Aβ_{40} and Aβ_{42}. Furthermore, Aβ monomers are not toxic, while oligomers are more toxic than mature fibrils.

Nowadays the computer-aided drug design becomes one of the most efficient methods complementary to experiment to screen out potential drug candidates for various diseases. Our main goal is to use this approach to find new inhibitors for AD based on the amyloid cascade hypothesis. From the data base of Vietnamese natural products Dracorubin, Taraxerol, Taraxasterol, Hinokiflavone and Diosgenin have been identified as good candidates to block Aβ aggregation. Using the QSAR method it was shown that these compounds meet pharmacological requirements for drug such as absorption, distribution, metabolism, excretion, and toxicity. Our *in silico* and *in vitro* studies revealed that vitamin K3 derivative VK3-9 can prevent formation of Aβ plaques and does not damage cells.

From the data base of all possible oral drugs we have identified Propafenone, anti-arrhythmic medication, as a promising candidate for AD treatment. The screening was performed using the criterion that potential AD drugs should have high similarity with Curcumin, which is in phase II of clinical trials.

We have demonstrated that, in accord with experiment, the binding affinity of Curcumin to Aβ is higher than nonsteroidal anti-inflammatory drugs Naproxen and Ibuprofen. Aromatic rings have been found to play the key role in stability of Aβ-ligand complexes. The van der Waals interaction dominates over the electrostatic interaction in ligand binding.

The molecular docking, MM-PBSA and free energy perturbation methods have been employed to estimate the binding free energy. Aβ monomers and fibrils were used as targets for drug design. Overall, our *in silico* results agree with the available experimental results.

Acknowledgments

First and foremost I would like to thank to my supervisor, Prof. dr hab Mai Suan Li, for supporting me during these past four years. Li is not only my advisor, but also my scientific friend who usually has great ideas and insightful discussions on my research.

I would like to thank Prof. dr Hoang Zung who has given me the opportunity to work in sciences.

I would like to thank my friends, Binh Khanh Mai, Tho Do Duc, Hsin-Lin Chiang, Chwastyk Mateusz, Cabaj Andrzej, Tchutchulashvili Giorgi, Nam Hoang, and my collaborators who share with me not only their work and ideas but also enjoyable things in life.

I will forever be thankful to my family who always support me spiritually throughout my life.

Last but not least, I want to thank staff of Institute for Computational Sciences and Technology in Ho Chi Minh City, Vietnam and Institute of Physics, Polish Academy of Sciences in Warsaw, Poland who supported me a lot during my PhD study.

Contents

1 Introduction **1**

2 Review of the Literature **5**

2.1 Alzheimer's disease and amyloid cascade hypothesis 5

2.1.1 Introduction to Alzheimer's disease 5

2.1.2 Cholinergic hypothesis 5

2.1.3 Tau hypothesis 7

2.1.4 Amyloid cascade hypothesis 7

2.1.5 Amyloid beta peptides 8

2.2 Treatment 9

2.2.1 Cholinesterase Inhibitors 9

2.2.2 Tau Inhibitors 9

2.2.3 Aβ Inhibitors 10

2.2.3.1 Compounds under clinical trials 10

2.2.3.2 Experiments on amyloid binding molecules 11

2.2.3.3 Computational studies of binding affinity of small molecules to Aβ 14

3 Computational approaches and analysis methods **18**

3.1 Molecular Docking 18

3.2 Molecular dynamics simulation 19

3.2.1 Modeling of solvated complex protein-ligand: all-atom model . 19

3.2.2 Non-bonded interactions 19

3.2.3 Bonded interactions 20

3.2.4 Stochastic dynamics 21

3.2.5 The leap-frog integrator 21

3.2.6 MD simulations with AMBER 22
3.2.7 MD simulation with GROMACS 22
3.3 Calculation of binding free energy for solvated complex protein-ligand 23
3.3.1 Solvated protein-ligand complex 23
3.3.2 MM-PBSA method 24
3.3.3 Free energy perturbation method 25
3.3.3.1 Free energy calculation 25
3.3.3.2 Dependence of interactions on λ 27
3.3.3.3 The double-annihilation binding-energy method . . . 28
3.4 Measures used for data analysis 28
3.4.1 Blood-brain barrier and human intestinal absorption 28
3.4.2 RMSD, hydrogen bond, side chain contacts, and secondary structures 29
3.4.3 Chemical and structural similarity 29

4 Curcumin binds to Aβ_{1-40} peptides and fibrils stronger than Ibuprofen and Naproxen 31

4.1 Introduction 31
4.2 Materials and Methods 32
4.2.1 Chemical structures and parameterization of Curcumin, Ibuprofen and Naproxen 32
4.2.2 Crystal structures of monomer Aβ_{1-40} 32
4.2.3 Solid state NMR structures of Aβ_{9-40} fibrils 35
4.2.4 Computational methods and measures used in structure analysis 35
4.3 Results and Discussion 36
4.3.1 Binding of three ligands to monomer Aβ_{1-40} 36
4.3.1.1 Docking results. 36
4.3.1.2 Estimation of binding free energies by MM-PBSA method. 36
4.3.1.3 Role of aromatic rings in binding affinity of ligands to Aβ_{1-40} 39
4.3.1.4 Hydrogen bonding and side chain interaction of Curcumin are stronger than Naproxen and Ibuprofen. . . 40
4.3.1.5 Binding site predicted by the docking method for Curcumin is the most probable. 43

4.3.2 Binding to two-fold symmetric fibril 6Aβ_{9-40} 44
4.3.2.1 Docking results. 44
4.3.2.2 Binding free energy: MM-PBSA results. 44
4.3.2.3 Nature of ligand binding to 6Aβ_{9-40}. 46
4.3.3 Binding to more complex Aβ fibril structures 47
4.3.3.1 Binding to 3-fold symmetric 9Aβ_{9-40}. 47
4.3.3.2 Binding to 2-fold symmetric 12Aβ_{9-40} and 3-fold symmetric 18Aβ_{9-40}. 49
4.3.3.3 Binding to fibril 5Aβ_{17-42} 51
4.3.4 Binding in low pH and hexafluoroisopropanol/water environment 51
4.4 Conclusion 51

5 Anti-arrhythmic medication Propafenone is potential drug for Alzheimer's disease by inhibiting aggregation of amyloid beta peptide: in silico and in vitro studies 53

5.1 Introduction 53
5.2 Methods & Materials 55
5.2.1 Screening top-hits by chemical and structural similarity with Curcumin 55
5.2.2 Crystal structure of fibril and ligands used in computational experiments. 55
5.2.3 Computational methods and measures used in structure analysis 55
5.2.4 Synthesis and purification of Aβ_{40} 56
5.2.5 Cell cultures 56
5.2.6 Cell viability assay 56
5.2.7 Aggregation assay 56
5.2.8 Transmission Electron Microscope (TEM) Analysis 57
5.2.9 Free radical assay 57
5.3 Results and Discussion 57
5.3.1 Selection of top-hits from orally available drugs 57
5.3.2 Binding of ligands to 12Aβ_{9-40} 58
5.3.3 Molecular dynamics simulation 58
5.3.4 Hydrogen bonds between ligands and 12Aβ_{9-40} 59
5.3.5 The absolute binding free energy 59

5.3.6 vdW interaction plays the important role but electrostatics interaction also has large impact on Propafenone binding to Aβ fibril . . . 60

5.3.7 Ligand-induced β-content change . . . 60

5.3.8 Cell viability in the presence and absence of Curcumin or Propafenone . . . 61

5.3.9 Aggregation assay of the Aβ peptide in the presence and absence of Curcumin or Propafenone . . . 63

5.3.10 TEM morphology of Aβ Fibrils . . . 63

5.3.11 Free radical assay with or without the treatment of Curcumin or Propafenone . . . 64

5.4 Conclusions . . . 65

6 Top-Leads from Natural Products for Treatment of Alzheimer's Disease: Docking and Molecular Dynamics Study 66

6.1 Introduction . . . 66

6.2 Materials and Methods . . . 67

6.2.1 Set of receptor-ligand complexes . . . 67

6.2.2 Molecular dynamic simulations . . . 67

6.2.3 Computational methods and studied quantities . . . 67

6.3 Results and discussions . . . 68

6.3.1 Human intestinal absorption. . . . 68

6.3.2 Blood-brain barrier. . . . 68

6.3.3 Docking results . . . 69

6.3.3.1 Binding energies: correlation between four sets . . . 69

6.3.3.2 Top-leads revealed by docking results . . . 71

6.3.3.3 Hydrogen networks . . . 76

6.3.4 Refinement of docking results by MM-PBSA method . . . 80

6.3.5 Comparison of pharmacological properties of top leads with Curcumin . . . 83

6.3.6 Competition between fibril growth and ligand binding . . . 85

6.4 Conclusion . . . 86

7 In silico and in vitro characterization of anti-amyloidogenic activity of vitamin K3 analogues for Alzheimer's disease 88

7.1 Introduction . . . 88

7.2 Materials and Methods . . . 89

7.2.1 Computational methods . . . 89

7.2.2 Synthesis of vitamin K3 analogues . . . 89

7.2.3 Synthesis and purification of Aβ_{1-40} . . . 89

7.2.4 Free radical assay . . . 89

7.2.5 Peptide aggregation assay . . . 93

7.2.6 Cell cultures . . . 93

7.2.7 Cell viability assay . . . 93

7.2.8 Fourier-transform infrared (FT-IR) spectroscopy . . . 94

7.3 Results . . . 94

7.3.1 Aβ_{1-40} aggregation in the presence and absence of VK3 analogues . . . 94

7.3.2 Secondary structure of Aβ_{1-40} in the presence and absence of VK3 analogues . . . 94

7.3.3 Cell viability in the presence and absence of VK3 analogues . 95

7.3.4 VK3 analogues attenuated Aβ_{1-40} induced free radical formation 96

7.3.5 Docking of VK3 analogues to Aβ_{1-40} . . . 96

7.3.6 MM-PBSA simulation . . . 100

7.3.7 Correlation of binding energy and experimental properties . . 101

7.4 Discussion . . . 104

CONCLUSIONS 107

APPENDIX 108

Bibliography 109

1

Introduction

Alzheimer's disease (AD) is one of the most popular forms of neurodegenerative disease which occurs among senior population [1]. AD affects approximately 5 million Americans causing an annual economic burden of about 214 billions USD for health care, long-term care and hospice for patients in 2014 [2]. As AD progresses living skills of patients slowly deteriorate [3, 4, 5]. Despite intense research for many decades the origin of this disease remains mysterious. Possible causes of AD may be grouped into these categories including cellular, genetic and molecular imbalances [6]. The aggregation of amyloid beta (Aβ) peptides [7] and tau protein [8], for instance, belongs to the category of molecular imbalance.

Accumulated over last two decades experimental evidences strongly support the amyloid cascade hypothesis [7, 9, 10] which suggests that the Aβ aggregation is the cause of AD. Aβ peptides may misfold to amyloid deposits with cross-β-sheet pattern[11, 12, 13, 14] damaging neurocells. Furthermore, soluble oligomers are presumably more toxic than mature fibrils [7, 15, 16]. The amyloid cascade hypothesis has been the predominant framework for experimental and theoretical research in AD [17, 18]. Because Aβ peptides are proteolytic by-products of the APP (amyloid precursor protein) and are most commonly composed of 40 (Aβ_{1-40}) and 42 (Aβ_{1-42}) amino acids, one of strategies to cure AD is to block generation of Aβ peptides. In this case one has to inhibit activity of β- and γ-secretases that cut APP into short Aβ peptides. In this thesis we will adopt the second strategy based on inhibition of misfolding and reversing Aβ aggregation [9].

A large number of inhibitors for Aβ aggregation have been discovered such as short β-sheet breaker peptides [19, 20, 21], natural compounds [22, 23, 24, 25, 26, 27], polyamines [28, 29], metal chelators [30], chaperones [31], carbohydrate-containing compounds [33, 34], osmolytes [35], RNA aptamers [36], Adenosine triphosphate (ATP) [37], Carvedilol [38], and Nilvadipine [39], etc. However, the lack of effective therapy for AD makes design of new inhibitors for Aβ as an urgent task.

Currently, computer simulation becomes a powerful method for virtual screening drug candidates. It was successful in obtaining a number of drugs approved by

FDA including Dorzolamide for treatment of cystoid macular edema [40], Zanamivir against influenza virus [41], Sildenafil for penile erectile dysfunction [42], and Amprenavir for treating HIV through preventing HIV-1 protease activity [43]. Here we combined pharmaco-informatics tools, molecular docking and molecular dynamics (MD) simulations to identify new potential inhibitors for Aβ self-assembly. Some of them were further validated using *in-vitro* experiments by our collaborators.

There are three strategies to design new potential drugs. One of them is to search for candidates among compounds available in data bases but with unknown pharmaceutical properties for a given disease. Along this line potential Aβ inhibitors have been discovered including short β- sheet breaker peptides [19, 20, 21], natural compounds [24, 25], etc. Second strategy is to screen out candidates among FDA-approved drugs [44]. For instance, ATP [37], Carvedilol [38], and Nilvadipine [39], are under clinical trials [45, 46, 47] as inhibitors for Aβ aggregation. Third strategy is to synthesize new compounds. In this thesis we tried to find potent Aβ inhibitors following all of these three strategies.

Adopting the first drug design strategy we have collected 342 compounds derived from Vietnamese plants [48] and studied their binding affinity to full-length Aβ_{40} and Aβ_{42} peptides and mature fibrils using the docking and MD simulations. We have predicted that five ligands Dracorubin, Taraxerol, Taraxasterol, Hinokiflavone, and Diosgenin are good candidates for treating AD [22].

To search for drug candidates from AD among all available drugs we select those which have high similarity with the well-known inhibitors [49]. Because Curcumin (diferulomethane), a low molecular weight molecule derived from the rhizome of curcuma longa, is prominent in blocking Aβ aggregation [25, 50] we narrow down our search to those FDA approved drugs that have high chemical and structural similarity with Curcumin. Using QikProp implemented in Schrodinger package [51] we have found eterilate, itopride, and Propafenone which have more than 80% similarity with Curcumin. Nature of their binding to Aβ has been examined in detail by MD simulations. Our collaborators from Taiwan succeeded in performing *in vitro* experiments for anti-arrhythmic medication Propafenone. In agreement with simulation results it was shown that Propafenone is a good candidate for Alzheimer's disease by blocking Aβ aggregation with inhibition constant IC50 in the sub-micro molar range [52].

The relationship between vitamin K and AD was first mentioned by Allison [54]. The overexpression of apolipoprotein E (ApoE) variant ApoE4 was observed at low concentration of vitamin K in the human blood. Because ApoE4 is one of possible genetic risk factors for AD, it was suggested that deficiency of this vitamin may contribute to the AD pathogenesis and vitamin K supplementation might be beneficial for AD treatment. Although vitamin K was shown to regulate several functions, such as sulfotransferase enzyme activity, and the activity of a growth factor/tyrosine kinase receptor, the molecular mechanism of action of vitamin K on AD remains unclear. This could be due to a lack of interest because of its neurotoxicity. Following the third strategy of drug design 15 derivatives of vitamin K3 (VK3) were synthesized. Their activity against Aβ self-assembly was studied by *in-silico* and *in-vitro* experiments. Although several VK3 analogues such as VK3-9, VK3-10, and VK3-6 inhibited the aggregation of Aβ_{40}, only VK3-9 was able to protect cells against

Aβ_{40} induced toxicity. This compound is, therefore, recommended for further *in vivo* studies.

Although potentially important Curcumin is under phase II clinical trial [55], the nature of its binding to Aβ peptides and fibrillar structures has not been understood at the atomic level. As evident from experiments, NSAID (non-steroidal anti-inflammatory drugs) (NSAID) Ibuprofen and Naproxen are potential candidates to control A aggregation. Their chronic consumption can not only inhibit inflammatory targets contributing to neuroprotection, but also slow down amyloid self-assembly by mechanisms which remain unknown [56]. MD simulations of influence of Ibuprofen and Naproxen on A aggregation were carried out by Klimov *et al* [57, 58] who showed that, in agreement with the experiments [59], Ibuprofen displays lower A binding affinity than Naproxen. However, the binding free energies ΔG_{bind} of Ibuprofen and Naproxen to Aβ peptides and their mature fibrils that can be directly compared with experimental constants [59, 50] have not been estimated. In addition, the experiments of Yang *et al* [25] have shown that Curcumin, which is non-toxic and able to cross the blood brain barrier (BBB) due to its high hydrophobicity, can interfere with Aβ oligomerization better than Ibuprofen and Naproxen. So, it is worth to address this question by computer simulations to shed more light on the binding nature of these ligands. Moreover, the binding free energy ΔG_{bind} of Curcumin to Aβ monomer and aggregates has not been also computed. As shown by the experiments [59] Ibuprofen and Naproxen have the same binding site but this question has not been addressed theoretically. In addition, an interesting question emerges is that does Curcumin bind to the same position as NSAIDs?

Consistent with the experiments [25] we have shown that Curcumin binds to Aβ_{40} fibrils stronger than NSAIDs [23]. ΔG_{bind} estimated by the all-atom MD simulations also agrees with experiments [59, 50]. Our analysis revealed that in the case of monomer Aβ_{40} Ibuprofen and Naproxen bind to the same position which is different from the binding site of Curcumin. However, for mature fibrils all of three ligands share the same binding site located inside fibrils near loop regions.

My thesis is organized as follows:

Chapter 2 is a review of literature on Alzheimers disease and its treatment.

Chapter 3 describes materials and methods which have been used in this thesis.

Chapter 4 presents presents computational study of binding affinity of Curcumin, Naproxen and Ibuprofen to Aβ.

Chapter 5 devotes to screening potential Aβ inhibitors from data base of FDA-proved drugs and *in silico* and *in vitro* studies anti-arrhythmic medication Propafenone.

Chapter 6 shows top leads obtained by computer-aided drug design procedure from natural products for treatment of AD.

Chapter 7 contains *in silico* and *in vitro* studies of VK3 analogues in inhibiting Aβ aggregation and their cytotoxicity.

List of publications presented in my thesis

1. **Ngo S. T.** and Li M. S., Curcumin binds to Ab40 peptides and fibrils stronger than Ibuprofen and Naproxen, J.Phys. Chem. B 116, 10165 (2012)

2. **Ngo S. T.** and Li M. S., Top-Leads from natural products for treatment of Alzheimer's disease: Docking and molecular dynamics study, Molecular Simulation 39, 279-291 (2013)

3. Huy* P. Q. D., Yu* Y. C., **Ngo S. T.***, Thao T. V., Chen C. P., Li M. S., and Chen Y. C., In silico and in vitro characterization of anti-amyloidogenic activity of vitamin K3 analogues for Alzheimer's disease, BBA-General Subjects 1380, 2960 (2013) (*: contribution equally to the work)

4. **Ngo S. T.**, Fang S. T., Huang S. H., Chou C., Li M. S. and Chen Y. C., Antiarrhythmic medication Propafenone is potential drug for Alzheimers disease by inhibiting aggregation of amyloid beta peptide: *in silico* and *in vitro* studies, *submitted for publication*

5. **Ngo S. T.** and Li M. S., Inhibitors for Amyloid beta peptides, *in preparation*

Other publications

1. **Ngo S. T.**, Kouza M., and Li M. S., Shanghai influenza A/H7N9 Virus Confers Resistance to Oseltamivir: Evidence from *in silico* Study *submitted*

2. **Ngo S. T.**, Mai B. K., Hiep D. M., and Li M. S., Estimation of the binding free energy of AC1NX476 to HIV-1 protease wild-type and mutations using free energy perturbation method, Chem. Biol. Drug Des. (2015), DOI: 10.1111/cbdd.12518

3. Viet M.H., Nguyen P.H., **Ngo S. T.**, Li M. S., and Derreumaux P., Effect of the Tottori familial disease mutation (D7N) on the monomers and dimers of Ab40 and Ab42 , ACS Neuroscience, 4(11), 1446-1457 (2013)

4. Chiang H. L., **Ngo S. T.**, Chen C.J., Hu C.K., and Li M. S., Oligomerization of peptides LVEALYL and RGFFYT and their binding affinity to insulin , Plos One, 8, 65358 (2013)

5. Viet M.H., **Ngo S. T.**, Lam N. S. , and Li M. S., Inhibition of aggregation of amyloid peptides by beta-sheet breaker peptides and their binding affinity, J. Phys. Chem. B 115, 7433 (2011)

Proceedings

1. Li M. S., and **Ngo S. T.**, Computational Study of Diseases Associated with Protein Aggregation, Springer Berlin Heidelberg, 4th International Conference on Biomedical Engineering in Vietnam, 391-395

Publication metrics (as of Sep 1^{st} 2015)

Total citations 85, H-index 3

2

Review of the Literature

2.1 Alzheimer's disease and amyloid cascade hypothesis

2.1.1 Introduction to Alzheimer's disease

As mentioned above, AD is a neurodegenerative disorder mainly recognized in elderly people [1]. The brain of patient is slowly destroyed (Fig. 2.2) causing the decline in cognition and living skill [60, 61]. AD affects millions people and assess huge amount of money for health care and treatment [2]. Numerous studies suggested a lot of possible causes of AD which may be grouped into 3 categories including molecular, cellular, and genetic imbalances (Fig. 2.1) [6]. Imbalance in Ca^{2+} homeostasis, for instance, belongs to the group of cell imbalances, while genetic imbalances involves DNA damage. Here we focus on the cholinergic, tau, and amyloid cascade hypotheses from the molecular imbalance category (Fig. 2.1). The last one is the most favorable because it is supported by a large number of experimental evidences.

2.1.2 Cholinergic hypothesis

This oldest hypothesis posits that the synaptic failure is the cause of AD [62]. The memory deficit is due to reduction of the neurotransmitter acetylcholine [63, 64, 65, 66, 67] which is associated with both memory and learning. Current drugs for AD such as Donepezil, Galantamine, Rivastigmine and Tacrine are acetylcholinesterase inhibitors that have been developed based on cholinergic hypothesis. Because these drugs can treat some symptoms but not cure the disease, the acetylcholine deficiencies may not be directly causal, but are a result of widespread brain tissue damage.

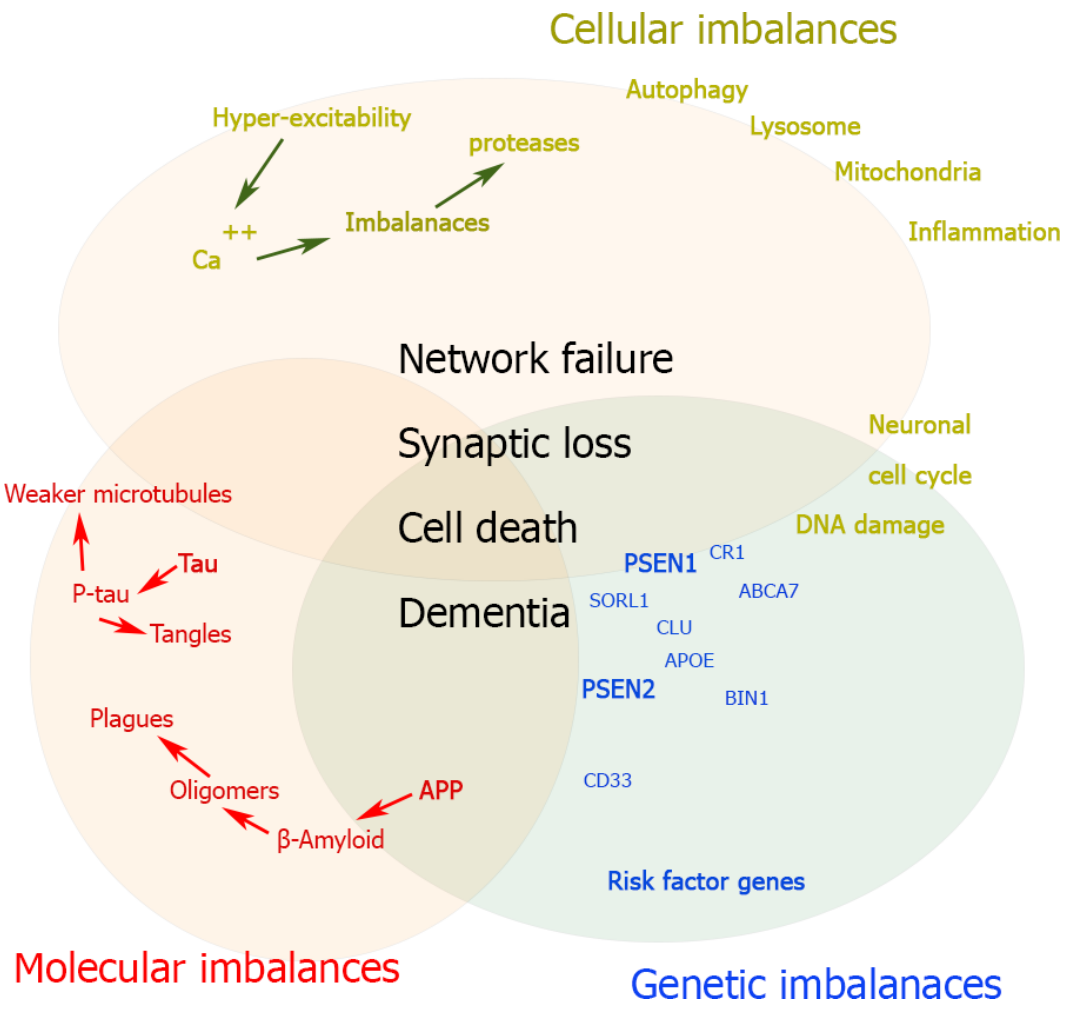

Figure 2.1 AD causes can be divided into three groups such as molecular, genetic, and cellular imbalances that are represented by shaded ovals. The Aβ aggregation which belongs to molecular events is our target.

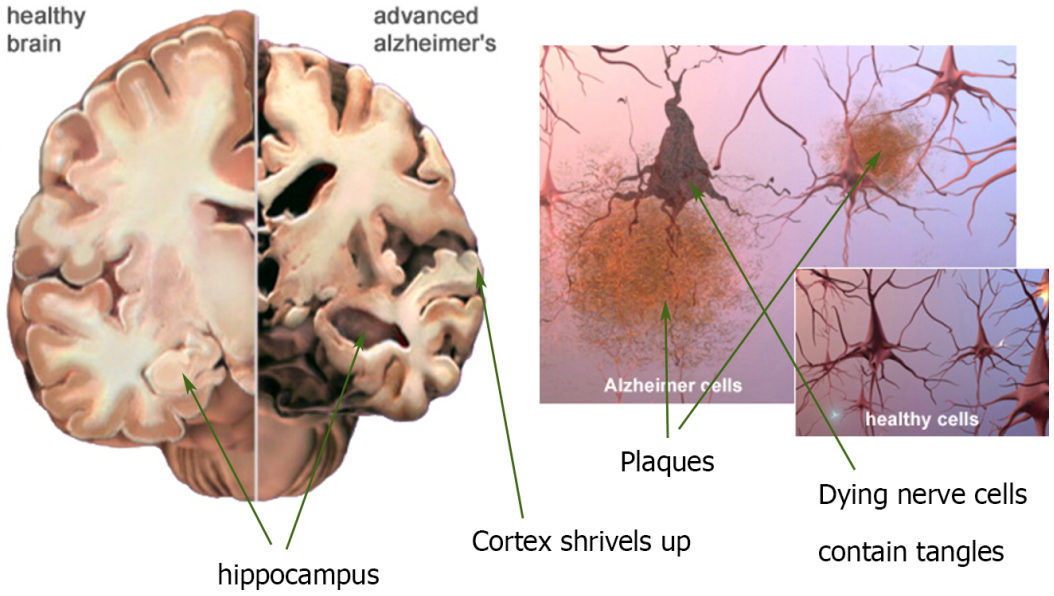

Figure 2.2 Comparison between healthy brain and advanced with AD in X-ray computed tomography scan (left) and under the microscope (right). The cortex of AD brain is slowly shriveled up. The AD hippocampus, which is related with formation of new memories, has same situation with the cortex. The figures have taken from www.alz.org

2.1.3 Tau hypothesis

Tau proteins have six main isoforms which have from 352 to 441 residues [68]. Aggregation of this protein in human brain is related to tauopathies which are a set of neurodegenerative pathologies [69, 70]. In the case of AD it is hypothesized that tau protein is accumulated within neurons in the form of neurofibrillary tangles (NFTs) leading to the neurotoxicity and reduced cognition [69, 70]. Tangles are formed by hyperphosphorylation of microtubule-associated tau protein causing it to self-assemble in an insoluble form. Overexpression of tau and increased phosphorylation were detected in patient cognitive deficiencies [71]. Tau was found to be related with Aβ-induced neurotoxicity [72].

2.1.4 Amyloid cascade hypothesis

The hypothesis that AD is directly associated with the aggregation of Aβ peptide, produced by cleavage of amyloid precursor protein (APP) was first asserted by Hardy and Allsop in 1991 [73]. This hypothesis is supported by a large number of experimental evidences [9, 10]. As AD progresses the brain is getting damaged by extracellular Aβ plaques (Fig. 2.2) causing neuron death.

In the years 1950-1960 of the last century it was believed that mature fibrils are neurotoxic, while monomers are not cytotoxic. However recent evidences have indicated that soluble oligomers are more toxic than mature fibrils [7, 15, 16, 74]. Mass spectroscopy revealed that the neurotoxicity is presumably depends on the size of

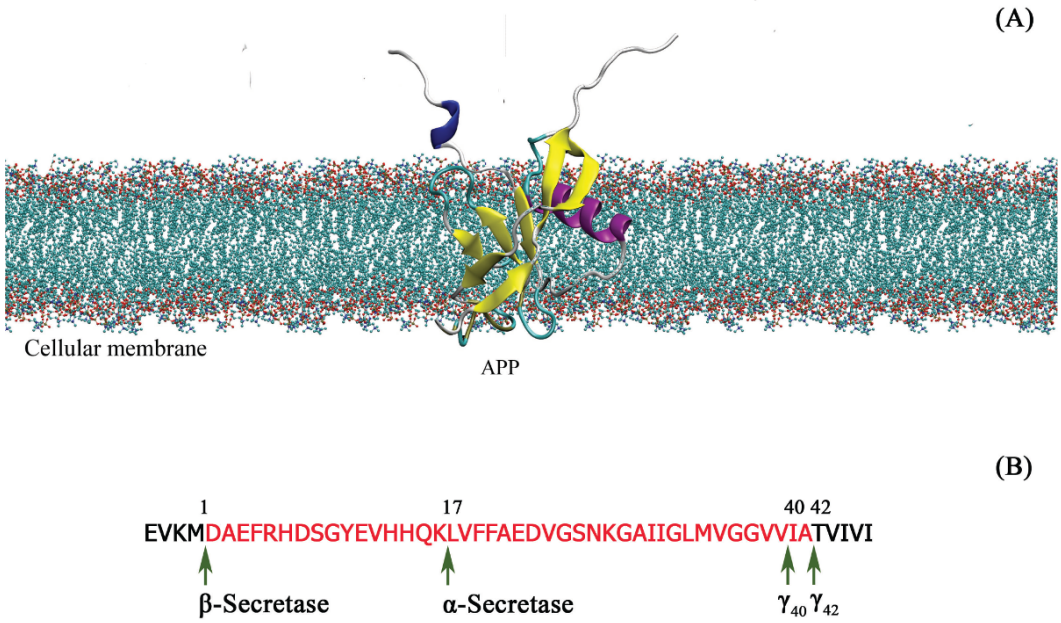

Figure 2.3 (A) APP in cellular membrane. (B) Pathways in APP proteolysis may be either nonamyloidegenic and amyloidegenic. In the first mode non-Aβ peptides are formed by APP cleavage by α- and β-secretases at specific sites. In the second pathway Aβ peptides of 36-43 residues are produced by cutting by γ- and β-secretases.

oligomers [75] and the Aβ_{42} dodecamer is a candidate for the primary toxic species in AD.

All computational studies performed in this thesis are based on the amyloid cascade hypothesis that Aβ is the target for AD drug design.

2.1.5 Amyloid beta peptides

APP is a neuron's transmembrane protein (Fig. 2.3) which alters the structure and function of synapse in cultured hippocampal neurons [76]. APP has three major isoforms APP_{695}, APP_{751} and APP_{770} that are abundant in hippocampus and cerebellum.

Multiple alternate pathways exist for APP proteolysis, some of which lead to production of Aβ peptides (amyloidogenic pathway) and some of which do not (non-amyloidogenic pathway). Non-amyloidogenic peptides are generated by α- and γ-secretases cutting, while Aβ peptides of 36-43 residues are cleavaged by β- and γ-secretases at specific sites (Fig. 2.3B). Note that β-secretase is also known as beta-site APP-cleaving enzyme 1 (BACE-1). About 90% of secreted peptides is Aβ_{40}, while Aβ_{42} accounts for $< 10\%$ of secreted Aβ.

Aβ_{40} is the most abundant but Aβ_{42} is more neurotoxic as the later aggregates faster [71]. The sequence of wild type Aβ_{42} is:

DAEFR^{5}HDSGY^{10}EVHHQ^{15}KLVFF^{20}AEDVG^{25}SNKGA^{30}IIGLM^{35}VGGVV^{40}IA.

Aβ_{40} has the same sequence as Aβ_{42} but without the last two residues. Aβ_{42} and Aβ_{40} have the same hydrophilic N-terminal extended from residue 1 to residue 15. The residues 17-21 form the so called central hydrophobic core, while the turn region includes residues 22-28. The hydrophobic C-terminal has 13 residues 30-42 and 11 residues 30-40 for Aβ_{42} and Aβ_{40}, respectively.

In water Aβ peptides are intrinsically disordered and they aggregate rapidly forming cross-beta fibril structures [11, 12, 13, 14]. The structures of Aβ monomers cannot be resolved experimentally in aqueous environment but they adopt mainly helices in micellar solutions (PDB codes are 1BA4 [77] and 1Z0Q [78] for Aβ_{40} and Aβ_{42}, respectively).

Structures of Aβ have not been also resolved experimentally. Therefore, as in the monomer case [79] they might be determined using all-atom MD simulations [18]. Crystal structures of Aβ fibrils (more precisely, protofibrils) have been resolved by the solid state NMR technique. Neglecting the first 9 disordered residues in the N-terminal, Tycko *at al.* have obtained two-fold symmetry (PDB codes 2LMN and 2LMO) [80] and three-fold symmetry (PDB codes 2LMP and 2LMQ) [81] structures for A$\beta 9-40$ fibrils. However recent studies suggest that the N-terminal is not disordered [18] and the fibril structure of full length Aβ_{1-40} was derived from the brain of AD patient was obtained [82]. The situation is different in the Aβ_{42} case, where residues 1-17 are disordered, but residues 18-42 form a β-strand-turn-β-strand motif that contains two in-register β-sheets (PDB code 2BEG) [14]. Remarkably, the triple-β-motif has been recently reported for Aβ_{42} fibril structure by Xiao *et al.* [83]. The structures of Aβ_{9-40} protofibrils have been used to study binding affinity in this thesis.

2.2 Treatment

2.2.1 Cholinesterase Inhibitors

Currently, the five available drugs for AD including Donepezil, Galantamine, Rivastigmine, Memantine and Tacrine, are the inhibitors of cholinesterase. These medications, though sometimes beneficial, cannot cure AD [71]. They are used to treat symptoms of the disease but have neither halted nor reversed it. Furthermore, current drugs have many side effect, such as headache, nausea, vomiting, and weight loss that have been reported [84].

2.2.2 Tau Inhibitors

A lot of candidates were identified for preventing the aggregation of tau protein. One of the first inhibitors is methylthioninium chloride (MTC) [85] which has the inhibition constant of 123 nM [86]. It was found in phase 2 of clinical [87] that MTC stablized the AD progression in both mid and moderate AD. The clinical

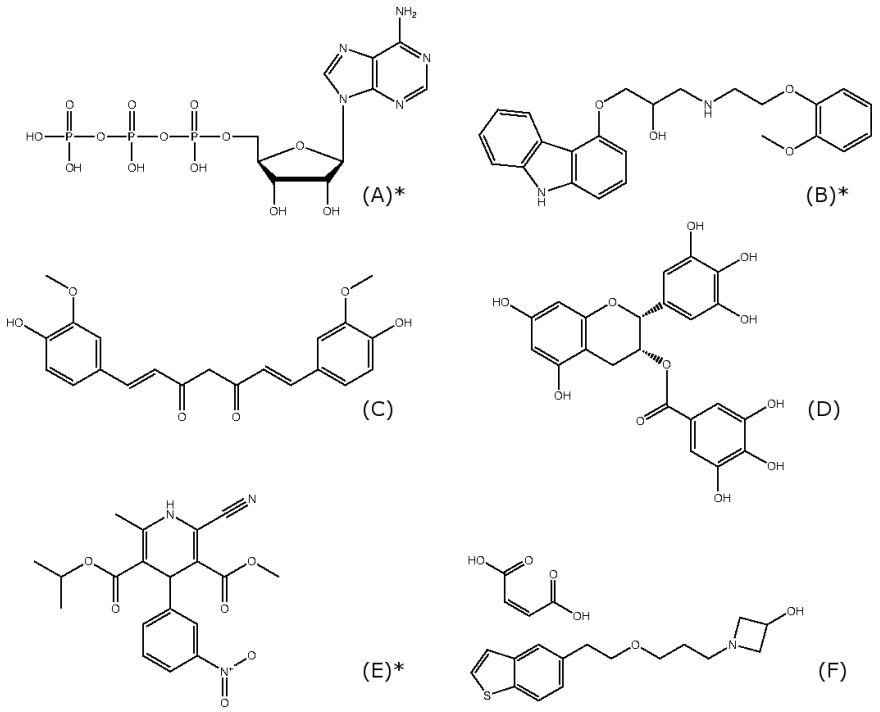

Figure 2.4 Structures of the compounds that are under clinical trial as potential drugs for treating AD. (A) ATP which is under phase 2 of clinical trial; (B) Carvedilol (phase 4); (C) Curcumin (phase 2); (D) (-)-Epigallocatechin-3-Gallate (EGCG) (phase 2); (E) Nilvadipine (phase 3) and (F) T-817MA (phase 2). * refers to compound which was approved for another disease.

phase 3 is processing with reduced version of methylthioninium [85]. Azure A and Anthraquinones also have low IC_{50} that are 2.6 μM, and 2 μM, respectively, that are closed to clinical trial [88, 89]. Many other inhibitors have been designed and studied such as rhodanie based compounds [90], phenylthiazolylhydrazide [91], N-phenylamines [92], Benzothiazoles [93] Phenothiazines, Porphyrins, and polyphenols [68, 94], but none of them has been approved FDA for AD therapy.

2.2.3 Aβ Inhibitors

2.2.3.1 Compounds under clinical trials

Following the amyloid cascade hypothesis [7, 9] many compounds have been explored as potential drugs for AD as they can blok Aβ aggregation. Currently, there are 6 small molecules that are under clinical trial and half of them were approved by FDA for another disease (Fig. 2.4).

The first one is ATP, a small molecule which is associated with intracellular energy transfer [95, 96], is used for nutritional supplementation. The first study on association of ATP with AD was completed by Vincent *et al* [97] showing that ATP is related to the reduction of the Alz-50 immunoreactive proteins. Then, this relationship has been clarified in many experiments [98, 99, 100]. The ability of ATP

in inhibiting Aβ misfolding was reported for the first time in 2001 by Exley *et al* [101] and confirmed by other experiments [37]. Contemporaneously, this compound is being trialled as a potential drug for AD in phase 2 by Rovira *et al* [45] starting from November 2014. The trial is expected to take about 2 years [45].

Carvedilol, a nonselective β-blocker compound, has been proved to impact on the human essential hypertension since 1984 [102]. Until September 2007, Carvedilol was approved for treating congestive heart failure [103]. Carvedilol was suggested as inhibitor of Aβ aggregation in 1999 by Howlett *et al.* [104] and this was supported by other groups [38, 105, 106] Moreover, Rosenberg *et al.* have started the phase 4 to trial ability of Carvedilol for AD treatment in May 2011 and this phase is estimated to complete in the beginning of 2016 [46].

Curcumin, a small compound with two aromatic rings, is derived from curcuma longa. Kim *et al.* were first to find that Curcumin can protect human umbilical vein endothelial cells from Aβ-induced damage [107]. The similar result was also reported by Lim *et al* [108]. Curcumin can degrade both Aβ oligomers and fibrils *in vitro* [109] and *in vivo* [25]. The binding of Curcumin to Aβ peptides was studied by experiments [25, 55, 50, 110] and its nature was understood at the atomic level [23, 111]. The phase 2 of clinical trial for Curcumin as drug to treat AD has been started from January 2014 and it will be completed at the end of 2016 [112]. Moreover, many groups have tried to synthesize Curcumin analogues and related compounds to find new potential inhibitors for Aβ aggregation [50, 113, 114, 115].

Nilvadipine, which is a calcium channel blocker, is used for treating hypertension [116, 117]. Its structure is similar up to 86% in comparison to Curcumin structure [51]. There are many evidences showing that Nilvadipine have positive effect in treatment of early and mild AD [118, 119]. Nilvadipine prevents AD through clearance of Aβ deposits as well as reduced production of Aβ peptides [39, 120, 121, 122]. The ability of Nilvadipine in crossing BBB was also tested [39, 122]. A phase 3 clinical trial for Nilvadipine as potential AD drug has been initiated by Lawlor *et al* [47] at St. James's Hospital, Ireland, from Oct 2012 and expected to finish in Dec 2017.

T-817MA was identified as potential drug by targeting Aβ_{42} aggregation [123]. It was not only powerful in preventing Aβ_{40}/Aβ_{42} and H2O2-induced neurotoxicity in rat brain [123, 124, 125, 126] but also in impairing the synaptic transmission failure of tau protein [127]. Takamura *et al* [128] have shown that T-817MA reduced both Aβ oligomer and oligomer of photo-cross-linked Aβ_{42} in long-term potentiation. Patients with mild and moderate AD have been trialled with T-817MA in phase 2 [129] starting from March 2014. The ages eligible for study range from 55 to 85 years old and the trial will be ended in March 2016.

2.2.3.2 Experiments on amyloid binding molecules

Currently about 160 compounds are under investigation as potential AD inhibitors [130]. Here we briefly review major classes of them.

Polyphenol inhibitors

Because aromatic rings have strong interaction with Aβ peptides [23, 22, 24, 49, 131, 132], polyphenol compounds appear to be potential candidates as Aβ self-assembly inhibitors due to existence of these rings in their structure. Curcumin

[25, 107], Rosmarinic acid [109], EGCG [133], Congo red [134], Resveratrol [135], Propafenone (chapter 5 of this thesis), Carvedilol [38], etc have high propensity to prevent Aβ aggregation. In particular, Curcumin is a good inhibitor of Aβ self-assembly [23, 25, 107] and nontoxic [25]. Due to two aromatic rings Curcumin has higher binding affinity to Aβ in comparison with Naproxen and Ibuprofen [25, 23]. Similar to Curcumin, EGCG, derivative from green tea, also has double aromatic rings playing the key role in its strong binding to Aβ [49]. Choi *at al* [136] was the first group to disclose the relationship between aging and EGCG, although the ability of green tea to slow the aging process was known long time ago in China.

Non-steroidal anti-inflammatory drugs

NSAIDs have high potential to treatment AD through preventing the self-assembly of Aβ. The most important NSAIDs are Naproxen, Ibuprofen, ketoprofen, sulindac, and indomethacin [137].

Natural products

The major advantage of natural compounds is that they are often less toxic compared to synthesized compounds and easy to absorb. Together with Curcumin and EGCG, Ginkgo biloba is beneficial in reduction of Aβ deposits [138]. Recently, Dihydrochalcone, which is available in the database of Chinese traditional medicines, has been confirmed to prevent Aβ aggregation not being cytotoxic [24].

Immunization In AD, the neurotoxicity is presumably associated with the self-assembly of various types of Aβ peptides. An ideal vaccine should function to promote the activity of human immune system to recognize and destroy Aβ plaques. For instance, the immunogen AN1792 is active because Aβ plaques in mice have been reduced in its presence [32]. Stimulated by this result, the clinical phase I was initiated [32] but the clinical phase II [139] terminated in Sep 2003 after the death of one patient. However, the immunogen AN1792 has opened up a new chapter in this field. More vaccines for Aβ are under investigation including immunogen ACC-001 [140], CAD-106 [141], and V950 [142]. In the meanwhile, passive immunization has also been developed including Bapineuzumab [143] and LY2062430 [144] However, clinical trials phase III of both bapineuzumab and solanezumab failed in 2012 [145, 146] showing that immunization is not as good as imagined before [18].

Anti-oxidant ligands

Oxidative injury in the brain is associated with cognitive problems [108, 147]. Many evidences have demonstrated that anti-oxidant compounds can prevent AD through blocking Aβ aggregation [148, 149]. The Aβ neurotoxicity is reduced by anti-oxidant compounds such as Ginkgo biloba [138], Vitamin A [150], Vitamin K [54], Curcumin [25], and EGCG [136]. Therefore, these inhibitors might protect from AD through dual process: one is reduced oxidative injury and the other one is blocking Aβ self-assembly.

Chaperones

Consistent with their main function, chaperone proteins facilitate correct folding and therefore they might prevent misfolding. Inspired by this observation many studies pointd out that HSPs (heat shock proteins) can prevent A aggregation [31] Chaperones Hsp70, and Hsp90 block early stages of Aβ_{42} self-association, while Hsp70 and

Hsp90 with their co-chaperone Hsp40 dissociate Aβ oligomers but not mature filbrils [31]. More information about activity of chaperones as Aβ self-assembly blockers may be found in Yamin *et al* [151].

Peptide inhibitors

Recently, peptide therapeutics has become more and more promising for various diseases [152]. One of popular strategies is using short peptides which are fragments of full length Aβ to prevent Aβ self-assembly. Particularly, Tjernberg *et al* [153] reported that a five residues β-sheet breaker peptide KLVFF from the central region of full length Aβ peptide, can inhibit the growth of Aβ fibrils. In contrast, LVFFA is not highly prone to preventing Aβ aggregation [154]. Replacing the residue Valine by Proline and Alanine by Aspartic acid, Soto *et al* showed that another β-sheet breaker peptide LPFFD is a very potent inhibitor due to its higher hydrophobicity compared with KLVFF [131]. Similarly, eleven-residue β-sheet breaker peptides Aβ11 and RGKLVFFGR have been shown to have the Aβ-blocking ability. All of them are N-methyl peptides. The mechanism of their anti Aβ aggregation is that these peptides are docked to the edge of strands blocking addition of new Aβ [155]. Although N-methyl peptides are critical for prevention of Aβ aggregation, their size is too big and might not cross the BBB. Therefore, Viet *et al* [156] generated all possible 8000 (20^3) three-residue peptides (tripeptides) and studied their activity. It has been shown that tripeptides prefer to bind to hydrophobic region and Proline play the critical role in binding affinity. Combining *in silico* and *in vitro* studies, the authors found WWW, WWP, WPW, and PWW as the most promising Aβ inhibitors [156].

Metal Chelation

Metal ions Cu^{2+}, Zn^{2+}, and Fe^{2+} can mainly bind to His6, His11 and His13 in the N-terminal of Aβ peptide. They alter not only self-assembly rates but also the morphology of aggregates [18]. *In vitro* experiments implied that these ions participate in production of hydrogen peroxide leading to pathologic sequelae [157]. Therefore an obvious therapeutic approach relies on sequestering metal ions by chelation agents. An analogue of 8-hydroxy-quinoline, clioquinol (CQ) is a particularly important metal chelator. It was found to block A self-assembly and production of reactive oxygen species *in vitro* [158]. The second generation of 8-hydroxy-quinoline, PBT2, is in phase II of clinical trials.

Inhibition constants of some compounds

Among 160 tested compounds [130] 128 compounds have the the inhibition constant K_i lower than μM. Here we will just list potent compounds that have K_i in the sub-nanomolar range. The most impressive candidate is fluoropropyl substituted Curcumin, synthesized by Ryu *et at* [50], has the inhibition constant against Aβ aggregation of 0.07 nM [50]. It also passed the examination for partition coefficient, biodistribution, and metabolism [50]. Isomers of styrylbenzene are good inhibitors [159] that K_i of four isomers, E,E-5, E,Z-5, Z,E-5, and Z,Z-5 is 0.11, 0.19, 0.27, and 0.13 nM, respectively [159]. Benzofuran derivatives also have low inhibition constant [160].

One can use the half maximal inhibitory concentration (IC_{50}), which is related to inhibition constant K_i through the Cheng-Prusoff equation [161], to characterize

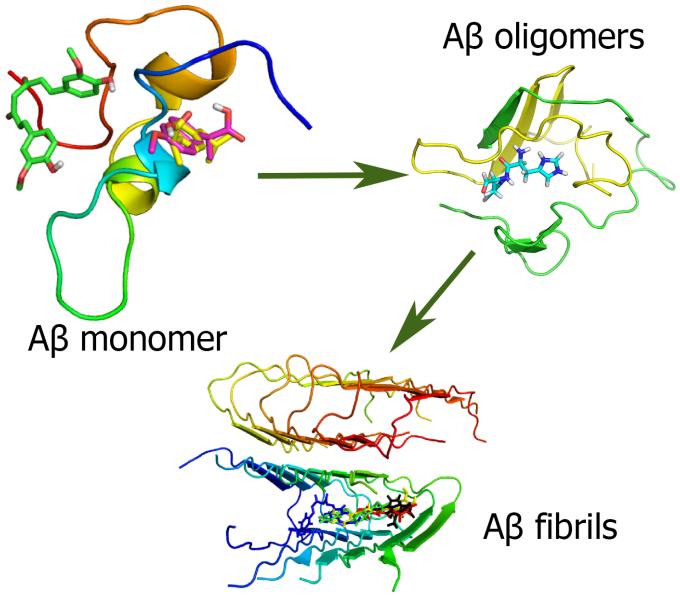

Figure 2.5 (A) Representative monomer structure generated by MD simulations [23]; (B) Oligomeric structure obtained by all-atom MD simulation [166]; (C) Solid state NMR structure of Aβ_{40} fibrils (PDB ID: 2LMN).

binding affinity of small molecules to Aβ [132, 162, 163, 164, 165]. Potential candidates for AD should have the value of IC_{50} in the range of μM to nM. The newest inhibitors for Aβ deposit has been identified by Dadashpour *et al* [162] showing that cyclooxygenase-1 and cyclooxygenase-2 have IC_{50} of 88.88 μM and 10.1 μM, respectively.

2.2.3.3 Computational studies of binding affinity of small molecules to Aβ

Targets

The first thing to do in drug design is to establish binding targets. To prevent Aβ aggregation one can inhibit the activity of monomers but their atomic structures were not resolved experimentally because Aβ peptides are intrinsically disordered in water. In this situation representative structures obtained by using all-atom MD simulations [79] can be used as binding targets (Fig. 2.5). Since oligomers are neurotoxic they become target for AD treatment. As in the monomer case the experimental structures of Aβ oligomers are not available. Again atomic structures of receptors obtained by all-atom MD simulations [166] are employed for *in silico* AD drug design (Fig. 2.5). Some Aβ fibril/protofibril structures are available in PDB [14, 80, 81] (Fig. 2.5) and they are used as targets for destroying Aβ aggregates.

Binding sites

Another serious problem in the computer-aided drug design for AD is that binding sites of small molecules in Aβ are not known a *priori*. Therefore the molecular docking is applied to locate possible binding sites [131]. One can show that binding sites in Aβ are not well defined because locations of ligands are scattered as shown in Fig. 2.6.

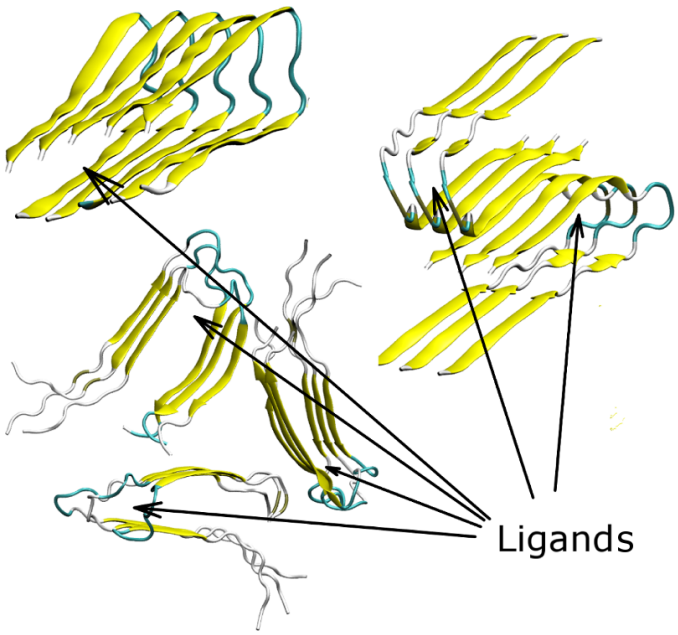

Figure 2.6 Favorite binding poses of ligands to Aβ fibrils. Results were obtained by the molecular docking [131].

Results obtained by molecular docking and conventional MD simulations

The traditional procedure to study binding affinity of small ligands to receptors that the docking method is first applied to find the binding site. Because this method is not accurate enough for estimation of the binding energy more precise methods like MM-PBSA, FEP etc are employed. Conformations obtained in the best docking mode with the lowest binding energy were employed as initial structures for simulations.

Viet *et al.* were the first who have applied molecular simulations to study the binding affinity of short peptides to Aβ peptides and fibrils [131]. Using the Gromos96 43a1 force field and SPC water model it was shown that beta-sheet breaker peptide LPFFD strongly binds to monomer Aβ_{40} and its binding affinity is higher than KLVFF. These findings are consistent with experimental evidences [21]. The binding modes and affinity of KLVFF, LPFFD and VVIA were also studied by MD and MM-PBSA simulations [167].

By the same scheme, it has been shown [23] that Curcumin is better than Naproxen and Ibuprofen in binding to Aβ_{40} monomer. Curcumin do not only have higher binding affinity than two NSAIDs but also reduce the β-content to the larger extent during MD simulations. Two aromatic rings of Curcimin play the important role in its stability in complex with Aβ. A similar study was performed by Zhao *et al* [111] for Aβ_{42} dimer using the GROMOS96 53a6 force field [168] and explicit solvent. The role of hydrophobicity and π-π stacking interaction between Curcumin and dimer was highlighted. The binding site involving Val24, Asn27, Glu11, Gln15, Leu34, and Ile41 is favorable for Curcumin.

The binding properties of 15 derivatives of vitamin K3 (VK3) were studied using representative structures generated by MD simulations for Aβ_{40} [132]. Surprisingly

the results obtained by the docking method for binding energy highly correlated with the experimental results with the correlation level $R = 0.88$. MM-PBSA calculations revealed that compounds VK3-9 and VK3-10 are more potent more Curcumin in inhibiting Aβ_{40} self-assembly. However, VK3-9 is more promising target because it does not show toxicity to cells [132].

Employing MD structures of Aβ_{42} and virtual screening with multi-step docking procedure including DOCK program and Meastro Glide with Pipeline Pilot 7.5 analysis one obtained 183 top hits from 200.000 compounds available in SPECS database [169]. Then by *in vitro* activity assays Wang *et al.* have identified 5 compounds that are dual inhibitors for Aβ aggregation and BACE1.

Du *et al* [164] screened out potential leads from the database of more than 600 natural compounds using their own docking program FlexX/SYBYL which adapts five scoring functions to rank binding affinities. Here Aβ_{42} fibril (PDB ID: 2BEG [14]) was taken as target for molecular docking. Brazilin was identified as the most potent candidate to degrade Aβ aggregates and recommended for further *in vitro* experiments on Aβ_{42} cytotoxicity and fibrillogenesis. The 100 ns MD simulations revealed that the degradation of pentamer proceeded via interruption of salt bridge Asp23-Lys28 and reduction in β-content leaded to decreased neurotoxicity.

By virtual screening top-leads for AD were searched among 32364 natural compounds from the Chinese database [170]. First, Lipinski's rule of five was applied to obtain 3699 drug-like ligands the binding affinity of which was further checked using the molecular docking method. From 10 top-leads revealed by the docking and MM-PBSA simulations one has carried *in vitro* study of dihydrochalcone in detail [24]. The binding free energy of dihydrochalcone to Aβ fibrils obtained by MD is in accord with experiment. Moreover, cell viability assays have shown that this might reduce the neurotoxicity of Aβ [24].

Combining the docking and MM-PBSA methods, from all possible 8000 (20^3) tripeptides one has screened out WWW, WWP, WPW and PWW as potential blockers Aβ fibrillization due to the presence of aromatic rings [156]. In this study the protofibril structure of Aβ_{9-40} [80] was used as the target. *In vitro* experiments have supported the theoretical prediction showing that these compounds have the inhibition constant IC50 in the μM range [156].

The binding of fullerene to Aβ_{17-42} fibrils has been considered using molecular simulations [171, 172]. It was shown that the binding affinity linearly increases with the fullerene size [171].

Although binding sites in Aβ are not well-defined, for the case of fibrils with known PDB structures small ligands prefer to locate next to the turn regions (Fig. 2.6). For monomer and dimer ligands move around the receptor [23, 111] during MD simulation course due to great flexibility of studied systems.

Results obtained by replica exchange molecular dynamics (REMD)

Contrary to the docking and conventional MD simulation, REMD [173] is not aimed at estimating the binding free energy. Therefore its results cannot be directly compared to experimental results on inhibition constant. Rather REMD provides insights on stability of receptor-ligand complex. The advantage of this approach is

that a *priori* information about the atomic structure of target and binding site is not required because the simulation usually initiates from random configurations.

Implicit solvent REMD study of the impact of Ibuprofen on Aβ_{9-40} monomer and oligomers was completed by Chang *et al* [174]. They have confirmed that the fibril growth through dock-lock mechanism [175]. In agreement with experiments [59], the mechanism of anti-aggregation of Ibuprofen has been found as through strong binding to Aβ fibril [174]. The ability of Naproxen to impede Aβ fibril growth has been also ascertained by REMD simulations by Klimov *et al.* [176]. It was found that Naproxen binds stronger than Ibuprofen having higher binding temperature.

Xie *et al* [172] employed REMD method to study the mechanism of fullerene-inhibited aggregation of Aβ fragments. 3C60 was shown to destroy Aβ_{16-22} fibrils stronger than C180 although they have them C60, 3C60, and C180 were located randomly near 8 Aβ_{16-22} fragment the same number of carbon atoms

The impact of NQTrp on structure of Aβ_{1-28} monomer was investigated by all-atom REMD simulations [177]. Because the β-content is reduced by a factor of 1.5, NQTrp can slow down aggregation. However, contrary to previous reports, the activity is not high as the fraction of free monomers is about 20-15% at concentration of 17.5 mM. The similar conclusion has been reached by REMD simulations of Aβ_{1-42} dimer with two NQTrp molecules [178]. The binding of five compounds including 2002-H20, Curcumin, EGCG, Nqtrp, and resveratrol to trimer of Aβ_{17-42} has been also studied by REMD [179]. Although the ligands have multiple binding modes with different binding affinities, they predominantly locate near the CHC (central hydrophobic core) region expanded over residues 17-21.

3

Computational approaches and analysis methods

3.1 Molecular Docking

Molecular docking is a method which is used to predict the most stable conformation of the noncovalently bound molecule to the other one as well as the binding energy. One of the popular scores is the binding energy ΔE_{bind} of ligand to receptor. The best docking mode corresponds to the lowest ΔE_{bind}.

Existing scoring functions may be divided into 4 groups: knowledge-based, force field, empirical, and consensus scoring functions [180]. In this thesis, Autodock Vina [181] is employed to estimate the binding affinity and generate starting conformations for MD simulation. It is also applied to virtual screening for potential drug candidates from the drug-like database. Autodock Vina uses an empirical scoring function

$$\Delta E = \sum_i W_i \Delta E_i, \tag{3.1}$$

where ΔE_i are differences in interaction energies (vdW, electrostatics, etc) between bound and unbound states. Wights W_i are estimated by fitting experimental data on binding energies of ligand-protein complexes with known holo structures. AutodockTools 1.5.4 [182] is used to prepare PDBQT file for the receptors and ligands, which is the input file of Autodock Vina. A modified version of the CHARMM force field was implemented [183, 184] to describe atomic interactions. In the Autodock Vina software, the Broyden-Fletcher-Goldfarb-Shanno (BFGS) method [185] is implemented for local optimization. To obtain accurate results we set the exhaustiveness of global search between 400 and 4000 depending on systems. The maximum energy difference between the worst and best binding modes was chosen equal 7 kcal/mol. Twenty binding modes were generated with random starting positions of ligand, which has

fully flexible torsion degrees of freedom. The receptor flexibility is not allowed in our simulations. The center of grids was placed at the center of mass of either the receptor or binding site. Grid dimensions were chosen large enough to cover the entire receptor or binding pocket. Autodock Vina can also run in parallel to speed up simulation. Although the molecular docking method provides a reasonable information about the location of binding pocket, it is not accurate enough for estimating the binding affinity because of lacking receptor dynamics and limited number of trial positions of ligand.

3.2 Molecular dynamics simulation

In the classical MD simulation the motion of atoms and molecules is described by classical physics. Trajectories of particles are determined by numerically solving the Langevin equations. Results of simulation can be used to analyze structure and dynamics of atoms and molecules at the atomic level that is difficult to gain from experiment. MD simulation was first applied in theoretical physics in the late 1950s [186, 187] but it is widely used today in many science and technology domains including computational biophysics and medicine. In this thesis, we employ all-atoms models for MD simulation of protein-ligand interaction in explicit water using GROMACS [168] and AMBER[188] softwares. A short introduction to MD simulation is given below.

3.2.1 Modeling of solvated complex protein-ligand: all-atom model

Several different force fields have been worked out to model both biomolecules and ligands at the most accurate atomic level such as GROMOS [189, 190], AMBER [191], OPSL [192], and CHARM [193]. Although the force fields are different, the interaction energies have the common functional form

$$E = E_{bonded} + E_{non-bonded}, \tag{3.2}$$

where E_{bonded} is the interaction energy of atoms which are connected by covalent bonds, and $E_{non-bonded}$ represents the non-bonding interactions such vdW and electrostatics interactions.

3.2.2 Non-bonded interactions

The non-bonded interaction involves vdW (Figure 3.1E) and electrostatic (Figure 3.1F) terms. The vdW interaction is defined by the Lennard-Jones potential

$$V_{LJ}(r_{ij}) = \frac{C_{ij}^{12}}{r_{ij}^{12}} - \frac{C_{ij}^{6}}{r_{ij}^{6}} \tag{3.3}$$

where C_{ij}^{12} and C_{ij}^{6} are specific Lennard-Jones parameters which are dependent on atom types and force fields.

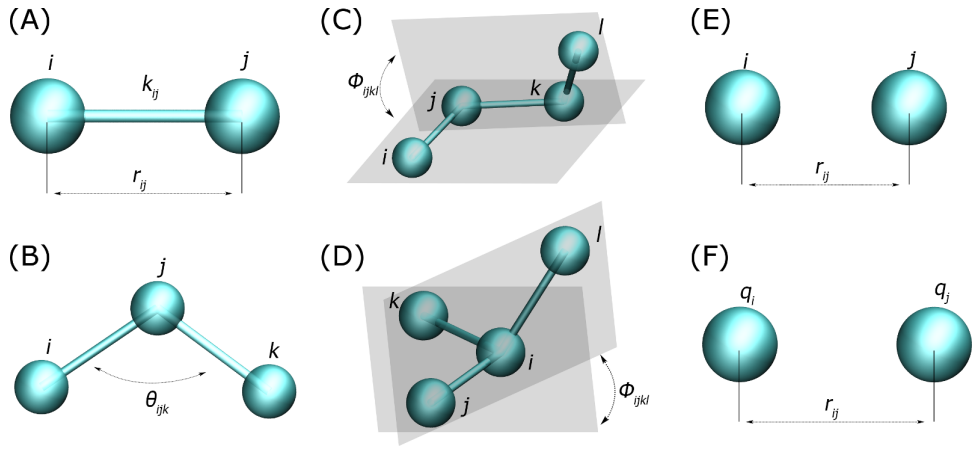

Figure 3.1 Bonded and non-bonded interactions between atom i and j. (A) Schematic representation for covalent bonding, (B) bond angle interactions, (C) proper torsion potential, (D) improper dihedral angles, (E) long range vdW interaction, (F) electrostatic interaction

The interaction between two charged atoms is described by the Coulomb potential

$$V_c(r_{ij}) = \frac{q_i q_j}{4\pi\epsilon_0 r_{ij}} \tag{3.4}$$

where r_{ij} is the distance separating atoms i and j with charges q_i and q_j , and ϵ_0 the electrical permittivity of space.

3.2.3 Bonded interactions

Bonded interactions are bond stretching (2-body), bond angle (3-body), and dihedral angle (4-body) interactions. The bond stretching corresponding to a covalent bond between atoms i and j is described by a simple harmonic potential.

$$V_b(r_{ij}) = \frac{1}{2}k^b_{ij}(r_{ij} - b_{ij})^2 \tag{3.5}$$

where r_{ij} is actual bond length, b_{ij} the reference bond length, k_{ij} the bond stretching force constant. Both reference bond length and force constant are specific for atom pairs and they are extracted from experimental data or quantum mechanical calculation.

The harmonic potential of the *bond angle* between a triple of atoms $i-j-k$ is related with angle θ_{ijk}

$$V_a(\theta_{ijk}) = \frac{1}{2}k^\theta_{ijk}(\theta_{ijk} - \theta^0_{ijk})^2, \tag{3.6}$$

where θ_{ijk} and θ^0_{ijk} are the actual and reference angles, k^θ_{ijk} is the angle bending force constant. Values of k^θ_{ijk} and θ^0_{ijk} depend on chemical type of atoms.

Improper potential is handled to manage planarity in a molecular structure. Figure 3.1D illustrates the improper torsional angle. The simplest improper dihedral potential is chosen as a harmonic potential.

$$V_{id}(\xi_{ijkl}) = \frac{1}{2}k_\xi(\xi_{ijkl} - \xi_0)^2, \tag{3.7}$$

where ξ_{ijkl} is improper dihedral angle and k_ξ is the corresponding bending force constant.

Proper dihedral angles are defined according to the IUPAC/IUB convention (Figure 3.1C), where ϕ_{ijk} is angle between ijk and ikl planes, with zero matching to the *cis* configuration (i and l on the same side). The periodic cosine type of proper dihedral potential is usually used.

$$V_d(\phi_{ijkl}) = k_\phi(1 + cos(n\phi - \phi_s)), \tag{3.8}$$

here k_ϕ is dihedral angle force constant, ϕ_s is dihedral angle (Figure 3.1C), and $n = 1, 2, 3$ is a coefficient of symmetry.

3.2.4 Stochastic dynamics

The stochastic dynamics adds a friction and noise terms into Newton's equation to approximate effects of temperature and environment that is also termed Langevin equation:

$$m\frac{d^2\vec{r}}{dt^2} = \vec{F}_c - \gamma\frac{d\vec{r}}{dt} + \vec{\Gamma} \equiv \vec{F}. \tag{3.9}$$

Here m is the typical mass of a bead, Γ is a random force, γ is the friction coefficient, and $\vec{F}_c = -d\vec{E}/d\vec{r}$. Here the configuration energy E given by Eq. (3.2). The random force Γ is a Gaussian random variable with white noise spectrum and obeys the fluctuation-dissipation relation:

$$< \Gamma(t)\Gamma(t') >= 2\gamma k_B T\delta(t - t'), \tag{3.10}$$

where k_B is a Boltzmann's constant, T temperature and $\delta(t - t')$ the Dirac delta function. The friction term only influences kinetic but not thermodynamic properties.

3.2.5 The leap-frog integrator

In stochastic dynamics simulations, Langevin equations (Eq. 3.9 and 3.10) are solved for discrete time intervals Δt by using leap-frog algorithm [194]. This algorithm is based on Taylor's expansions of positions, velocities or higher-order derivatives. It is fast and requires only little memory storage. The leap-frog algorithm uses position

$\mathbf{r}_i$ at time t and velocity $\mathbf{v}_i$ at time $t - \Delta t/2$ updating positions and velocities using the forces $\mathbf{f}_i(t)$ determined by the positions at time t:

$$\mathbf{v}_i(t + \frac{\Delta t}{2}) = \mathbf{v}_i(t - \frac{\Delta t}{2}) + \frac{\mathbf{F}_i}{m_i}\Delta t$$
$$\mathbf{r}_i(t + \Delta t) = \mathbf{r}_i(t) + \mathbf{v}_i(t + \frac{\Delta t}{2})\Delta t. \tag{3.11}$$

For iteration stability, the maximum time step Δt should be small in comparing to the cycle of the fastest shaking within the system. Its value is usually chosen equal 1 or 2 fs.

3.2.6 MD simulations with AMBER

We have used AMBER 10 package [188] to run MD simulations. The AMBER 99SB force field [191] was employed to represent small molecules and proteins. The ligand parameters were provided by the general AMBER force field [195] except for charges, which taken from MOPAC 2002 [196] using AM1-BCC [197, 198] in the gas phase. Solvated protein-ligand complexes were placed in a triclinic box with at least 0.8 nm distance between the solute and box. The water model TIP3P [199] has been chosen for explicit solvent. To neutralize systems, ions Na^+ or Cl^- were added.

The long range electrostatic interaction is computed by particle-mesh Ewald (PME) summation method [200]. Equations of motion were integrated using the leap-frog algorithm [194] with a time step 1 fs. The non-bonded interaction pair-list was updated every 10 fs with the cut-off of 0.8 nm. The systems were minimized to remove bad vdW contacts with water. Then the temperature was gradually increased from 0 to 300K during 100 ps. For density equilibration the MD simulation has been carried out with weak restraints on all bonds of the complex for 100 ps at constant temperature 300 K [201, 202]. Restraints have been implemented by the LINCS algorithm [203]. Constant temperature 300 K was enforced using Berendsen algorithm [204] under 500 ps NVT simulation with a damping coefficient of 0.1 ps. Then the NPT simulation is performed using Parrinello-Rahman pressure coupling [205] at 1 atm with the damping coefficient of 0.5 ps. The final MD runs has been carried out and snapshots collected in equilibrium were used to study binding affinity of ligand to protein.

3.2.7 MD simulation with GROMACS

We have also performed MD simulations using GROMACS 4.5.5 package [168] with the GROMOS96 43a1 force field [189, 190] and SPC water model [206]. The PRODRG2 beta server [207] was used to generate topology parameters for ligands. Since charges assigned by this server [207] provide unrealistic partitioning between water and cyclohexane phases [208], we used Mulliken partial charges [209] calculated at the AM1-BCC [197, 198] level in the gas phase using MOPAC2002 [196].

The accurate leap-frog stochastic dynamics integrator was employed for MD simulation [210] at 300 K with a relaxation time of 0.1 ps. The pressure was kept at

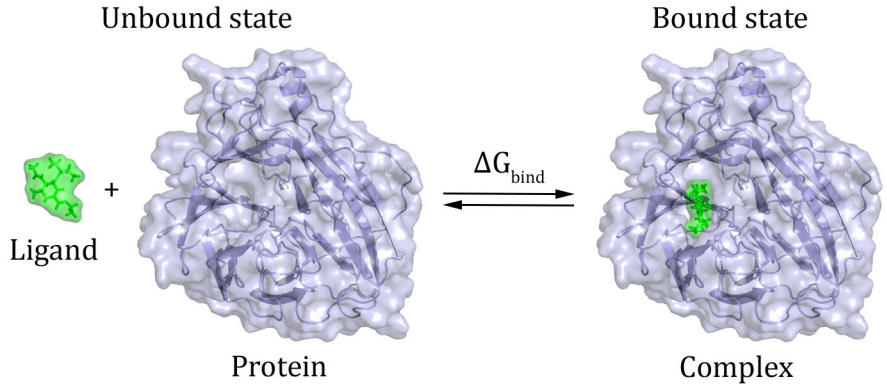

Figure 3.2 Protein and ligand in unbound and bound states.

1.0 atm using Parrinello-Rahman pressure control [205]. We used LINCS [203] for constraining bonds, while the time step 2 fs was chosen. The PME method [200] was employed to compute the electrostatic interaction. The cutoff the Lennard-Jones interaction was set equal 0.9 nm, while the non-bonded interaction pair list with a cutoff of 1.0 nm was updated every 10 fs. Solvated systems were placed in the dodecahedron and cubic boxes 1 nm distance between the solute and box with periodic boundary conditions.

By carrying out energy minimization steps, the solvated complex and ligand systems were first minimized until the maximum force becomes smaller than $2\text{x}10^{-6}$ kJ/(mol.nm) for the solvated systems. We applied a weak restrained force for solvated systems using harmonic potential and performed constant temperature MD simulations for 100 ps. To reach equilibrium NPT simulations of 0.5 ns for the solvated systems were carried out. Equilibrium configurations were used to estimate the binding free energy using MM-PBSA method and other quantities such as hydrogen bonds (HB), hydrophobic interactions, second structures, free energy landscape, etc.

3.3 Calculation of binding free energy for solvated complex protein-ligand

Because molecular docking ignores the receptor dynamics and the number of trial positions of ligand is limited, the prediction power of this method is low. The more accurate methods for estimating the binding free energy should be employed. The MM-PBSA method which is usually used because its input is reasonable. The more expensive but more accurate method is FEP method that is also employed in this thesis for studying stability of protein-ligand complexes.

3.3.1 Solvated protein-ligand complex

Finding the free energy difference between different states of a physical system is of great interest in many scientific fields, including drug design [211]. Here we are in-

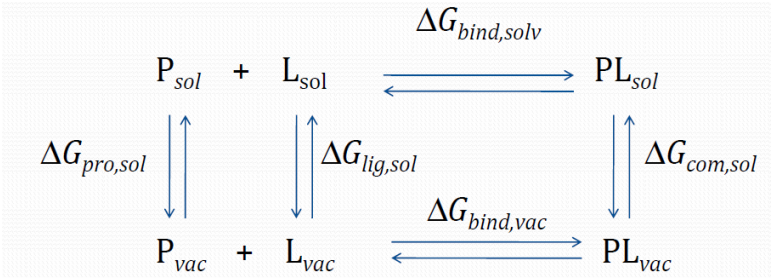

Figure 3.3 The diagram of protein-ligand binding/unbinding. Here P_{sol} represents solvated protein, L_{sol} solvated ligand, PL_{sol} solvated complex, P_{vac} L_{vac}, and PL_{vac} are protein, ligand and protein-ligand complex in vacuum. $\Delta G_{pro,sol}$, $\Delta G_{lig,sol}$, and $\Delta G_{lig,sol}$ are free energy difference between solvated and vacuum states of protein, ligand and protein-ligand complex, respectively. $\Delta G_{bind,vac}$ is binding free energy of protein-ligand in vacuum, while $\Delta G_{bind,sol}$ is binding free energy of solvated complex protein-ligand in environment.

terested in the difference between free energies of bound and unbound states (Figure 3.2). There are many numerical methods which have been employed to predict the binding affinity such as MM-PBSA, linear-response approximate, linear interaction energy FEP, thermodynamics integration methods and others. The calculated binding free energy ΔG_{bind} is related with experimentally determined binding constant K_i through the following equation

$$\Delta G_{bind} = RTln(K_i), \tag{3.12}$$

where gas constant $R = 1.989$ cal.mol^{-1}K^{-1} and K_i is measured in mole.

3.3.2 MM-PBSA method

In the MM-PBSA method, the binding free energy is defined as follows

$$\Delta G_{\text{bind}} = G_{\text{complex}} - G_{\text{free-protein}} - G_{\text{free-ligand}}. \tag{3.13}$$

Calculations of the free energy of each molecule were carried out according to

$$G = E_{\text{mm}} + G_{\text{solvation}} - TS. \tag{3.14}$$

The molecular mechanics energy of the solute in the gas phase E_{mm} includes bond, bond-angle, dihedral-angle, electrostatics and vdW (Lennard-Jones) terms,

$$E_{\text{mm}} = E_{\text{bond}} + E_{\text{angle}} + E_{\text{torsion}} + E_{\text{elec}} + E_{\text{vdW}}. \tag{3.15}$$

The intramolecular electrostatic (E_{elec}) and vdW (E_{vdw}) interactions are calculated by the Gromacs or Amber tool.

The free energy of solvation, $G_{\text{solvation}}$ was approximated as the sum of electrostatic and nonpolar contributions,

$$G_{\text{solvation}} = G_{\text{PB}} + G_{\text{sur}}. \tag{3.16}$$

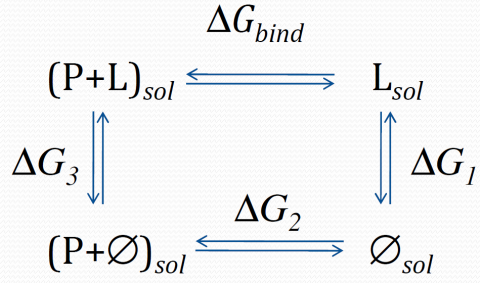

Figure 3.4 The free energy cycle to calculate ΔG_{bind}, the free energy difference between the bind of inhibitor L to protein P in solvent. $\oslash$ is ligand without any non-bonding interactions with environment.

Here G_{PB} derived from the electrostatic potential between solute and solvent using the continuum solvent approximation [212] (Figure 3.3). It is the change of electrostatic energy from transferring solute in a continuum medium, from a low solute dielectric constant (ϵ=2) to higher one with water without salt (ϵ=78.45). G_{PB} is the numerical solution of the corresponding linear Poisson Boltzmann equation. The nonpolar solvation term G_{sur} was approximated as linearly dependent on the solvent accessible surface area (SASA), derived using the Shrake-Rupley numerical method [213].

$$G_{\mathrm{sur}} = \gamma SASA + \beta \tag{3.17}$$

where $\gamma = 0.0072$ kcal/mol.Å^2 and $\beta = 0$ [214]. Solute entropy contributions were estimated using snapshots taken from MD runs. Structures were first minimized with no cut-off for non-bonded interactions by using steepest decent, conjugate gradient and low-memory BFGS method [185] until the maximum force drops below 10^{-6} kJ/(mol.nm). The conformational entropy of the solute S, estimated from normal mode analysis by calculating and diagonalizing the mass-weighted Hessian matrix [215], is as follows

$$S_{\mathrm{vib}} = -R\ln(1 - e^{-h\nu_0/k_BT}) + \frac{N_A\nu_0 e^{-h\nu_0/k_BT}}{T(1 - e^{-h\nu_0/k_BT})}. \tag{3.18}$$

Here S_{vib} is the vibrational entropy, h Plank's constant, ν_0 the frequency of the normal mode, k_B the Boltzmann constant, $T = 300$ K, and N_A Avogadro's number.

3.3.3 Free energy perturbation method

3.3.3.1 Free energy calculation

The binding free energy ΔG_{bind} between ligand and protein is the sum of the free energy change of complex protein-ligand and the free energy of desolvation:

$$\Delta G_{bind} = \Delta G_{complex} + \Delta G_{desolvation} \tag{3.19}$$

$$\Delta G_{solvation} = -\Delta G_{desolvation} \tag{3.20}$$

$$\Delta G_{bind} = \Delta G_{complex} - \Delta G_{solvation} \tag{3.21}$$

The absolute binding free energy ΔG might be calculated using the following the diagram of free energy cycle (Figure 3.4):

$$\Delta G_{bind} = \Delta G_3 + \Delta G_1, \tag{3.22}$$

where ΔG_3 is $\Delta G_{complex}$ and ΔG_1 is $\Delta G_{solvation}$

In the FEP method, the free energy difference between two states A and B is obtained using a simulation where the Hamiltonian changes from the A Hamiltonian to the B Hamiltonian in discrete stages called lambda intervals. The transformation between states must be slow that system remains in equilibrium during the process. The Hamiltonian has been changed from pure state A ($\lambda = 0$) to pure state B ($\lambda = 1$) tuning parameter λ,

$$H_{\lambda=0}(p,q) = H^A(p,q), \tag{3.23}$$

$$H_{\lambda=1}(p,q) = H^B(p,q) \tag{3.24}$$

In NVT ensemble, the Helmholtz free energy A is related to the partition function Q obtained at constant volume and temperature using MD simulation:

$$A(\lambda) = -k_B T ln Q \tag{3.25}$$

$$Q = \frac{1}{N!h^{3N}} \int\int e^{-H_\lambda(p,q)/k_B T} dpdq. \tag{3.26}$$

In classical physics h is an arbitrary quantity but one may choose it as Plank constant. In NPT ensemble, the Gibbs free energy G is related to the partition function Δ obtained in equilibrium at constant pressure and temperature:

$$G_\lambda = -k_B T ln \Delta \tag{3.27}$$

$$\Delta = \frac{1}{N!h^{3N}} \int\int\int e^{-(H_\lambda(p,q)+pV)/k_B T} dpdqdV. \tag{3.28}$$

$$G = A + pV \tag{3.29}$$

Integrals over the whole phase space cannot be evaluated from MD simulation, but it is possible to estimate the derivative with respect to λ as an ensemble average:

$$\frac{dG}{d\lambda} = \frac{\int\int\int (\partial H/\partial\lambda) e^{-(H_\lambda(p,q)+pV)/k_B T} dpdqdV}{\int\int e^{-(H_\lambda(p,q)/+pV)/k_B T} dpdqV} = \left\langle \frac{\partial H}{\partial \lambda} \right\rangle_{NPT,\lambda} \tag{3.30}$$

with a similar relation for $dA/d\lambda$ in the NVT ensemble. The difference in free energy between A and B can be found by integrating the derivative over λ:

$$\Delta G = G^B(p,T) - G^A(p,T) = \int_0^1 \left\langle \frac{\partial H}{\partial \lambda} \right\rangle_{NPT,\lambda} d\lambda. \tag{3.31}$$

3.3.3.2 Dependence of interactions on λ

To describe the transformation between states A and B one can use a simple dependence of the interaction energy on λ.

Coulomb interaction

The λ-dependent Coulomb interaction between two particles is:

$$V_c = \frac{f}{\epsilon_{rf} r_{ij}}[(1-\lambda)q_i^A q_j^A + \lambda q_i^B q_j^B] \tag{3.32}$$

$$\frac{\partial V_c}{\partial \lambda} = \frac{f}{\epsilon_{rf} rij}[-q_i^A q_j^A + q_i^B q_j^B] \tag{3.33}$$

where $f = 1/4\pi\epsilon_0$.

Van der Waals interaction

For the vdW (Lennard-Jones) interactions one chooses

$$V_{vdW} = \frac{(1-\lambda)C_{12}^A + \lambda C_{12}^B}{r_{ij}^{12}} - \frac{(1-\lambda)C_6^A + \lambda C_6^B}{r_{ij}^6} \tag{3.34}$$

$$\frac{\partial V_{vdW}}{\partial \lambda} = \frac{C_{12}^B - C_{12}^A}{r_{ij}^{12}} - \frac{C_6^B - C_6^A}{r_{_{ij}}^{6}} \tag{3.35}$$

Soft-core interaction

In a free-energy calculation where particles appear or disappear, the use of the simple linear interpolation of the Lennard-Jones and Coulomb potentials as described in Eqs 3.34 and 3.35 may lead to poor convergence. When the particles have nearly disappeared, or are close to appearing (at λ close to 0 or 1), the interaction energy will be weak enough for particles to get very close to each other, leading to large fluctuations in values of $\partial V/\partial\lambda$.

To overcome these difficulties, the singularities in the potentials need to be removed by modifying the regular Lennard-Jones and Coulomb potentials with "soft-core" potentials that limit the energies and forces involved at values between 0 and 1, but not at λ =0 or 1.

In GROMACS the soft-core potential V_{sc} are shifted versions of the regular potentials:

$$V_{sc}(r) = (1-\lambda)V^A(r_A + \lambda V^B(r_B) \tag{3.36}$$

$$r_A = (\alpha\sigma_A^6\lambda^p + r^6)^{\frac{1}{6}} \tag{3.37}$$

$$r_B = (\alpha\sigma_B^6(1-\lambda)^p + r^6)^{\frac{1}{6}} \tag{3.38}$$

where V^A and V^B are the normal vdW or electrostatics potentials in state A ($\lambda = 0$) and state B ($\lambda = 1$) respectively, α is the soft-core parameter, p is the soft-core λ power, σ is the radius of the interaction.

The soft-core forces are given by the following expressions

$$F_{sc}(r) = \frac{\partial V_{sc}(r)}{\partial r} = (1-\lambda)F^A(r_A)(\frac{r}{r_A})^5 + \lambda F^B(r_B)(\frac{r}{r_B})^5 \tag{3.39}$$

where F^A and F^B are normal forces. The contribution to the derivative of the free energy is:

$$\frac{\partial V_{sc}(r)}{\partial \lambda} = V^B(r_B) - V^A(r_A) + (1-\lambda)\frac{\partial V^A(r_A)}{\partial r_A}\frac{\partial r_A}{\partial \lambda} + \lambda\frac{\partial V^B(r_B)}{\partial r_B}\frac{\partial r_B}{\partial \lambda} \tag{3.40}$$

$$\frac{\partial V_{sc}(r)}{\partial \lambda} = V^B(r_B) - V^A(r_A) + \frac{p\alpha}{6}[\lambda F^B(r_B) r_B^{-5}\sigma_B^6(1-\lambda)^{p-1} - (1-\lambda)F^A(r_A)r_A^{-5}\sigma_A^6\lambda^{p-1}] \tag{3.41}$$

In GROMACS vdW soft-core function uses $p = 2$, but $p = 1$ gives a smoother $\partial H/\partial\lambda$ curve. For suitable changes between the two state A ($\lambda = 0$) and B ($\lambda = 1$), it is important that the overlapping should occur around $\lambda = 0.5$. This can usually be satisfied setting $\alpha \approx 0.7$ for $p = 1$ and $\alpha \approx 1.5$ for $p = 2$.

3.3.3.3 The double-annihilation binding-energy method

Details of the FEP may be found [217] Typically, we used the coupling parameter λ to adjust the non-bonded interactions. 21 values of λ were used to reduce the vdW interaction from full ($\lambda = 1$) to none ($\lambda = 0$). Similarly, 12 values of λ were chosen to decrease the electrostatics interaction using a soft core potential [218, 219]. The set of coupling parameter λ are the same in both the solvated complex and ligand systems that are λ = 0.0, 0.1, 0.2, 0.275, 0.375, 0.45, 0.55, 0.65, 0.675, 0.725, 0.75, 0.775, 0.8, 0.825, 0.85, 0.875, 0.9, 0.925, 0.95, 0.975, and 1.0 for adjustment of vdW interaction and λ = 0.00, 0.10, 0.25, 0.45, 0.55, 0.65, 0.70, 0.75, 0.80, 0.90, 0.95, and 1.00 for adjustment of Coulomb interaction. Therefore, one set of free energy calculation requires a total 33 independent MD simulations of 1 ns each with different λ but having the same starting configurations and velocities. The binding free energy ΔG_{bind} was estimated using BAR (Bennett's acceptance ratio) method [220], ΔG_{bind} = G_A - G_B. Here G_A is the free energy of ligand desolvation from solvated complex and G_B is the free energy of ligand ligand from solvated ligand system. For each system the results were averaged over 8 independent MD runs.

3.4 Measures used for data analysis

3.4.1 Blood-brain barrier and human intestinal absorption

The BBB is a physical barrier in the circulatory system that compounds should across in order to travel into the central nervous area [221]. Thus the requirement

of passing this barrier is necessary for any AD drug candidate. The crossing ability through the BBB is measured by the logarithm base 10 of the ratio of the compound concentration in the brain, C_{brain}, to that in the blood, C_{blood}:

$$\log(BB) = \log_{10}\left[\frac{C_{\text{brain}}}{C_{\text{blood}}}\right]. \tag{3.42}$$

BB is likely related to local hydrophobicity, molecular size, lipophilicity, and molecular flexibility [222]. In the present work BB is computed using the QSAR model [221, 223] implemented in the PreADME prediction software [224]. This method was proved to provide estimations highly correlated with experimental data [223].

Another important aspect of oral drug design is HIA [225] which measures drug percentage that can be absorbed by human body. HIA should be high enough for drug efficacy. It depends on molecular weight, number of HB donors, number of HB acceptors, $C\log P$ and $M\log P$ [224, 226]. HIA of all compounds is estimated by the QSAR method [224, 225, 227, 228] which is also implemented in the PreADME suit [224].

3.4.2 RMSD, hydrogen bond, side chain contacts, and secondary structures

The root mean square deviation (RMSD) is a measure of the deviation of structure from its initial configuration. RMSD is used to monitor the approach of studied system to equilibrium where this quantity becomes saturated.

The HB is assumed to be formed if the distance between proton donor (D) and proton acceptor (A) is less than 0.35 nm and the H-D-A angle is also less than 30^o.

The time evolution of formation of contacts between SC (side chain) of receptor and the ligand is also monitored. SC contact is formed if the distance between the centers of mass of the ligand and receptor SC $\leq$ 6.5 Å.

To estimate the content of secondary structures of proteins/peptides, we used the DSSP tool [229, 230].

3.4.3 Chemical and structural similarity

The similarity between two compounds was estimated through association and distance coefficients. The Tanimoto's association coefficient [231, 232] is characterized for binary data:

$$S_{A,B} = \frac{\sum_{i=1}^{n} p_{iA}p_{iB}}{\sum_{i=1}^{n} p_{iA}^2 + \sum_{i=1}^{n} p_{iB}^2 - \sum_{i=1}^{n} p_{iA}p_{iB}} \tag{3.43}$$

where $S_{A,B}$ is the similarity score between molecules A and B, and p_{iA} and p_{iB} are the values describing properties of the molecules A and B such as hydrophobic and hydrophilic SASA, donor HB, acceptor HB, polarizability, and aqueous solubility.

The distance coefficient $D_{A,B}$ is the score for the difference between two molecules A and B [232]:

$$D_{A,B} = [\sum_{i=1}^{n} m_i(p_{iA} - p_{iB})^2]^{1/2} \tag{3.44}$$

where m_i is the corresponding mass. To screen out potential candidates for AD we used QikProp implemented in Schroedinger package [51]. Compounds that share $>$ 80% similarity with Curcumin were selected.

4

Curcumin binds to Aβ_{1-40} peptides and fibrils stronger than Ibuprofen and Naproxen

4.1 Introduction

As mentioned above, Curcumin can inhibit Aβ aggregation [25, 50], but the nature of its binding to Aβ has not been explored at the atomic level. *In vitro* studies showed that NSAIDs naproxen and ibuprofen can interfere with Aβ aggregation, but inhibitory mechanisms remain mysterious [56, 59, 233, 234]. The impact of these compounds on Aβ was studied by REMD [57, 58, 176, 235] showing that consistent with the experiments [59] ibuprofen has lower binding propensity than naproxen. However, the binding free energies ΔG_{bind} of these NSAIDs to Aβ peptides that might be directly compared with experimental inhibition constants [50, 59] have not been computed. As evident from the experiments [59], ibuprofen and naproxen have the same binding site but, this problem has not been addressed theoretically. On the other hand, the experiments [25] showed that Curcumin inhibits Aβ oligomerization to the greater extent than ibuprofen and naproxen. As in the case of NSAIDs, ΔG_{bind} of Curcumin to Aβ has not been estimated.

Motivated by mentioned here open problems, in this chapter we address the following questions: 1) calculation of the binding free energies of Curcumin, Ibuprofen and Naproxen to monomer Aβ_{1-40} and its mature fibrils using the docking and MM-PBSA method; 2) finding binding sites of these ligands and 3) elucidating the role of aromatic rings in ligand binding.

4.2 Materials and Methods

4.2.1 Chemical structures and parameterization of Curcumin, Ibuprofen and Naproxen

The chemical structures of Curcumin ($C_{21}H_{20}O_6$), Naproxen ($C_{14}H_{14}O_3$) and Ibuprofen ($C_{13}H_{18}O_2$) were taken from Pubchem with ID 969516, 156391 and 3672 [236]. Note that there are R- and S-form of Ibuprofen. The latter has been chosen for simulation and will be referred to as Ibuprofen. Two-dimensional plots of three ligands are shown in Fig. 4.1 (A). We used the PRODRG server [207] to generate their parameters to perform MD simulations with GROMOS96 43a1 force field. Names and types of atoms, masses and charges of ligands are shown in Table S1-S3 in Supporting Information [23].

4.2.2 Crystal structures of monomer Aβ_{1-40}

Since Aβ peptides are highly aggregation-prone in water their monomer structures have not been experimentally resolved yet. In the Protein Data Bank (PDB) two structures with PDB codes 1AML [237] and 1BA4 [77] are available for the full-length Aβ_{1-40}. However, these structures are not suitable for aqueous environment as they were obtained in the water-micelle environment with pH= 2.8 and 5.1 [77, 237]. In order to obtain the structure reliable for docking simulations we have carried out the following simulation. The structure taken from PDB with ID 1BA4 was first heated up to $T = 500$ K using the GROMOS96 43a1 force field [189] in explicit water. Then subsequent 5 ns MD simulation was carried at this temperature until the peptide becomes unstructured. A random coil conformation was used as a starting configuration for 300 ns MD simulations at $T = 300$ K. As follow from the time dependence of the C_α root mean square displacement (RMSD) (Fig. 4.3) the system reaches equilibrium after about 120 ns.

To check if our canonical 300 ns MD simulation generates structures relevant to experimental ones, we calculate chemical shifts δ using snapshots collected during last 180 ns and the SHIFT program [238, 239]. Our *in silico* result is in excellent agreement with the NMR experiments of Hou *et al* [240] with correlation level $R = 0.98$ (Fig. 4.2). The same correlation level has been obtained in 500 ns MD simulation [241], while Yang and Teplow have reported $R = 0.994$ [79] using the replica exchange molecular dynamics (REMD) and recently improved Amber force field PARM99SB [191]. However, the correlation factor of chemical shifts cannot serve as a good indicator of reliability of *in-silico* structural distributions [241]. To understand this problem we calculate the secondary chemical shift defined as $\Delta\delta = \delta - \delta_{\mathrm{RC}}$, where δ_{RC} is a chemical shift for amino acids in random coil state. Using values of NMR δ_{RC} from Wishart *et al* [242] we have the correlation coefficient between the experimental $\Delta\delta_{\mathrm{exp}}$ and our conventional MD (CMD) simulation results $R = 0.42$ (Fig. 4.2). This correlation level is close to $R = 0.45$ obtained by REMD method [79] (see Fig. S5 in SI of our previous work [241]).

Because, in term of primary and secondary chemical shifts, the quality of structure ensemble obtained by 300 ns CMD is compatible with that of REMD we use the

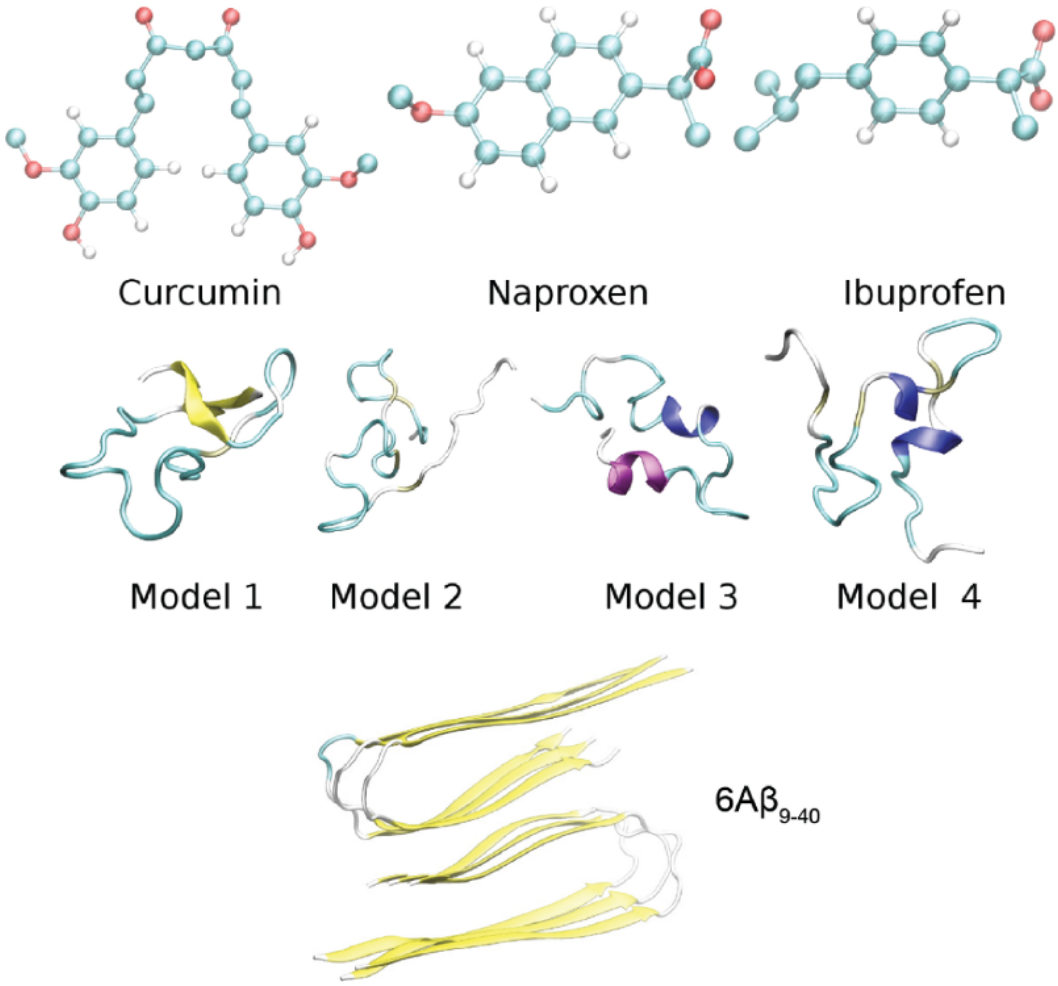

Figure 4.1 Chemical structures of Curcumin, Ibuprofen and Naproxen (upper panel). Here we use the S-form of Ibuprofen. Model 1 (middle panel) is the most populated structure obtained by CMD simulations starting from the random coil configuration for full length monomer Aβ_{40}. Model 2, 3, and 4 were obtained by REMD [79] for monomer. These 4 structures are used for the docking and MD simulations to estimate the binding free energy by the MM-PBSA method. The two-fold symmetric 6Aβ_{9-40} fibril structure, resolved by the solid state NMR technique [80] (bottom panel).

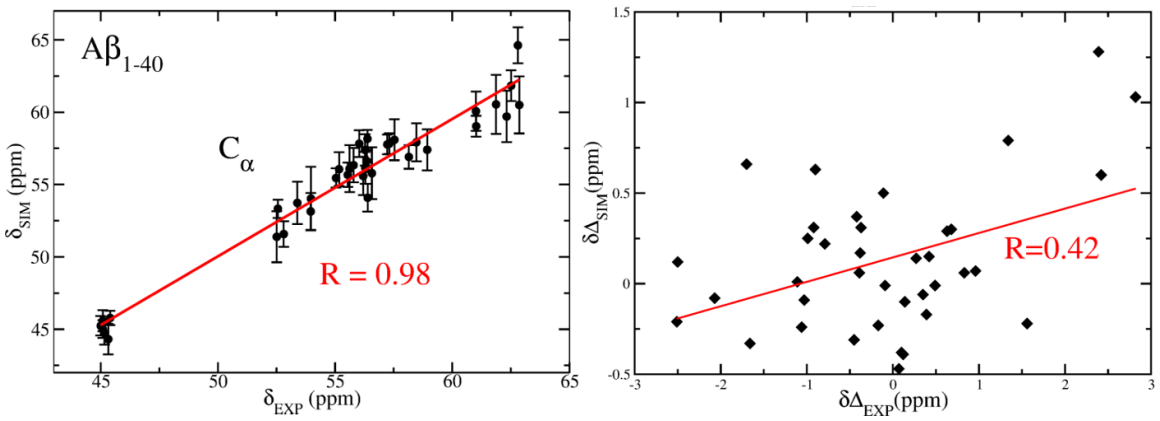

Figure 4.2 Correlation between theoretical and experimental C_α chemical shifts (upper panel) and secondary chemical shifts (lower panel) of monomer AAβ_{1-40}. The correlation level R is shown next to data points.

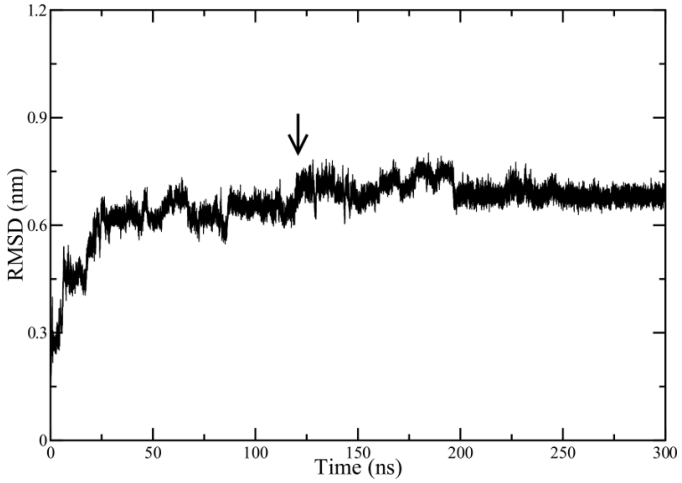

Figure 4.3 Time dependence of C_α RMSD of Aβ_{1-40}. The arrow roughly refers to time when the system reaches equilibrium.

C_α RMSD conformational clustering method [243] implemented in the GROMACS software to screen out dominant structures for studying ligand binding. With the clustering tolerance of 1.0 we have obtained 5 representative structures from snapshots collected in equilibrium during last 180 ns of MD run. We choose a typical structure of the most populated cluster (population is about 84%) as Model 1 (Fig. 4.1) for further docking and MD simulations. Since one structure obtained from 300 ns CMD simulation may not provide unbiased results on binding affinity we will also use structures of three dominant clusters obtained by REMD [79] as receptors. These structures have been provided by Prof. D. Teplow and will be referred to as Models 2, 3 and 4 (Fig. 4.1). Note that REMD study of Aβ_{1-40} has been also carried by Sgourakis and Garcia [244] but their structures are not available for us.

4.2.3 Solid state NMR structures of Aβ_{9-40} fibrils

Because eight residues of the N-terminus of Aβ_{1-40} are disordered in the fibrillar state [80], they are neglected in the construction of fibril structures. We perform docking simulation using 2-fold-symmetric fibrils of six (6Aβ_{9-40}) and twelve (12Aβ_{9-40}) [80] peptides and 3-fold symmetric fibrils of nine (9Aβ_{9-40}) and 18 (18Aβ_{9-40}) Aβ_{9-40} chains [81]. The corresponding structures were kindly provided by Dr. R. Tycko. Structure of 6Aβ_{9-40} (Fig. 4.1) will be also used for MD simulations in the presence of ligands. Note that experimental structures for 6Aβ_{9-40}-ligand complexes are not available. Therefore initial conformations, used for MD simulation, have been generated by docking ligand to NMR structures of receptor.

4.2.4 Computational methods and measures used in structure analysis

Docking method

As we told above, docking method is used to search binding pose and binding energy of Curcumin, Naproxen, and Ibuprofen to receptors. In this problem, exhaustiveness is chose 400 for monomer receptor and 4000 for fibril receptor. The center of grids was put at the center of mass of receptors and grid dimensions were chosen 60x40x40 $Å^3$ and 90x70x50 $Å^3$ for Aβ_{40} and 6Aβ_{9-40} in respectively that covered all parts of receptors.

MD Simulations

The solvated complexes have simulated using the GROMACS 4.5.5 package [168]. The parameters of MD simulations have described in Chapter 3. In particular, the complex Aβ_{1-40} monomer and 6 Aβ_{9-40}-ligands have been put in PBC box that contain approximate 2500 and 26000 water molecule, respectively.

MM-PBSA Method

The MM-PBSA method has been employed to estimate the binding free energy between receptors and ligands. The details of MM-PBSA method are given in Chapter 3.

In this chapter, the time dependence of the number of HB and SC contacts is monitored to study structures of Aβ-ligand complexes (Chapter 3).

	Aβ_{1-40}	2-fold 6Aβ_{9-40}	2-fold 12Aβ_{9-40}	3-fold 9Aβ_{9-40}	3-fold 18Aβ_{9-40}
Curcumin	-5.4±0.5	-7.0	-8.6	-8.8	-9.5
Naproxen	-5.3±0.4	-6.7	-7.7	-7.9	-9.1
Ibuprofen	-4.9±0.3	-6.0	-6.9	-7.5	-8.3

Table 4.1 Shown are binding energies ΔE_{bind} (in kcal/mol) of Curcumin, Naproxen, and Ibuprofen to monomer Aβ_{1-40} and mature fibrils. Results have been obtained in the best mode by the docking method. For Aβ_{1-40} error bars come from averaging over 4 Models.

4.3 Results and Discussion

4.3.1 Binding of three ligands to monomer Aβ_{1-40}

4.3.1.1 Docking results.

We first dock three ligands to 4 structures of Aβ_{1-40} (Fig. 4.1) using Autodock Vina version 1.1[181]. The binding energies ΔE_{bind}, obtained in the best mode (lowest values), are averaged over 4 structures and shown in Table 4.1. Within the error bars the binding energies are the same for three ligand. Thus the docking method is not able to distinguish binding affinities of these ligands to monomer Aβ_{1-40}. However, as evident below, more accurate MD simulations support the superiority of Curcumin.

For the model 1 of monomer Aβ_{1-40} Curcumin is located near both terminals while Naproxen and Ibuprofen bind to the same site near the loop containing GLU11 and GLY12 (Fig. 4.4). Interestingly, for models 2, 3 and 4 Naproxen and Ibuprofen also have the same binding position in the best docking mode (Fig. 4.4). The binding position of Curcumin in Model 2 is closer to these ligands compared to other models (Fig. 4.4). The fact that NSAIDs share the same binding position agrees with the autoradiography and fluorescence experiments by Agdeppa *et al* [59].

The HB networks between ligands and Aβ_{1-40} (Model 1) in the best docking mode are shown in lower panel of Fig. 4.4. Curcumin has one HB with ASP1 of the receptor, while Naproxen and Ibuprofen have three HBs with GLU11 and GLY12. Obviously, the HB interaction is not a key factor controlling binding affinity because Ibuprofen has ΔE_{bind} higher than Curcumin despite the former has more HBs than the latter. Since Curcumin, Naproxen and Ibuprofen have 10, 7 and 6 SC contacts the SC interaction plays a decisive role in their binding affinity. This conclusion is also valid for Models 2, 3 and 4 of Aβ_{1-40} (results not shown).

4.3.1.2 Estimation of binding free energies by MM-PBSA method.

The docking method is good for predicting a binding position of ligand, but not accurate enough for estimation of binding energies. Therefore, in this section we

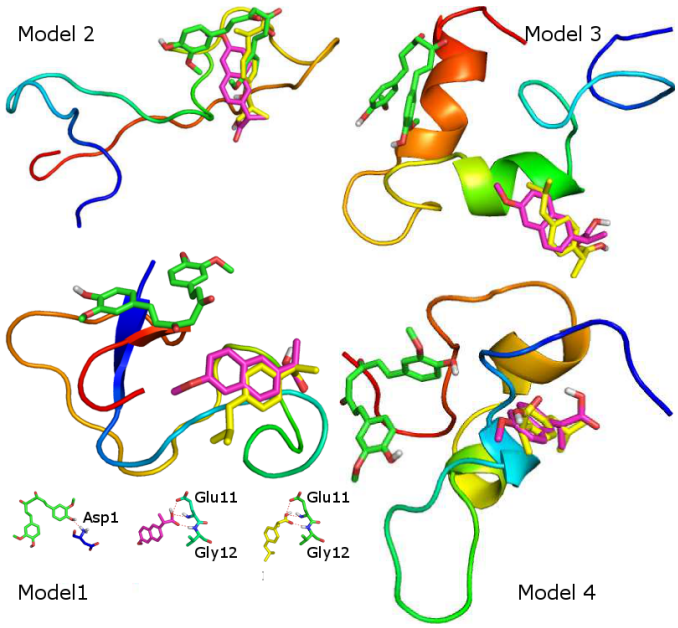

Figure 4.4 Binding sites of Curcumin (green), Naproxen (magenta), and Ibuprofen (orange) obtained in the best docking mode for receptor Aβ_{1-40}-Model 1,2, 3, and 4. The lower panel of the Molel 1 shows the HB networks for three ligands with the receptor.

estimate ΔG_{bind} by the MM-PBSA method [245, 246]. The structures of Aβ_{1-40}–ligand complexes obtained in the best docking mode (upper panel of Fig. 4.4 for Model 1 and Figs. S3-S5 for Models 2-4) were used as starting conformations for MD simulations with GROMACS 4.5.5 package [168]. As follows from the time dependence of the interaction energy between receptor and ligand the systems reach equilibrium at different time scales marked by arrows (Fig. 4.5). For Model 1, 3 and 4 (Fig. 4.5) the equilibration time of Aβ_{1-40}–Curcumin complex is larger than complexes with Naproxen and Ibuprofen. This is presumably because Curcumin is bigger leading to more complex interactions with the receptor. The situation becomes different for Model 2 where the complex with Curcumin gets equilibrated even faster than Naproxen and Ibuprofen (Fig. 4.5) suggesting that the equilibration time depends not only on ligand structure but also on topological and chemical properties of the binding site.

As shown below, within the same GROMOS force field the time scale to reach equilibrium for complex of fibril 6Aβ_{9-40} and ligand is about one order of magnitude shorter than Aβ_{1-40}. This is because Aβ_{1-40} lacks a well-defined binding site (Fig. 4.4), while a ligand moves within the binding pocket of 6Aβ_{9-40}. For other systems with well-defined binding pocket the relaxation time is of $\approx$ 10 ns [247].

Snapshots collected every 100 ps in equilibrium were used to estimate ΔG_{bind} by the MM-PBSA protocol. The results that have been averaged over four models are shown in Table 4.2. For Curcumin the vdW contribution dominates over the electrostatic interaction, but for Naproxen and Ibuprofen the Coulomb contribution is larger in magnitude than the vdW term. ΔE_{elec} is positive for NSAIDs because these ligands have charge of -1 while the total charge of Aβ_{1-40} is -3. The charge

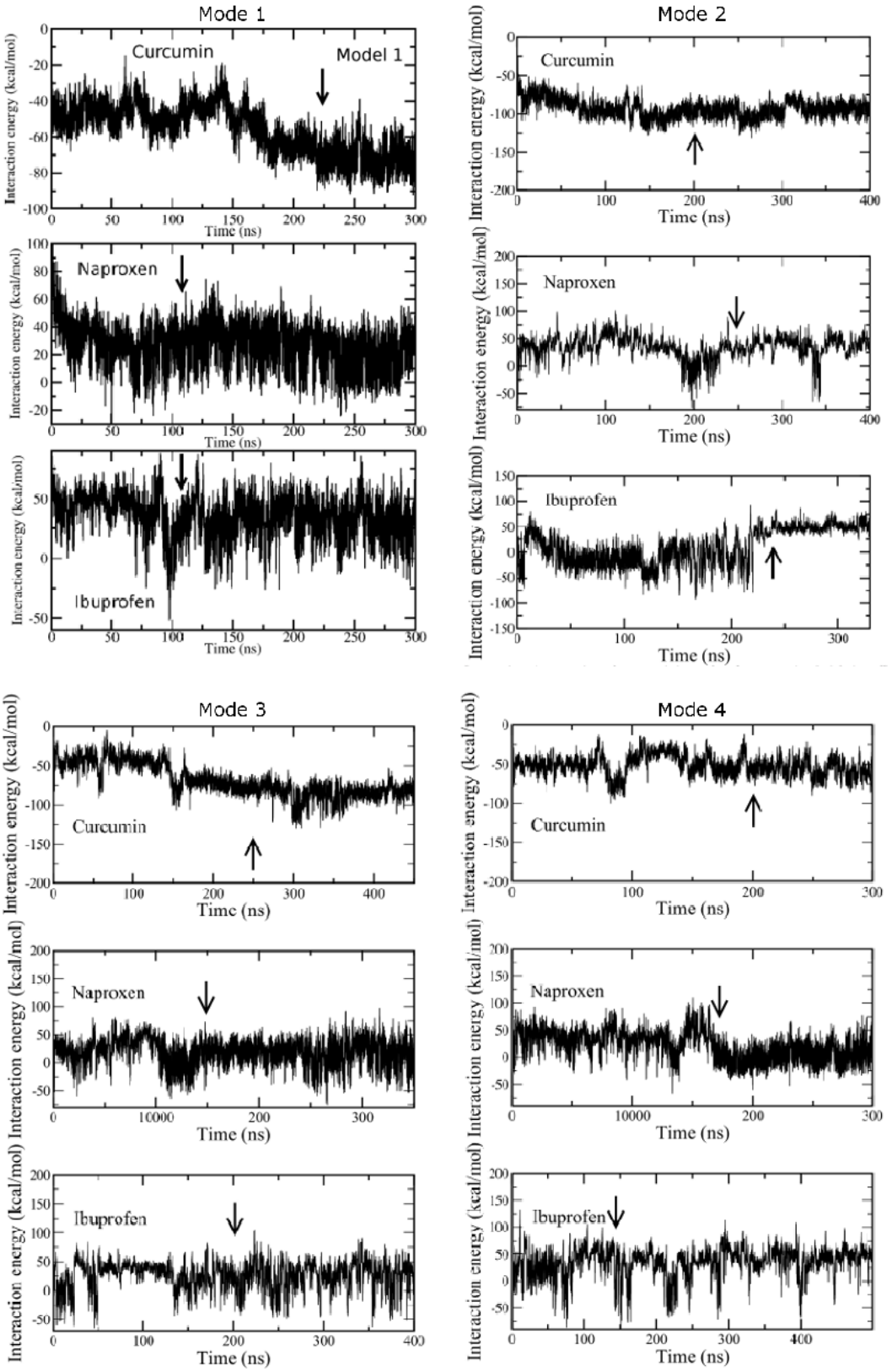

Figure 4.5 Time dependence of the interaction energy between Curcumin (upper), Naproxen (middle) and Ibuprofen (lower panel) with Aβ_{140}. The results have been obtained using the complex of structure of Model 1 with ligands as a starting configuration (Fig. 4.4). Arrows roughly refer to times when complexes reach equilibrium.

		$\Delta E_{\rm elec}$	$\Delta E_{\rm vdw}$	$\Delta G_{\rm sur}$	$\Delta G_{\rm PB}$	$-T\Delta S$	$\Delta G_{\rm bind}$	$\Delta G^{\rm exp}_{\rm bind}$
Curcumin	Aβ_{1-40}	-28.5±6.5	-46.2±6.7	-5.2±0.5	37.3±4.1	23.5±0.6	-19.1±6.4	
	6Aβ_{9-40}	-21.99	-49.96	-6.30	39.31	25.44	-13.50	-13.33
Naproxen	Aβ_{1-40}	43.7±8.4	-23.4±4.4	-3.0±0.4	-34.5±11.0	8.3±0.5	-8.7±2.4	
	6Aβ_{9-40}	52.40	-31.73	-4.18	-36.57	10.46	-9.45	-11.33
Ibuprofen	Aβ_{1-40}	45.9±5.3	-14.4±2.5	-2.2±0.4	-40.2±5.3	7.7±1.0	-3.2±2.0	
	6Aβ_{9-40}	30.78	-21.53	-3.97	-22.53	8.94	-8.31	-6.8

Table 4.2 Binding free energies $\Delta G_{\rm bind}$ (kcal/mol) of three inhibitors to monomer Aβ_{1-40} and 2-fold symmetric 6Aβ_{9-40} fibril obtained by the MM-PBSA method. For Aβ_{1-40} error bars come from averaging over 4 Models. The experimental values of $\Delta G_{\rm bind}$ are estimated from the inhibition constants $K_{\rm i}$ using the formula $\Delta G_{\rm bind} = RT\ln(K_{\rm i})$. Here $R = 1.987\times10^{-3}$ kcal/mol, T = 300 K, and $K_{\rm i}$ is measured in M. K_i of Curcumin and NSAIDs was taken from Ryu *et al*[50] and Agdeppa *et al* [59], respectively.

of Naproxen and Ibuprofen is non-zero due to the carboxyl group that becomes carboxylate group in the aqueous environment. Having total zero charge Curcumin displays attractive Coulomb interaction with the receptor (Table 4.2). Note that the contribution of electrostatic interactions is largely compensated by the polarization term $\Delta G_{\rm PB}$.

In the harmonic approximation the solute entropy contribution is nearly the same for Naproxen and Ibuprofen complexes, but two-fold smaller than Curcumin (Table 4.2). This is because Curcumin has 21 carbon atoms, while Naproxen and Ibuprofen have 14 and 13 carbon atoms only. For this very reason the nonpolar term $\Delta G_{\rm sur}$ of NSAIDs is also twice smaller than Curcumin.

Curcumin and Naproxen show very strong binding affinity to monomer Aβ_{1-40} having $\Delta G_{\rm bind} = -19.1 \pm 6.4$ and -8.7 $\pm$ 2.4 kcal/mol, respectively (Table 4.2). Within the error bars these estimations are close to the experimental values obtained for fibrillar structures [59, 50]. Much weaker binding affinity was observed for Ibuprofen with $\Delta G_{\rm bind} \approx$ -3.2 kcal/mol which is higher the experimental result -6.8 kcal/mol measured for fibrils (Table 4.2). MM-PBSA calculations give the following ranking for binding affinity to monomer Aβ_{1-40}:

$$Ibuprofen \rightarrow Naproxen \rightarrow Curcumin, \tag{4.1}$$

where the ascending ordering is used. As will be shown below, this ranking also holds for ligand binding to fibrils.

4.3.1.3 Role of aromatic rings in binding affinity of ligands to Aβ_{1-40}

. Since the vdW interaction dominates over the electrostatic interaction in binding affinity we consider the contribution of individual atoms of ligand to the vdW interaction energy. Curcumin, Naproxen and Ibuprofen, respectively, have 35, 23 and 19 atoms that are numbered as shown in Fig. S10 [23]. Using the GROMACS software we have calculated the vdW interaction energy of each atom with receptor in equilibrium (only snapshots collected after arrows in Fig. 4.5 are used for calculation) and the results have been averaged over four models. Curcumin has 4 key atoms

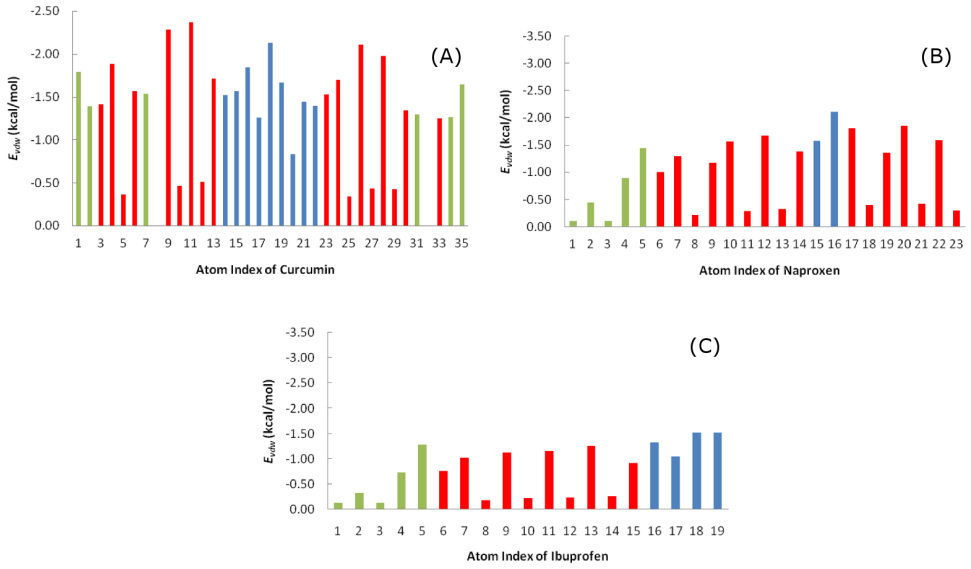

Figure 4.6 Contributions of individual atoms of three ligands to the vdW interaction energy. The results have been obtained in equilibrium for four models of monomer Aβ_{1-40}. Red color refers to atoms belonging to aromatic rings. For Curcumin blue refers to atoms between two rings, while remaining atoms are in green. In the case of Naproxen and Ibuprofen blue and green indicate atoms on the left and right of aromatic rings, respectively.

(9, 11, 18 and 26) that have vdW interaction energy $E_{\rm vdW} < -2$ kcal/mol (Fig. 4.6) but three of them belong to aromatic rings. However, contributions from aromatic ring atoms are not homogeneous leading to their total contribution of about 51.4%. Thus, aromatic rings of Curcumin do not dominate over other parts in vdW interaction with monomer Aβ_{1-40} although they have three key residues.

Similar to Curcumin the aromatic ring of Ibuprofen, which involves 10 atoms, has almost the same contribution to $E_{\rm vdW}$ (46,7%) as other fragments. Among 9 key atoms (5, 7, 9, 11, 13, and 16-19) which have $E_{\rm vdW} < -1$ kcal/mol (Fig. 4.6) one has four atoms 7, 9, 11 and 13 from the aromatic ring.

The situation becomes different in the case of Naproxen (Fig. 4.6), where aromatic rings dominate over other parts as their contribution is 71.1%. Five (atoms 10, 12, 20 and 22) of 7 key atoms with $E_{\rm vdW} < -1.5$ kcal/mol belong to aromatic rings.

4.3.1.4 Hydrogen bonding and side chain interaction of Curcumin are stronger than Naproxen and Ibuprofen.

Since qualitative results are the same for four models of monomer Aβ_{1-40} we will focus on the Model 1. In order to better understand the nature of binding of three ligands we monitor the time dependence of HBs between receptor and ligand (Fig. 4.7). Having calculated the time average of the number of HBs in equilibrium we obtain $\overline{HB(t)} = 2.34$, 0.27 and 0.07 for Curcumin, Naproxen and Ibuprofen, respectively. Thus, contrary to the docking result (Fig. 4.4), Curcumin has more HBs

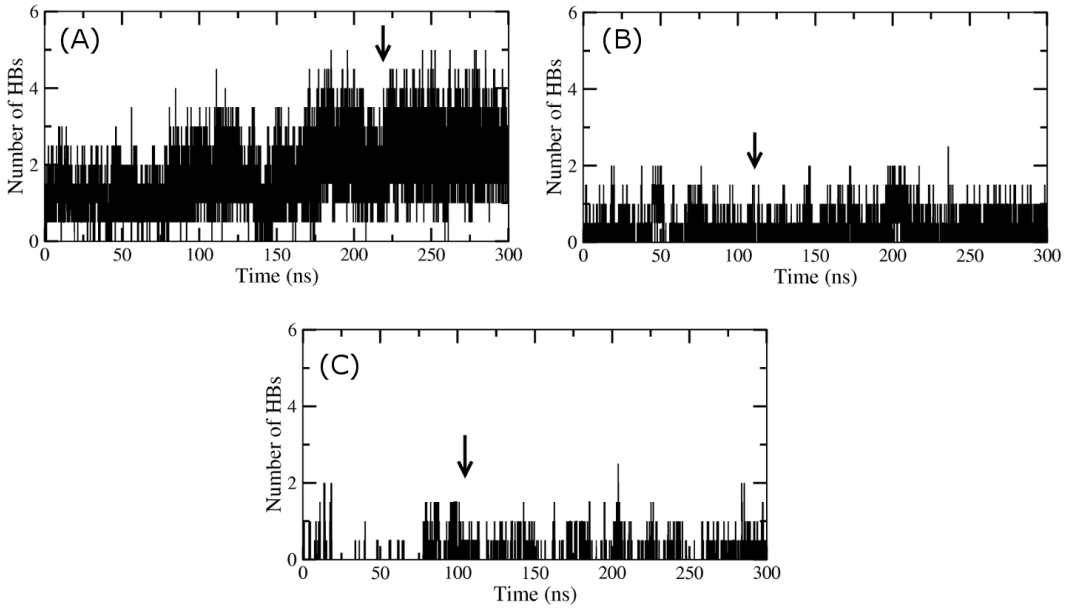

Figure 4.7 Time dependence of HBs between receptor Aβ_{1-40} and Curcumin (A), Naproxen (B) and Ibuprofen (C). The results have been obtained for Model 1. Arrows roughly refer to times when systems reach equilibrium. Using values of HBs collected in equilibrium (after arrows) we obtain the average $\overline{HB(t)}$ =2.34, 0.27, and 0.07 for Curcumin, Naproxen and Ibuprofen, respectively.

than NSAIDs and the binding ranking (Eq. 4.1) is consistent with our MD results on HB networks.

Fig. 4.8 (A) shows the probability of occurrence of HB between ligand and a given residue of receptor. This quantity is defined as the number of HB formation times divided by the total number of recorded snapshots. Curcumin prefers to form HBs with both terminals with very strong binding to residue GLY-38, while NSAIDs have more HBs with the region 10-16 (Fig. 4.8 (A)). The HB network of Curcumin with monomer Aβ_{1-40} is much stronger than Naproxen and Ibuprofen. This is in accord with the estimations of ΔG_{bind} (Table 4.2).

Fig. 4.9 shows time dependence of SC contacts between Aβ_{1-40}-Model 1 and three ligands. The average numbers of SC contacts, obtained in equilibrium for Curcumin, Naproxen and Ibuprofen (Fig. 4.9) indicate that together with hydrogen bonding the SC interaction plays an important role in ligand association. In order to get a more detailed picture on binding we have constructed SC contact map (Fig. 4.10) which shows the probability of occurrence of contacts between each atom of ligand and the SC of receptor amino acids. In agreement with the HB picture (Fig. 4.8 (A)) Curcumin spends more time near two ends of Aβ_{1-40} than other regions, frequently binding to residue GLY-37 and GLY-38. Naproxen has less SC contacts compared to Curcumin displaying strong binding to PHE-20. Contrary to Curcumin and Naproxen, Ibuprofen does not bind to specific residues (Fig. 4.10) and this is a reason why Ibuprofen has the lowest SC interaction and binding affinity. Comparing Fig. 4.8 (A) and Fig. 4.10 one can see that both HB and SC data support the binding ranking given by Eq. 4.1.

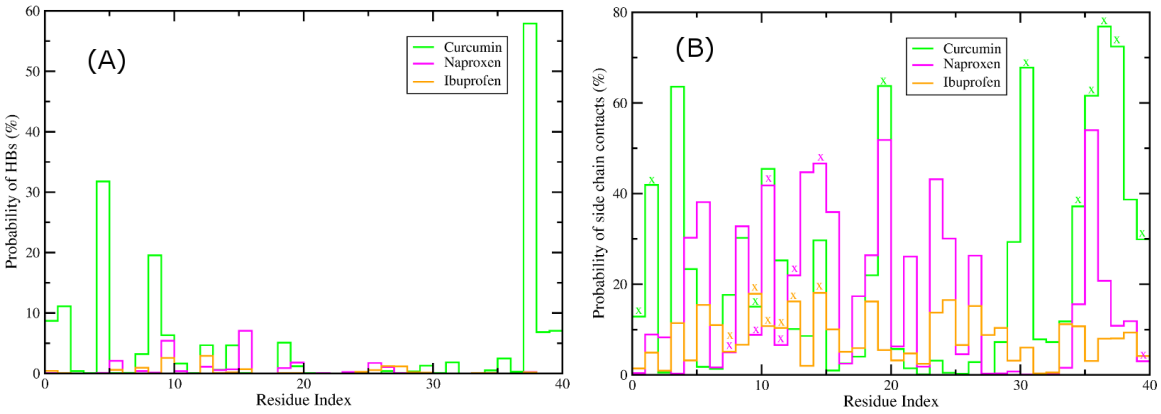

Figure 4.8 (A) Probability of formation of HBs between Curcumin, Naproxen and Ibuprofen and individual residues of Aβ_{1-40}-Model1. (B) Probability of formation of SC contacts of Curcumin, Naproxen and Ibuprofen with Aβ_{1-40}-Model 1. The results have been obtained from 300 ns MD simulations. Symbol X refer to those residues that have the SC with ligand in the best mode conformation obtained by the docking method (see Fig. 4.4).

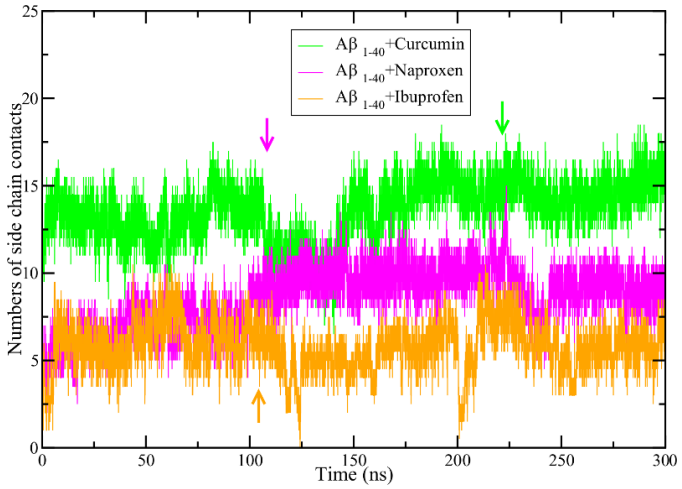

Figure 4.9 Time dependence of the SC contacts between monomer Aβ_{1-40} and Curcumin (green), Naproxen (magenta) and Ibuprofen (orange). The results were obtained for Model 1. Arrows refer to times of reaching equilibrium (see Fig. 4.5). In the equilinrium we have the average value $\overline{SC(t)}$=14.64, 9.47, and 5.63 for Curcumin, Naproxen and Ibuprofen, respectively.

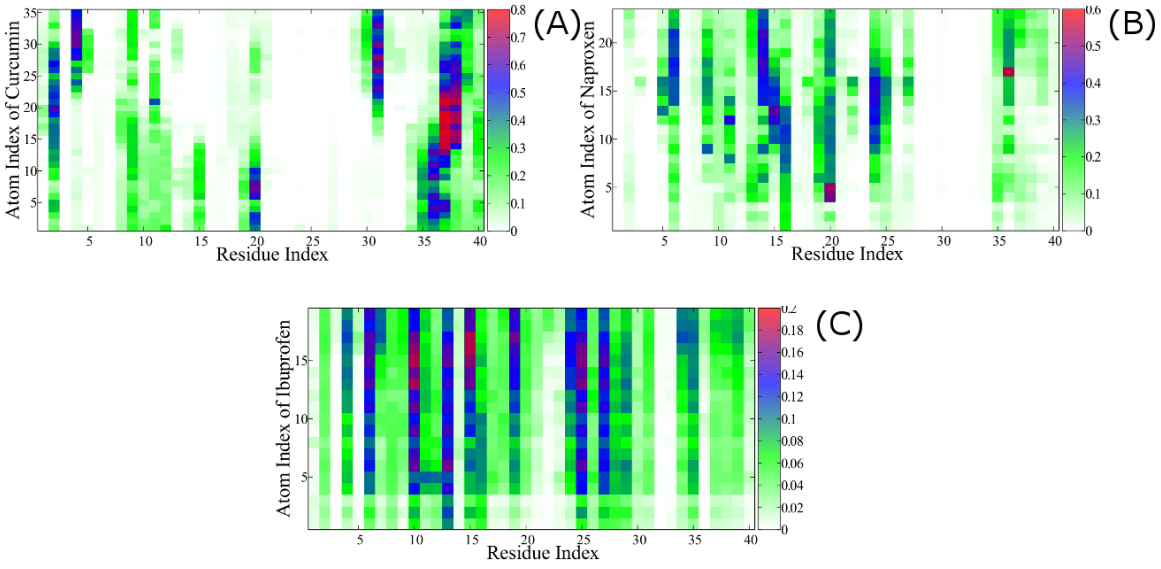

Figure 4.10 SC contact maps for complexes of Aβ_{1-40} (Model 1) with Curcumin (A), Naproxen (B), and Ibuprofen (C). Here one considers contacts between each atom of ligand and amino acids of receptor. The results have been obtained from 300 ns MD simulations.

4.3.1.5 Binding site predicted by the docking method for Curcumin is the most probable.

Since monomer Aβ_{1-40} is almost unstructured and does not have a well-defined binding pocket it is interesting to know if the binding site predicted by the docking method (Fig. 4.4) remains the most probable in MD runs. We will consider Model 1 because similar results have been also obtained for three remaining models. Starting from the conformation obtained in the best docking mode during 300 ns simulations Curcumin may run away from the binding location but revisits it again and again (Movie S1 in SI). Naproxen and Ibuprofen spend less time around their binding sites obtained by docking than Curcumin (Movies S2 and S3 in SI). In order to demonstrate this clearly we plot data shown in Fig. 4.10 in a different way (Fig. 4.8 (B)). In Fig. 4.8 (B) the probability of formation of SC contacts between ligand and receptor is defined in such a way that a contact is considered as formed if the distance between any ligand atom and the center of mass of residue < 6.5 Å. Symbol X refers to those residues that have SC contacts with ligand in the best docking mode conformation. Clearly, residues of the binding site predicted by the docking method for Curcumin are the most visited by ligand during MD simulation. However this does not hold for NSAIDs. Naproxen binds to PHE20 (51.8%) and VAL36 (54%) very often but these residues do not belong to the binding site followed from the docking calculation (Fig. 4.8 (B)). Ibuprofen displays the binding propensity to residues HIS6 (15.4%), TYR10 (17.9%), HIS13 (16.2%), GLN12 (18.1%), VAL18 (16.2%) and GLY25 (16.5%) higher than to others but only TYR10, HIS13 and GLN15 belong to the docking binding region. Nevertheless, Naproxen and Ibuprofen have the tendency to bind to the same place (Fig. 4.8 (B)).

4.3.2 Binding to two-fold symmetric fibril 6Aβ_{9-40}

The results obtained for monomer Aβ_{1-40} by MD simulations indicate that Curcumin is the most prominent ligand. However, they can not be directly compared with the experiments [25, 50, 59] which have been carried out on mature fibrils. Recall that it is very difficult to perform experiments for Aβ monomer in water as it has high propensity to aggregation. Therefore, to make the direct comparison of theoretical results with the experiments one should consider fibril structures. Here we consider 6Aβ_{9-40} system but more complex structures will be discussed with the help of the docking method in the next section.

4.3.2.1 Docking results.

Binding positions in the best mode obtained by the Autodock Vina version 1.1 are shown in Fig. 4.11. In difference from the monomer case (Fig. 4.4), all of three ligands have the same binding site inside the upper patch of three β-hairpins. The corresponding binding energies of ligands to 6Aβ_{9-40} are listed in Table 4.1. In agreement with the experiments [25, 50, 59] and results obtained by the MM-PBSA method for monomer (Eq. 4.1), Curcumin at least marginally dominates over NSAIDs having $\Delta E_{\rm bind} = -7.0$ kcal/mol that is lower than $\Delta E_{\rm bind} = -6.7$ and -6.0 kcal/mol for Naproxen and Ibuprofen, respectively.

Curcumin forms 3 HBs with the receptor including two with LYS28 and one with SER26 from peptide III (lower panel of Fig. 4.11). Naproxen has 2 HBs with LYS28(I) and PHE20 (III), while Ibuprofen has only one HB with LYS28(II). Thus based on the HB networks one can explain the ranking of binding affinity in Eq. 4.1 that the lower is $\Delta E_{\rm bind}$ the larger is the number of HBs.

4.3.2.2 Binding free energy: MM-PBSA results.

The conformations obtained by the docking method (Fig. 4.11), are used as starting configurations for 20 ns MD simulations. The systems reach equilibrium at time scales of $\approx$ 10 ns (Fig. 4.12) that are much shorter than the monomer case (Fig. 4.5). This is because ligands have the binding pocket inside fibrils and they stay there during the whole MD run (Movies 4, 5 and 6 in SI). Snapshots collected in equilibrium, i.e. after times marked by arrows in Fig. 4.12 are used for estimating the binding free energy by MM-PBSA method[245, 246] (Table 4.2). For Curcumin we have $\Delta G_{\rm bind}$ = -13.5 kcal/mol which is in excellent agreement with the experimental value of -13.33 kcal/mol [50]. Thus both experiment and simulation indicate that Curcumin has very strong binding affinity with the inhibition constant IC50 $\sim$ nM. For Naproxen, the agreement between theory and experiment is not as good as Curcumin but the simulation correctly captures the experimental range of IC50 $\sim \mu$M [59]. For Ibuprofen the MM-PBSA method provides $\Delta G_{\rm bind} = -8.31$ kcal/mol that is lower than the experimental value -6.8 kcal/mol (Table 4.2). Given that this approach involves a number of approximations our simulation results should be considered as reasonable.

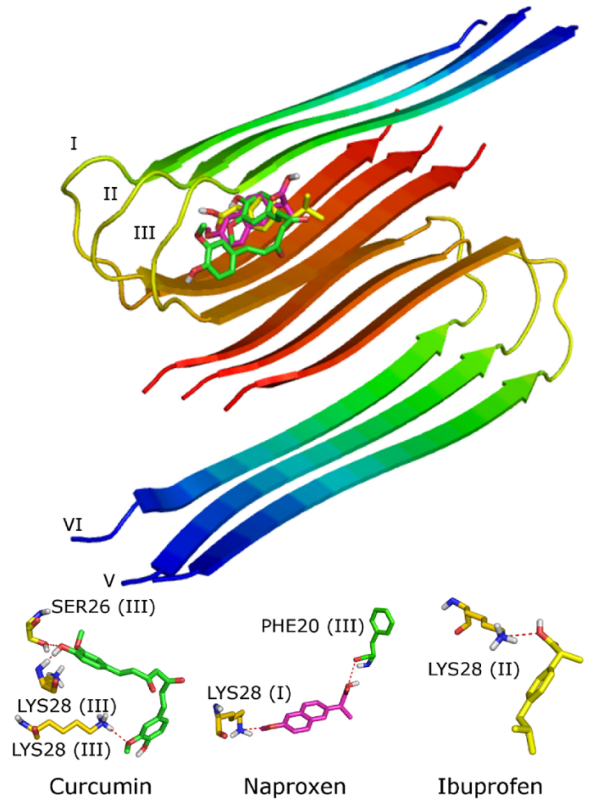

Figure 4.11 Binding sites of Curcumin (green), Naproxen (magenta) and Ibuprofen (orange) to 2-fold symmetric 6Aβ_{9-40} fibril. The results were obtained in the best mode of docking. The lower panel shows the HB networks for Curcumin, Naproxen and Ibuprofen.

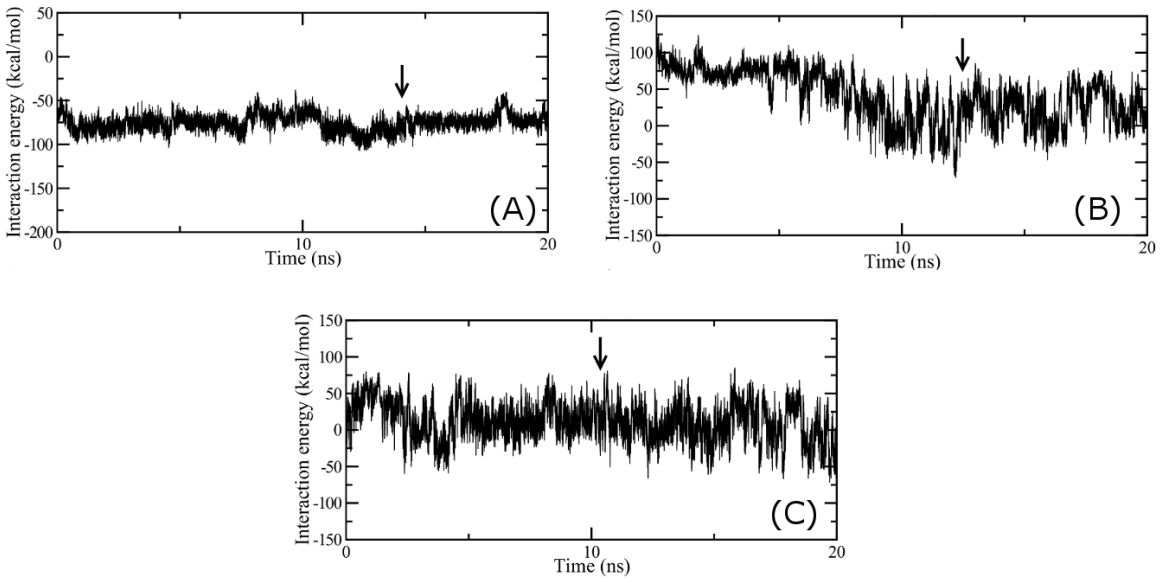

Figure 4.12 Time dependence of the interaction energy between 6Aβ_{9-40} and Curcumin (A), Naproxen (B) and Ibuprofen (C). Arrows refer to times when complexes reach equilibration.

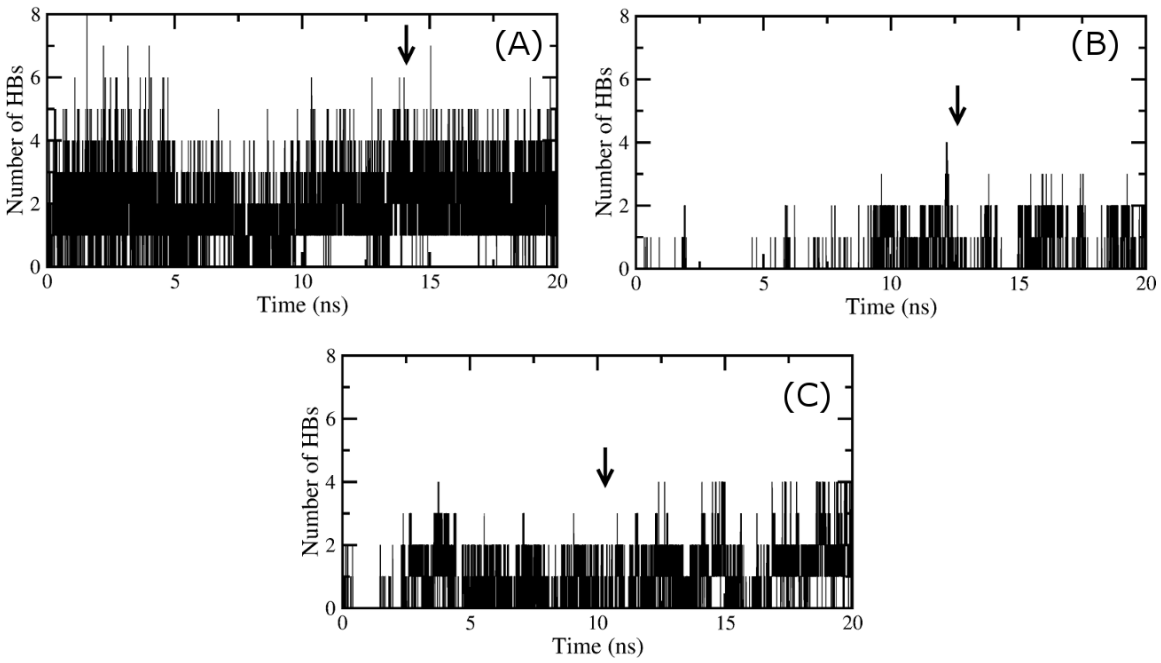

Figure 4.13 Time dependence of HBs between receptor 6Aβ_{9-40} and ligands Curcumin (A), Naproxen (B) and Ibuprofen (C). Arrows refer to times of reaching equilibrium (see Fig. 4.12). In equilibrium $\overline{HB(t)}$ =2.19, 0.56, and 1.21 for Curcumin, Naproxen, and Ibuprofen, respectively.

4.3.2.3 Nature of ligand binding to 6Aβ_{9-40}.

The time dependence of the number of HBs between ligand and receptor is shown in Fig. 4.13. Their time average value estimated in equilibrium $\overline{HB(t)}$ = 2.19, 0.56, and 1.21 for Curcumin, Naproxen and Ibuprofen, respectively. The strong HB interaction between Curcumin and 6Aβ_{9-40} causes its high binding affinity. However, this scenario is not valid if one compares Naproxen with Ibuprofen as the latter has more HBs but the binding is less tight. To shed more light on their binding nature we calculate SC contacts (Fig. 4.14). In equilibrium one has the average number of SC contacts $\overline{SC(t)}$ = 25.17, 18.16 and 17.06 for Curcumin, Naproxen and Ibuprofen, respectively. Therefore, the fact that the binding of Ibuprofen is weaker than Naproxen is caused by the smaller number of SC contacts or weaker SC interaction.

As in the monomer Aβ_{1-40} case, the electrostatic interaction between Curcumin and 6Aβ_{9-40} is attractive while it becomes repulsive for NSAIDs due to difference in charges of ligands (Table 4.2). The nonpolar solvation energy $\Delta G_{\rm sur}$ is smaller compared to the monomer case as the SASA is larger in the presence of more peptides. $\Delta G_{\rm sur}$ of Curcumin is lower because its size is bigger than others. For all of ligands the vdW interaction dominates over the combined contribution of electrostatic and polar terms playing the decisive role in binding affinity to 6Aβ_{9-40}.

Fig. 4.15 shows the contributions of ligand individual atoms to the the vdW interaction with receptor. The results have been obtained in equilibrium MD simulations. For Curcumin atoms 3, 4, 6, 9, 11, 13, 23, 24, 26, 28, 30 and 33 of aromatic rings and atoms 1, 2, 7, 31, 34 and 35 from other fragments are important for both monomer

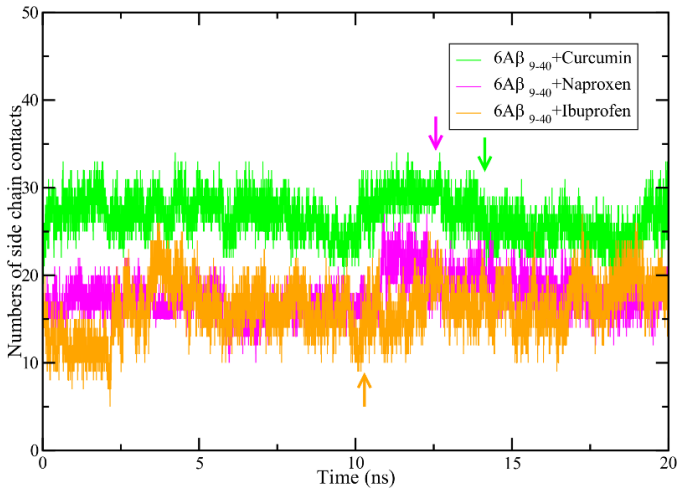

Figure 4.14 The same as in Fig. 4.9 but for receptor 6Aβ_{9-40}. In equilibrium we have the average value $\overline{SC(t)}$=25.17, 18.16, and 17.06 for Curcumin, Naproxen and Ibuprofen, respectively.

and fibril (compare Fig. 4.6 and Fig. 4.15). A difference is seen for carbon atom 20 which has slightly positive contribution in the fibril case. The role of individual atoms is also almost the same for monomer and fibril complexes with Naproxen and Ibuprofen (Fig. 4.6 and Fig. 4.15). However, atoms 1 and 3 of Ibuprofen have negative and positive contribution for monomer (Fig. 4.6) and fibril (Fig. 4.15), respectively.

Overall, as in the monomer Aβ_{1-40} case aromatic rings of Naproxen dominate over the remaining parts while for curcimin and Ibuprofen they have the same contribution to the vdW interaction energy as other fragments. One can show that the contribution from aromatic ring atoms is 52.7, 70.4 and 49.2% for Curcumin, Naproxen and Ibuprofen, respectively. These percentages are very close to those of the monomer case.

4.3.3 Binding to more complex Aβ fibril structures

The results, obtained for binding affinity of ligands to the fibril structure 6Aβ_{9-40} and monomer Aβ_{1-40}, unambiguously support domination of Curcumin over Naproxen and Ibuprofen in binding affinity, but it remains unclear if this does hold for more complex fibril structures. In this section we restrict ourselves to study of 2-fold symmetric 12Aβ_{9-40}, and 3-fold symmetric 9Aβ_{9-40}, and 18Aβ_{9-40} fibrils using AutodockTools 1.5.4[182].

4.3.3.1 Binding to 3-fold symmetric 9Aβ_{9-40}.

For docking we use the structure, resolved by Paravastu et al[81]. The lowest energy conformations of the receptor with three ligands are shown in Fig. 4.16. Similar to the 6Aβ_{9-40} case (Fig. 4.11) all of ligands bind to the same place inside the patch of three peptides. The binding energies ΔE_{bind} =-8.8, -7.9 and 7.5 kcal/mol

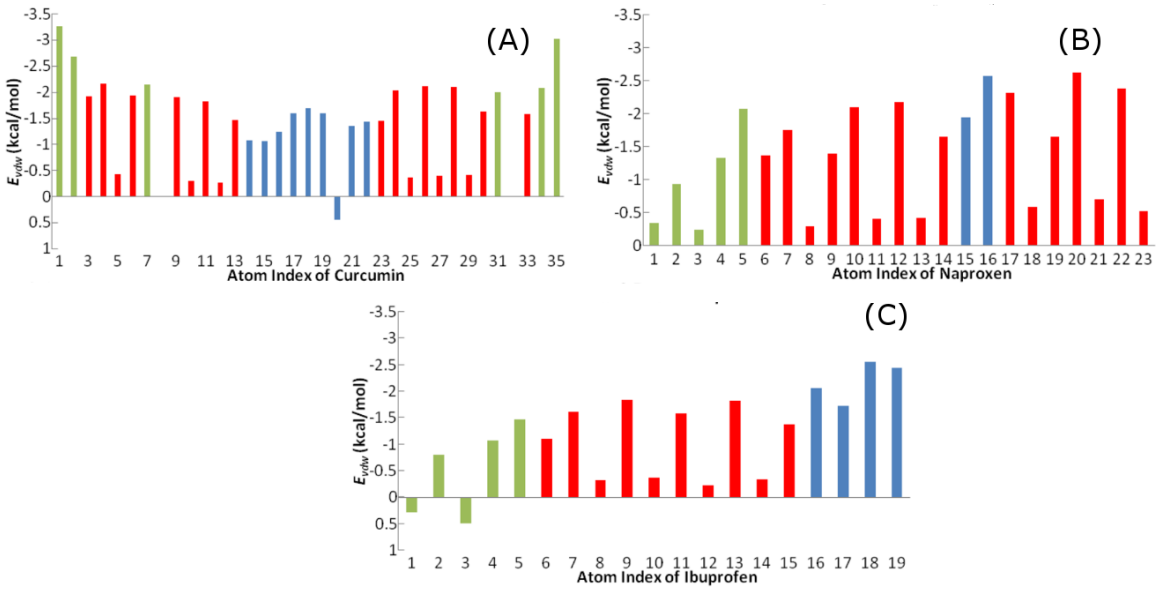

Figure 4.15 Contributions of individual atoms of three ligands to the vdW interaction energy. The results have been obtained in equilibrium for fibril 6Aβ_{9-40} Red color refers to atoms belonging to aromatic rings.

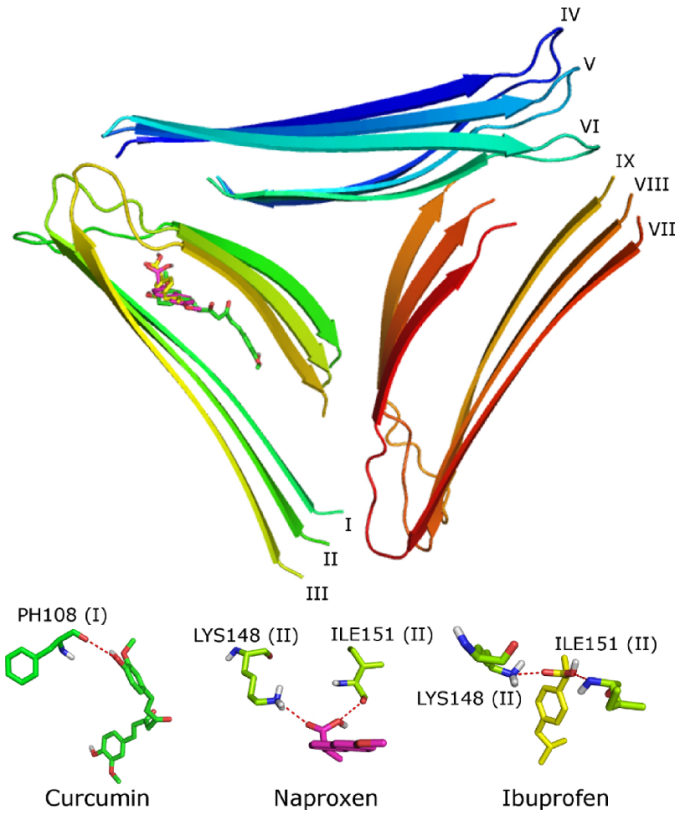

Figure 4.16 Binding sites of Curcumin (green), Naproxen (magenta) and Ibuprofen (orange) to 3-fold symmetric 9Aβ_{9-40}. The results have been obtained in the best docking mode. The lower panel shows HB networks for three ligands with the receptor. Curcumin has one HB while Naproxen and Ibuprofen have two HBs.

for Curcumin, Naproxen and Ibuprofen, respectively. Thus, as in the monomer and 6Aβ_{9-40} cases the binding affinity of Curcumin is the highest and one can expect that this ligand is the most efficient in degradation of 9Aβ_{1-40} aggregates.

Although Curcumin displays the highest propensity to binding, its HB network the weakest one. It has only one HB with PHE108 (I) of 9Aβ_{9-40}, while Naproxen forms two HBs with LYS148 (II) and ILE151 (II). Ibuprofen even has three HBs with LYS148 (II) and ILE151 (II) (Fig. 4.16). Therefore, HB network itself does not control binding affinity of these ligands. The high binding of Curcumin comes from the strong SC interaction having 21 SC contacts that are much more than 13 and 16 SC contacts of Naproxen and Ibuprofen. However the situation remains ambiguous for NSAIDs because the binding energy of Naproxen is lower than Ibuprofen despite Naproxen has less HB as well as SC contacts. The solution of this issue requires further investigation but one can believe that the binding ranking (Eq. 4.1) predicted by the docking method remains valid for three-fold symmetric 9Aβ_{9-40} fibril for the following reason. According to our recent study (MH Viet and MS Li, unpublished results), the higher is binding affinity to Aβ fibrils the larger is the total number of carbon atoms of ligand. Because Naproxen has more carbon atoms than Ibuprofen one can expect that the former has higher binding affinity.

4.3.3.2 Binding to 2-fold symmetric 12Aβ_{9-40} and 3-fold symmetric 18Aβ_{9-40}.

We now consider larger targets of 12 and 18 Aβ_{9-40} peptides. The binding energies obtained by the docking method are listed on Table 4.1. Clearly for both targets, in accord with the experiments [25], curcurin remains the best binder with the ranking given by Eq. 4.1. In the best binding mode Curcumin, Naproxen and Ibuprofen have 2, 3 and 0 HBs with receptor 12Aβ_{9-40}, respectively (Fig. 4.17 (D)). The strong binding of Curcumin with ΔE_{bind} =-8.6 kcal/mol comes from strong SC interaction having 24 SC contacts. NSAIDs have lower binding affinity (ΔE_{bind} =-7.7, and -6.9 kcal/mol for Naproxen and Ibuprofen) because they have less SC contacts (18 and 20 SC contacts for Naproxen and Ibuprofen). The lower binding of Ibuprofen compared to Naproxen is probably due to the weaker HB network and smaller number of carbon atoms.

For the three-fold symmetric 18Aβ_{9-40} (Fig. 4.17 (E)), we have the same binding ranking (Eq. 4.1) with ΔE_{bind} =-9.5, -9.1 and -8.3 kcal/mol for Curcumin, Naproxen and Ibuprofen. Curcumin has no HB contact with the receptor, whereas Naproxen and Ibuprofen have 2 and 3 HBs. Therefore, HB is not responsible for its strong binding affinity. One can show that SC interaction plays a decisive role because 18Aβ_{9-40} has 31 SC contacts with Curcumin. This number of contacts is markedly larger than 21 and 18 contacts for Naproxen and Ibuprofen. Thus, the binding nature is defined by the SC interaction.

It should be noted that, in agreement with the experiment [59], NSAIDs have the same binding site (Fig. 4.17 (D)) near the loop region inside the upper 6-peptide patch of 12Aβ_{9-40}. Curcumin also docks near the loop region but inside the lower patch. However, due to structure symmetry one may observe the same binding site for three ligands on experiments. For 18Aβ_{9-40} Curcumin and NSAIDs are located at the same position near loops (Fig. 4.17 (E)) where they can have more contacts with the receptor than other places.

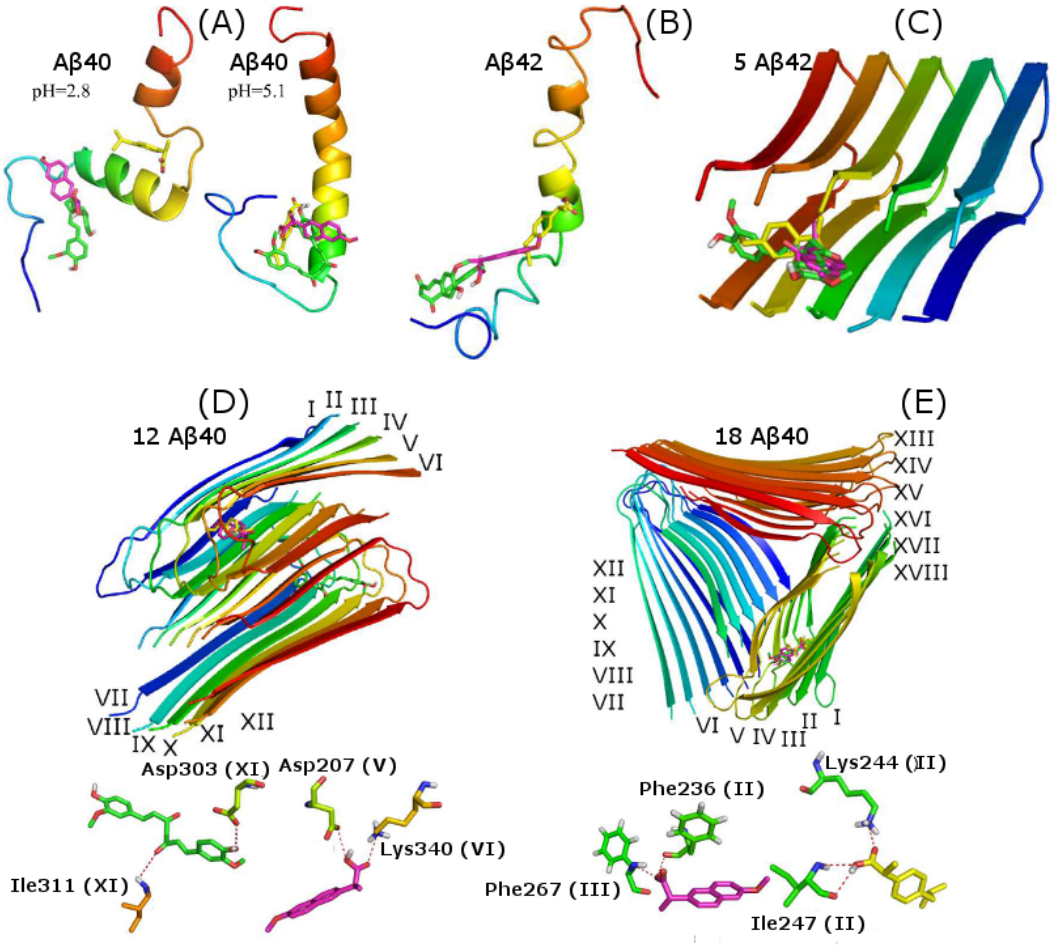

Figure 4.17 (A) Binding sites of three ligand to Aβ_{1-40} at pH=2.8 (left) and 5.1 (right). For pH=2.8 (5.1) one has ΔE_{bind} =-5.7 (-6.3), -5.4 (-5.7), and -5.1 (-5.1) kcal/mol for Curcumin, Naproxen and Ibuprofen, respectively. The values in parentheses are for pH=5.1. For docking we used the structures from PDB with ID 1AML [237] and 1BA4 [77] for pH=2.8 and 5.1, respectively. (B) Binding sites of three ligand to Aβ_{142} in water with hexafluoroisopropanol (HFIP). We have ΔE_{bind} =-5.8, -5.4, and -4.8 kcal/mol for Curcumin, Naproxen and Ibuprofen, respectively. For docking we used the structure from PDB with ID 1Z0Q [78]. (C) Binding sites, obtained in the best mode by the docking method, for Curcumin (green), Naproxen (magenta) and Ibuprofen (orange) to 5 Aβ_{17-42} fibril. The fibril structure has been taken from PDB (PDB ID: 2BEG [14]). One has ΔE_{bind} =-7.5 kcal/mol for Curcumin, while Naproxen and Ibuprofen has ΔE_{bind} = -6.8 kcal/mol. (D) Binding sites, obtained in the best mode by the docking method, for Curcumin (green), Naproxen (magenta) and Ibuprofen (orange) to 2-fold symmetry 12Aβ_{9-40} fibril. Both Curcumin and Naproxen have 2 HBs while Ibuprofen has no HB with the receptor (plot not shown). (E) Binding sites, obtained in the best mode by the docking method, for Curcumin (green), Naproxen (magenta) and Ibuprofen (orange) to three-fold symmetry 18β_{9-40} fibril. Curcumin has no HB with the receptor (plot not shown) but Naproxen and Ibuprofen have 2 and 3 HBs, respectively.

4.3.3.3 Binding to fibril 5Aβ_{17-42}

Using the docking method we have also calculated the binding energy of three ligands to fibril of five truncated peptides 5Aβ_{17-42} (PDB ID: 2BEG [14]). In the best mode the they have the same binding site inside the fibril (Fig. 4.17 (C)). The binding energy $\Delta E_{\rm bind}$ = -7.5, -6.8 and -6.8 kcal/mol for Curcumin, Naproxen and Ibuprofen, respectively, suggesting that Curcumin also binds to Aβ_{1-42} aggregates more tightly than NSAIDs.

4.3.4 Binding in low pH and hexafluoroisopropanol/water environment

At pH= 2.8 and 5.1 monomer Aβ_{1-40} adopts the helix-rich structure with PBD ID 1AML [237] and 1BA4 [77] (Fig. 4.17 (A)). In the best docking mode, for pH=2.8 (5.1) one has $\Delta E_{\rm bind}$ =-5.7 (-6.3), -5.4 (-5.7), and -5.1 (-5.1) kcal/mol for Curcumin, Naproxen and Ibuprofen, respectively. The values in parentheses are for pH=5.1. Therefore, NSAIDs also show the lower binding affinity than Curcumin at low pH.

Upon addition of a certain amount of hexafluoroisopropanol (HFIP) to water Aβ_{1-42} becomes structured and the corresponding structure has been solved by Tomaselli *et al* [78] (PDB ID: 1Z0Q). Using this structure and the docking method we obtain $\Delta E_{\rm bind}$ = -5.8, -5.4 and -4.8 kcal/mol for Curcumin, Naproxen and Ibuprofen (Fig. 4.17 (B)). This result implies that the ranking of binding affinity given by Eq. 4.1 remains valid for Aβ_{1-42} in the HFIP/water environment.

4.4 Conclusion

1. The effect of Naproxen and Ibuprofen on degradation of Aβ fibrils has been studied by Klimov *et al* [57, 58, 176, 235] but they have focused on the multi-ligand collective dynamics. In contrast, our study concerns pharmaceutical aspects of this problem calculating the binding free energies that can be directly compared with experimental results on inhibition constants. Our estimates of $\Delta G_{\rm bind}$ (Table 4.2) are in good agreement with experiments [50, 59] showing that Curcumin is the most potent ligand [25]. Our study also reveals that Curcumin and Naproxen may be used as a drug to interfere Aβ fibrillogenesis but not Ibuprofen. Thus, Naproxen is not only a NSAID but also as a good inhibitor for Aβ aggregation having IC50 in the range of 10 nM.

2. Consistent with experiments, our study disclosed that Ibuprofen and Naproxen bind to the same position in monomer Aβ_{1-40} which is not the same for Curcumin.

3. Based on the results obtained by the docking and MD simulations we predict that Curcumin has the same binding pocket as NSAIDs inside Aβ fibrils. It would be interesting to check validity of this prediction for other ligands.

4. The vdW interaction is found to dominate over the electrostatic interaction in binding affinity. The detailed analysis about contributions of individual

ligand atoms to the vdW interaction energy shows that aromatic rings of Curcumin and Ibuprofen have almost the same contribution as remaining parts, while they dominate in the case of Naproxen. This conclusion holds for both monomer and fibril cases.

5. It is well known that Curcumin strongly interferes with Aβ aggregation. On the other hand, as follows from our and experimental study it can tightly binds to fibrils. This suggests that inhibition of fibril formation is via the binding mechanism. Namely, Curcumin binds to Aβ fibrils modulating their propensity to aggregation. Such a mechanism has been observed for other systems [241, 248].

6. The fact that NSAIDs also show the lower binding affinity than Curcumin is presumably valid at low pH and HFIP/water environment. However this result has been obtained by the docking method its validity should be checked by more sophisticated methods.

5

Anti-arrhythmic medication Propafenone is potential drug for Alzheimer's disease by inhibiting aggregation of amyloid beta peptide: in silico and in vitro studies

5.1 Introduction

In this chapter we will search for potential AD inhibitors among all possible oral drugs available on market. Since Curcumin is prominent in blocking Aβ aggregation [23] we restricted our search to those oral drugs that are highly similar to Curcumin. By QikProp implemented in Schrodinger package [51] we have identified Propafenone, Eterilate, and Itopride that share more than 80% similarity with Curcumin (Fig. 5.1B). A QSAR (quantitative structure-activity relationship) study on capability of Propafenone in inhibiting Aβ aggregation [216], but the nature of its binding to Aβ has not been examined by all-atom MD simulation and experiment. Fluoropropyl-substituted Curcumin (FSC), synthesized by Yang *et al* [50], is a potent inhibitor of Aβ aggregation having very low inhibition constant $K_i = 0.07$ nM. However, the binding mechanism of FSC to Aβ peptide has not been studied at the atomic level.

Using the docking and FEP methods [217, 218, 220] we have found that Propafenone has the highest binding affinity to Aβ_{40} fibrils. This compound was further studied in our *in vitro* experiment and was compared with activity of Curcumin. The number of the death cells under treatment by Curcumin is slightly larger than Propafenone. Through aggregation assay test it was found that the anti-amyloid activity of Propafenone is better than that of Curcumin. This result is in accord

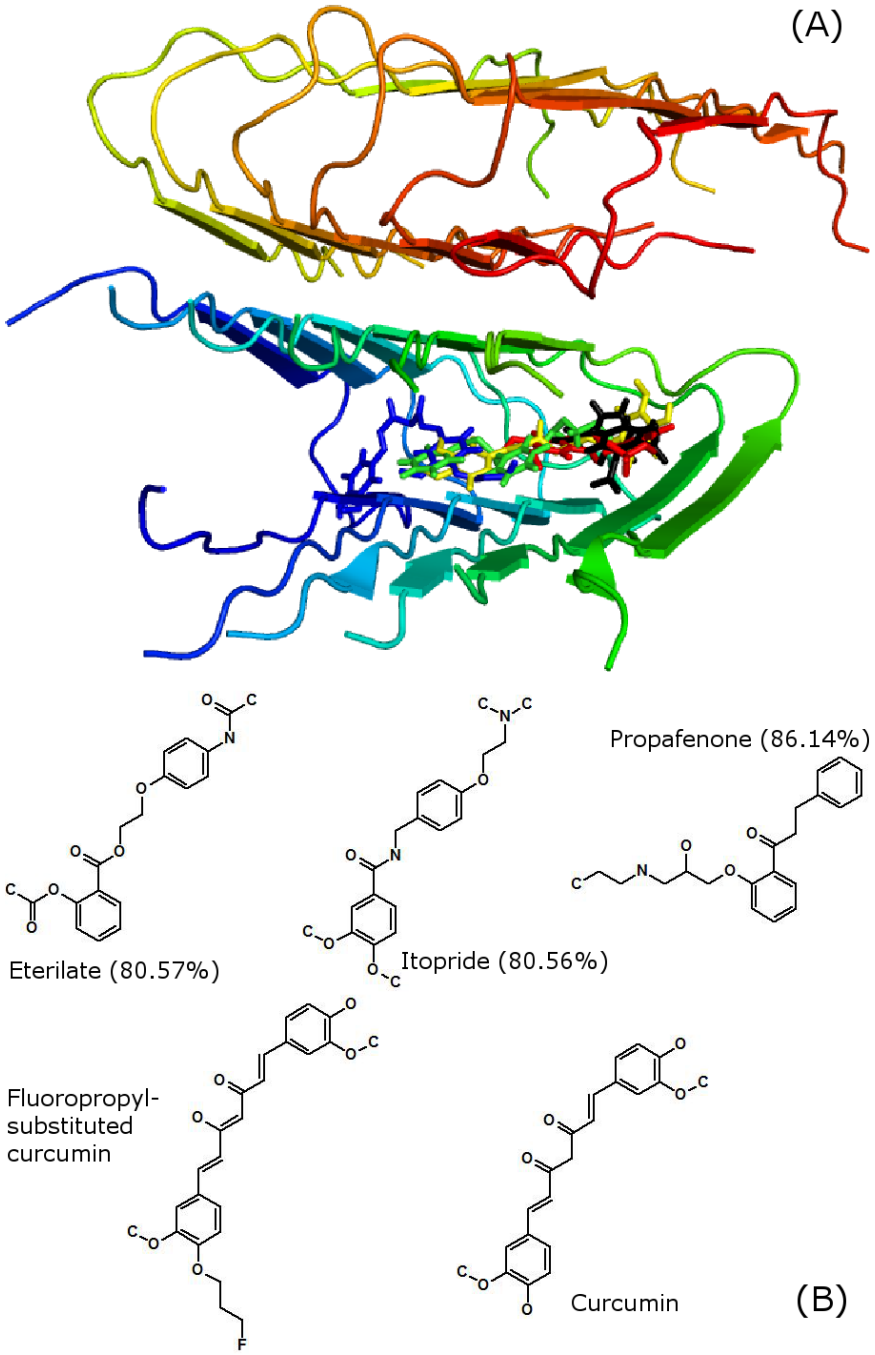

Figure 5.1 Structures and binding poses of five ligands to two-fold 12 Aβ_{40} peptide. The conformations of complexes were obtained in the best docking mode with the lowest binding energy. These conformations were used as starting conformations for MD simulation (A). Chemical structure of five ligands (B). Similarities with Curcumin are 80.57, 80.56, and 86.14 % for Eterilate, Itopride, and Propafenone, respectively.

with TEM morphology of Aβ in the appearance and non-appearance of trial inhibitors. The DCF fluorescence intensity was also measured. The results provided by free radical assays also indicate that the reduction of Aβ toxicity may cause by reduction of Aβ aggregation and subsequent induced free radical damage. The concentrations of both Curcumin and Propafenone should be higher than 10 μM to inhibiting Aβ aggregation. Thus, both theoretical and experimental results indicated that anti-arrhythmic Propafenone is a potential inhibitor for preventing Aβ deposits.

5.2 Methods & Materials

5.2.1 Screening top-hits by chemical and structural similarity with Curcumin

Chemical and structural similarity of two compounds A and B were described in Chapter 3. To screen out potential candidates for AD we used QikProp implemented in Schroedinger package [51]. Compounds that share $\geq 80\%$ similarity with Curcumin have been selected.

5.2.2 Crystal structure of fibril and ligands used in computational experiments.

Chemical structures of Eterilate ($C_{19}H_{19}NO_6$), Itopride ($C_{20}H_{26}N_2O_4$), Propafenone ($C_{21}H_{27}NO_3$), FSC ($C_{24}H_{25}FO_6$), and Curcumin ($C_{21}H_{20}O_6$) are downloaded from Pubchem database [249] with ID 44258, 3792, 4932, 16087306, and 969516 (Fig. 5.1B). For simulation we used the atomic structure of fibril 12Aβ_{9-40} retrieved from PDB with ID 2LMN [80]. This model consists of 12 truncated peptides.

5.2.3 Computational methods and measures used in structure analysis

Docking method.

Details of the docking method were described in Chapter 3. Here, the center of grids was placed at the center of receptor and grid dimensions were chosen large enough (80x60x40 $\AA^3$) to cover the whole 12Aβ_{9-40} .

Molecular dynamics simulation

GROMACS is employed to perform MD simulations. Details of MD simulations were mentioned in Chapter 3.

Free energy perturbation method.

The binding free energy of ligands to Aβ fibril was calculated using FEP method (Chapter 3).

The criteria for HB formation are shown in Chaper 3 and secondary structures were analyzed using DSSP tool [229, 230].

5.2.4 Synthesis and purification of Aβ_{40}

The synthesis of Aβ_{40} peptides was performed in a solid-phase peptide synthesizer (PS3, Protein Technologies, Inc., AZ) using standard FMOC protocols with HMP resin. After cleavage from the resin by stirring with a mixture of trifluoroacetic acid/H2O/ethanedithiol thiol anisole/phenol for 3 hr, the peptides were then extracted using ether: H2O (1:1/ v:v) containing 0.1% 2-mercaptothanol. The synthesized Aβ_{40} peptides were purified using a C18 reverse-phase column with a linear gradient from 0% to 80% acetonitrile. Peptide purity was over 95% as identified by mass spectroscopy. One milligram of Aβ_{40} peptide was dissolved in 1 mL trifluoroethanol and then centrifuged (20,000Œg) to precipitate the insoluble particles. This Aβ_{40} solution was then dried using freeze dryer (FDU-1200, EYELA) and stored at -80 ^{O}C until used.

5.2.5 Cell cultures

Human blastoma SH-SY5Y cellswere cultured in minimum essential medium supplemented with 50% (v/v) F-12 nutrient mixture, 10% (v/v) heat-inactivated fetal bovine serum, and 1% (v/v) antibiotics comprised of penicillin and streptomycin. Cells were kept at 37 ^{O}C in a humidified atmosphere of 5% CO2. SH-SY5Y cells were plated at a density of 5Œ104 viable cells per well in 96-well plates for further analysis.

5.2.6 Cell viability assay

The cell viability was measured using the MTT assay. One mg of Aβ_{40} was dissolved in 1000 μL trifluoroethanol, dried under N2 gas, redissolved in dimethyl sulfoxide, and incubated at 4^{O}C for 12 h to make a 500 μM of peptide stock solution. For the viability assay, 5Œ104 cells were incubated in a 96-well microtiter plate containing either 10 μM incubated Aβ peptides only, diluted from the incubated peptide stock solution, or 10 μM incubated Aβ peptides, in the presence of Curcumin or Propafenone, with concentrations ranging from 0.001 to 50 μM. The reaction was carried out for 48 h at 37^{O}C in a humidified atmosphere containing 5% CO2 before cell viability was assayed. MTT solution (10 μL) was added to each well, and the wells were incubated for another 8 h at room temperature. The optical density was determined at 450 nm, using a microplate reader (FlexStation 3, MD).

5.2.7 Aggregation assay

Thioflavin-T (ThT) was used to monitor the aggregation state of Aβ_{40}. Ten μM of Aβ_{40} was freshly diluted from peptide stock solution (500 μM in DMSO) in phosphate buffer, pH 7.4, for peptide aggregation assay. All samples containing a peptide concentration of10 μM in the absence and presence of various concentrations of Curcumin or Propafenone and 3 μM ThT were incubated at 37^{O}C. Samples containing either Aβ peptide only (as a control) or Aβ with Curcumin or Propafenone, taken daily from 0 to 72 h, were used to measure the ThT intensity. The Th-T fluorescence

intensity was measured using a microplate reader (FlexStation 3, MD) at 37^{O}C with the excitation and emission wavelengths of 440 nm and 485 nm, respectively.

5.2.8 Transmission Electron Microscope (TEM) Analysis

Five microliters of the Aβ peptide samples without or with treatment of 10 μM Curcumin or Propafenone used for the aggregation assay at day1, day3 and day5 was placed onto a carbon-coated 200 mesh copper grid (Pelco, Ca, USA). The grid containing sample was allowed to air dry. Then the TEM sample was stained with 1 ml of 2% uranyl acetate for 30 seconds. The grid was firstly wicked dry with tissue paper to remove the excess solution and then allowed to air dry before TEM analysis. A TEM (JEM-2000 EXII, JEOL, Japan) with an accelerating voltage of 100 KeV was used to analyze the morphology of Aβ peptides.

5.2.9 Free radical assay

The level of hydroxyl radicals induced by Aβ_{40} in cell free conditions was analyzed using the dichlorofluorescein diacetate (DCFH-DA) as proposed by Bush *et al* [250]. In principle, Dichlorofluorescein (DCF) diacetate was firstly deacetylated with 50% (v/v) 0.05 M NaOH for 30 min and then neutralized to pH 7.5. A final concentration of 200 μM deacetylated DCF was prepared as a stock solution and kept on ice in the dark until further use. The reactions were carried out in a 96-well plate (200 μl/well) containing 10 μM of Aβ_{40} peptides, 5 μM horseradish peroxidase and 15 μM deacetylated DCF, in Dulbecco's phosphate-buffered saline, pH 7.5 (Sigma, USA). To determine the inhibitory effects of Curcumin and Propafenone on inhibition of free radical formation, either Curcumin or Propafenone with concentrations of 0.001-50 μM were added and incubated at 37^{O}C. Fluorescence readings were recorded on a microplate reader (FlexStation 3, MD) with the excitation wavelength of 485 nm and the emission wavelength of 530 nm. The fluorescence intensity of DCF (H2O2 level) was measured every 12 h and from 0 to 48 h.

5.3 Results and Discussion

5.3.1 Selection of top-hits from orally available drugs

A Schroedinger package Qikprop [51] involving the chemical similarity searching functions [251], was used to search orally available drugs which have more than 80% of chemical and structural similarity with Curcumin. Four drugs Eterilate, Itopride, Propafenone, and Nilvadipine has been found. Because Nilvadipine is currently under phase 3 of clinical trial for AD [47], we have studied only Eterilate, Itopride, and Propafenone (Fig. 5.1B) as potential blockers of Aβ aggregation using both theoretical and experimental tools. Similar to Curcumin all of them have two aromatic rings. For comparison compound FSC has been also studied.

	ΔE_{bind}	$\Delta G_{\text{FEP}}^{\text{vdW}}$	$\Delta G_{\text{FEP}}^{\text{elec}}$	ΔG_{FEP}	ΔG_{exp}
Eterilate	-7.9	-19.47	4.34	-15.13 ± 2.22	
Itopride	-7.8	-21.72	-3.62	-25.33 ± 2.58	
Propafenone	-8.2	-23.15	-10.66	-33.81 ± 2.64	
FSC	-8.6	-31.05	6.76	-24.29 ± 3.31	-13.95
Curcumin	-8.8	-21.90	3.62	-18.28 ± 3.94	-13.33

Table 5.1 The binding energy is estimated using the docking (ΔE_{bind}) and FEP (ΔG_{FEP}) methods. The experimental binding free energy was calculated from formula $\Delta G_{\text{exp}} = RT \ln K_i$, where gas constant $R = 1.987 * 10^{-3}$ kcal K^{-1} mol^{-1}, $T = 300\ K$, and inhibition constant K_i is measured in mol. Energy is measured in kcal/mol. The results obtained for ΔG_{FEP} were averaged over 8 independent MD trajectories.

5.3.2 Binding of ligands to 12Aβ_{9-40}

Sharing more than 80% of chemical and structural similarities with Curcumin (Fig. 5.1B), the binding properties of candidates to Aβ fibrils are expected to be similar to each other. This might be the reason for their close binding positions to Curcumin, except a small deviation observed for FSC (Fig. 5.1A). The docking binding energy ΔE_{dock} varies little from ligand to ligand (in Table 5.1). It seems that Curcumin is the best one but this is not certain as the docking energies usually have low correlation with experiments [23, 217]. However, binding positions found in the best docking mode are good enough to be used as initial conformations for MD simulations [22, 23, 217].

5.3.3 Molecular dynamics simulation

For each solvated complex, we performed 8 independent trajectories of MD simulations with same starting structure but different randomly initial velocity momentum. After three step of energy minimizations and 100 ps of NVT simulation, 5 ns NPT simulation has been performed to search equilibrium structures of solvated receptor-ligand complexes. As follows from the time dependence of the root mean square displacement (RMSD), all solvated systems reached equilibrium approximately after 3 ns when RMSD got saturation (Fig. 5.2). Conformations, in which a ligand changes its binding position, has not been found. The last snapshot from 5 ns of NPT simulations were used to start new 1 ns MD runs for estimation of ΔG_{bind} using the FEP method. To compute the desolvation free energy of ligands in solvent, we have also followed the same protocol as for the solvated complex. After energy minimizations of solvated ligands, 100 ps NVT MD runs were carried out and then 2 ns NPT simulations were followed. The ligand in solvation stays very stable during NPT runs.

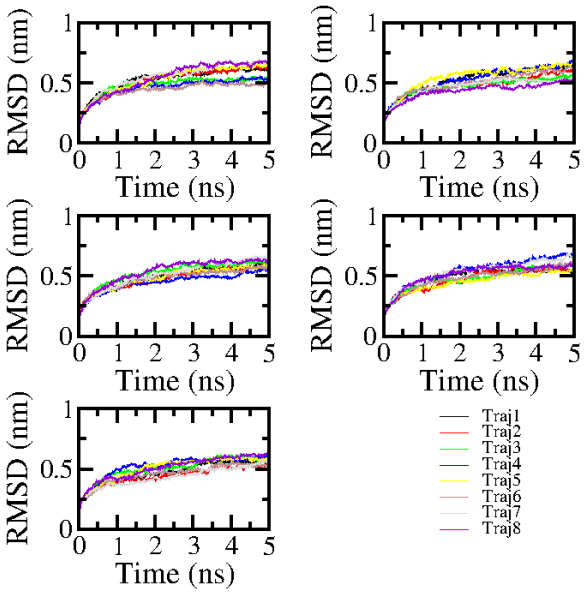

Figure 5.2 Time dependence of RMSD during 8 NPT MD trajectories of 5 solvated complexes. All systems reached equilibrium after about 3 ns. The last snapshots of these runs were used as initial conformations for subsequent 1ns MD simulations for free energy calculation by the FEP method.

5.3.4 Hydrogen bonds between ligands and 12Aβ_{9-40}

Fig. 5.3 shows the number of HBs (NHB) between five ligands and fibril as a function of time during 5 ns NPT MD runs. Initially, one has NHB =1.13, 1.25, 2, 0.5, and 2.75 for Eterilate, Itopride, Propafenone, FSC, and Curcumin in respectively. Non-interger value of NHB comes from averaging over 8 snapshots. After 2.5 ns, the number of HBs in all systems fluctuates around its equilibrium value. Averaging over snapshots collected in equilibrium of 8 MD trajectories we obtained NHB $\simeq$ 1.46, 1.60, 0.81, 0.57, and 1.99 for Eterilate, Itopride, Propafenone, FSC, and Curcumin, respectively. One can show that NHB does not correlate with the binding free energies (Table 5.1) suggesting that the hydrogen bonding is not a key factor to control ligand binding to Aβ fibril.

5.3.5 The absolute binding free energy

As mentioned in the Materials and Methods section, the 33 independent 1 ns MD simulations have been carried for the solvated complexes and ligands with different coupling parameter λ. The free energy was computed every 50 ps. It converged after 200 ps for solvated fibril complexed with Eterilate, Itopride, and Curcumin, while 300 ps is needed for Propafenone and FSC (Fig. 5.4). The annihilation free energy of ligands from both solvated complex and solvated ligand systems fluctuate a little bit because coupling parameter λ has changed from 1 to 33 different values. The difference between the annihilation free energies of ligand from solvated ligand and from solvated complex is the absolute binding free energies [252]. Skipping the

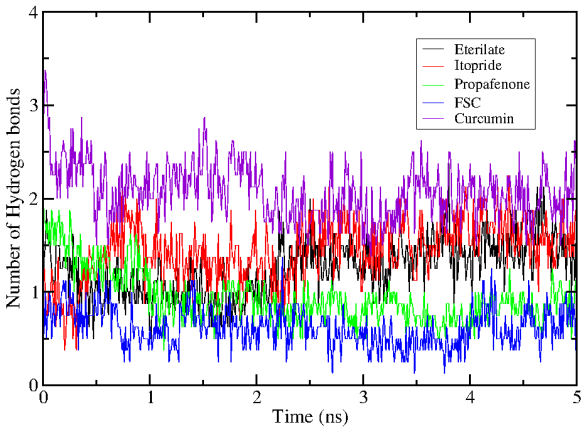

Figure 5.3 Time evolution of number of HBs between five ligands and 12Aβ_{9-40} peptides in time evolution. The results are average of 8 independent MD trajectories.

first 300 ps and averaging over 8 independence trajectories, we obtained the absolute binding free energy of ligands to 12Aβ_{9-40} (Table 5.1). Because the FEP method is one of the most accurate methods, the calculated binding free energies can be used to predict inhibitory activity of candidate compounds. From the top-hits only Eterilate has weaker binding affinity in comparison with Curcumin. Thus, Itopride, FSC, and Propafenone are presumably prominent inhibitors for Aβ aggregation. Having the lowest ΔG_{bind} = -33.81 $\pm$ 2.64 kcal/mol Propafenone is a champion and we will further test its activity in in vitro experiment.

5.3.6 vdW interaction plays the important role but electrostatics interaction also has large impact on Propafenone binding to Aβ fibril

The contribution of vdW and electrostatics interactions to ΔG_{bind} are shown in Table 5.1. In all cases, in agreement with previous study [23], the vdW interaction is a main contributor. The vdW term of Propafenone is almost equal to Itopride and Curcumin, but the electrostatics interaction of Propafenone with receptor, which contributes $\simeq$ 31.5 % of total ΔG_{bind} is larger than Itopride and Curcumin. This rationales the domination of Propafenone over other compounds in binding affinity to 12Aβ_{9-40}. Propafenone also has an advantage that together with the vdW part its electrostatics interaction with receptor is also strong.

5.3.7 Ligand-induced β-content change

Prior works [23, 131] have provided evidences that the higher binding affinity is the stronger is Aβ aggregation inhibition. Using snapshots collected in equilibrium for solvated complexes, the β-content of 12Aβ_{9-40} fibril has been analyzed using DSSP tool [229, 230] (Fig. 5.5). In the presence of Propafenone the β-content decreased to the largest extent. This result is in the line with the hypothesis that the tight ligand

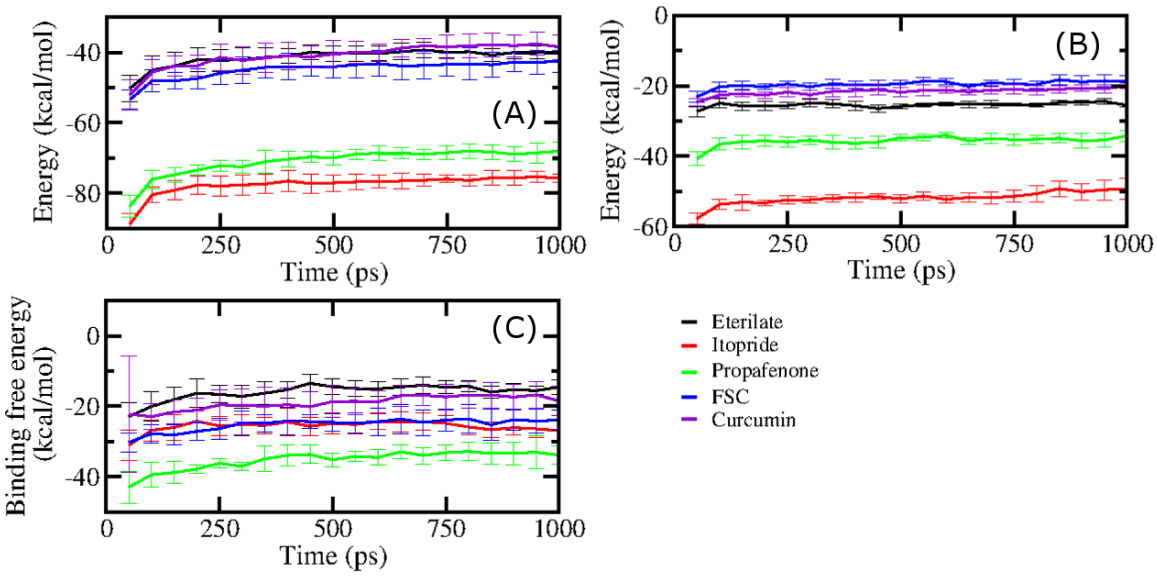

Figure 5.4 Time dependence of binding free energy of five complexes (C). It is defined as a difference between the desolvation free energy of ligand from solvated complexes (A) and desolvation free energy of ligand from solvated ligand (B). The free energy was calculated every 50 ps.

binding would strongly degrade fibers. In equilibrium the fibril with Curcumin has β-content of 58 % which is higher than 54.6% of the Propafenone complex. Thus, Propafenone is slightly better than Curcumin in destroying Aβ aggregates. This observation will be further supported by our in vitro experiment.

5.3.8 Cell viability in the presence and absence of Curcumin or Propafenone

The main cause of AD pathogenesis is the formation of toxic Aβ_{40} aggregates in the brain of AD patients [148, 149]. Therefore, preventing or reducing the toxicity induced by Aβ has been the primary goal of a number of therapeutic strategies under development or in clinical trials [253, 254, 255]. In the present study, we firstly examined the protective effects of Curcumin and Propafenone on the Aβ induced toxicity using MTT cell viability assay. Fig. 5.6 shows the related cell viability with the treatment of different concentrations of Curcumin and Propafenone incubated for 48 hrs. The cell survival rate showed a dose-dependent mode for both Curcumin and Propafenone. When the concentration above 1 μM, both Curcumin and Propafenone showed a significant effect to protect SH-SY5Y cells against Aβ toxicity. Cell survival rate was increased from 60%, without any treatment of Curcumin or Propafenone but 10 μM Aβ only, to more than 90%, with the treatment of 50 μM Curcumin or Propafenone. However, the cell survival rate shows no significant difference with the treatment of Curcumin and Propafenone when the concentration is $\geq$ 10 μM or $\leq$ 0.01 μM. At the concentration between 0.1 and 1 μM, the cell survival rate with the treatment of Propafenone is slightly better than that with the treatment of Curcumin.

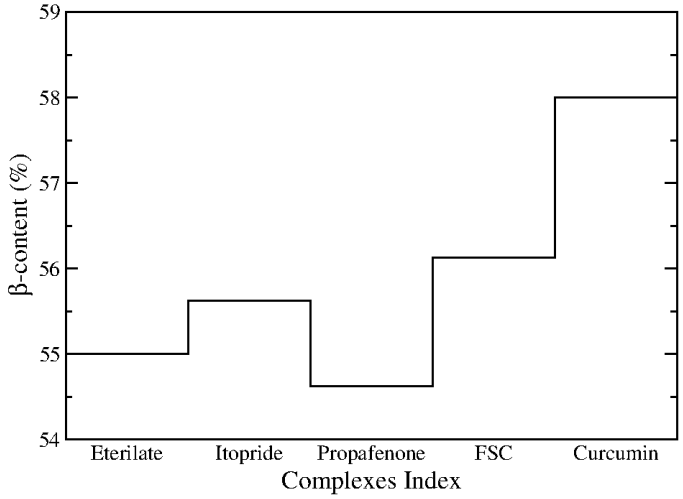

Figure 5.5 The β-content of two-fold Aβ_{40} peptides in complex with five ligands. The secondary structure of Aβ peptide were estimated using DSSP tool. These results were averaged all equilibrium snapshots.

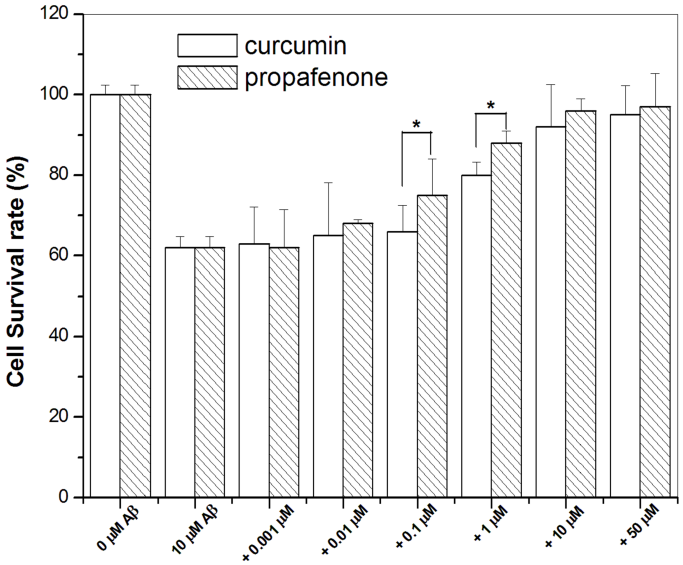

Figure 5.6 Cell viability with or without treatment of Curcumin or Propafenone determined by the MTT assay. Survival percentages of SH-SY5Y cells incubated with 10 μM Aβ_{40} for 48 h. Wells containing SH-SY5Y cells without Aβ peptides were used as a control group. The difference of cell survival rate between the treatment of Curcumin and Propafenone at concentration of 0.1 and 1 μM was significant. *p $\leq$ 0.05 versus control was considered statistically significant.

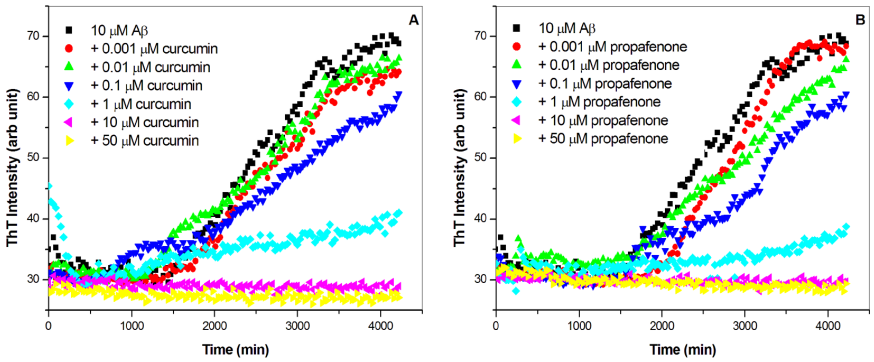

Figure 5.7 Kinetics of the aggregation process of Aβ_{40} with or without treatment of Curcumin or Propafenone. (A) The aggregation process of Aβ_{40} with the treatment of various concentration of Curcumin. (B) The aggregation process of Aβ_{40} with the treatment of various concentrations of Propafenone. The aggregation assay was performed with 10 μM Aβ peptides

5.3.9 Aggregation assay of the Aβ peptide in the presence and absence of Curcumin or Propafenone

The cytotoxicity induced by Aβ is raised from the property of Aβ self-aggregation. As shown in the previous result, both Curcumin and Propafenone could protect the cell against Aβ induced toxicity on a dose-dependent manner. Therefore, we then investigated the inhibitory ability of Curcumin and propfenone on the aggregation kinetics for Aβ_{40}.

Fig. 5.7 (A) and (B) show the aggregation process for Aβ_{40} in the presence of Curcumin and Propafenone using the Th-T binding assay, respectively. It can be seen that the inhibition of Aβ aggregation by Curcumin and Propafenone was also concentration-dependent. In consistent with the result of cell viability assay, both Curcumin and Propafenone showed to significantly inhibit Aβ aggregation at concentration $\geq$ 10 μM. At concentration $\leq$ 0.1 μM, both Curcumin and Propafenone could not inhibit the aggregation of Aβ_{40} peptides. At concentration between 10 and 0.1 μM, the anti-aggregation of Propafenone is slightly better than that of Curcumin.

IC_{50} values for Curcumin and Propafenone were estimated from the plot of Th-T intensity vs. concentration of Curcumin and Propafenone as shown in Fig 7 and (D), respectively. The estimated IC_{50} values are 3.0 and .5 μM for Curcumin and Propafenone, respectively. Our obtained IC_{50} is very close the reported values which IC_{50} values for Curcumin reported in literature were ranged 0.8-10 μM [25, 256]. Obviously, Propafenone has lower IC_{50} value than Curcumin. Taken together, the inhibitory ability of Propafenone basically is better than that of Curcumin.

5.3.10 TEM morphology of Aβ Fibrils

As demonstrated in the aggregation assay, both Curcumin and Propafenone can significantly inhibit the aggregation of Aβ_{40} at the concentration higher than 10

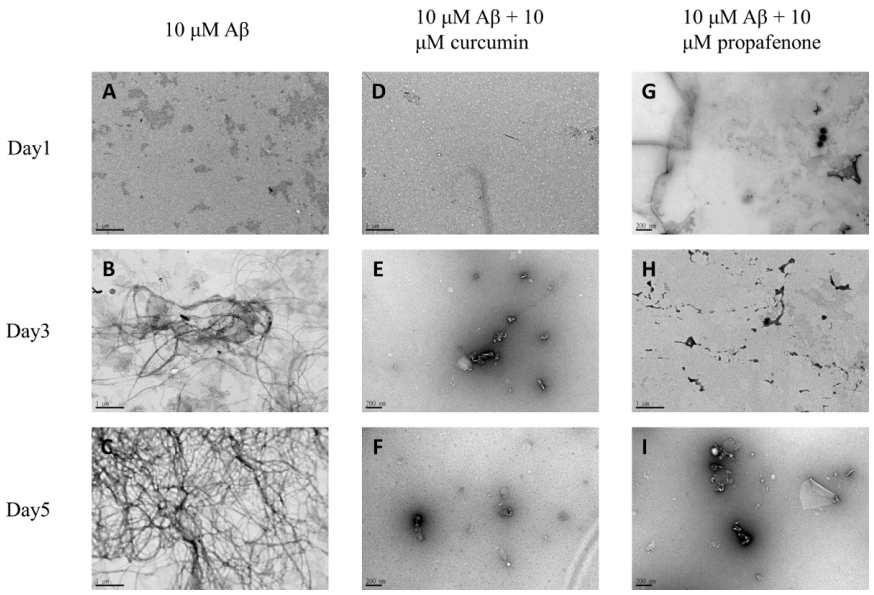

Figure 5.8 TEM images of Aβ_{40} morphologies with or without treatment of Curcumin or Propafenone. Fibrils formed from 10 μM Aβ peptides without or with treatment of Curcumin or Propafenone in phosphate buffer, pH 7.0, 37řC at day1, day3 and day5, (A-C) with 10 μM Aβ_{40} only, (D-F) with treatment of 10 μM Curcumin and (G-I) with treatment of 10 μM Propafenone. All TEM images are 200,000 x magnification. The scale bar indicates 200 nm.

μM. Therefore, we applied TEM to observe the morphology of Aβ in the absence and presence of Curcumin and Propafenone. The TEM morphologies of Aβ_{40} at various days are shown in Fig. 5.8 (A)(I). As shown in Fig. 5.8 (A), (B), and (C), in the absence of Curcumin (1 μM) and Propafenone (1 μM), the morphology of Aβ_{40} gradually aggregated into a fibril at day3 and day5, while as shown in Fig. 5.8 (D-F) and (G I) for the existence of 10μM Curcumin and Propafenone respectively, no fibrillary morphologies could be observed through the whole process incubation at 37^{O}C, further showing that the aggregation of Aβ_{40} was effectively inhibited by both Curcumin and Propafenone.

5.3.11 Free radical assay with or without the treatment of Curcumin or Propafenone

The production of ROS by Aβ peptide has been proposed as one of the possible mechanisms causing cell death [148, 149, 257]. Therefore, we examined the role of Curcumin and Propafenone on free radical generation induced by Aβ_{40} using the DCF assay. Fig. 5.9 (A) and (B) show the DCF fluorescence intensity of Aβ_{40} alone and in the presence of various concentration Curcumin and Propafenone incubated for 0, 12, 24, 36 and 48 h, respectively. In both Fig. 5.9 (A) and (B), the DCF fluorescence intensity of Aβ_{40} in the absence of Curcumin or Propafenone was generally increased with an increase of incubation time and reached peak at 36h. For the concentration lower than 1 μM, the inhibition of free radical production was not

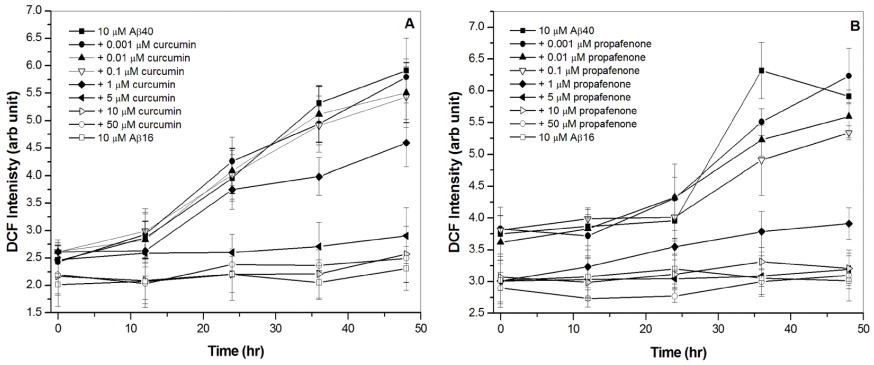

Figure 5.9 DCF free radical assay in the presence and absence of Curcumin or Propafenone. (A) the free radical generation for either 10 μM of Aβ_{40} alone or 10 μM of Aβ_{40} in the presence of 0.001, 0.01, 0.1, 1, 5, 10 and 50 μM Curcumin at 0, 12, 24, 36 and 48 h. (B) the free radical generation for either 10 μM of Aβ_{40} alone or 10 μM of Aβ_{40} in the presence of 0.001, 0.01, 0.1, 1, 5, 10 and 50 μM Propafenone at 0, 12, 24, 36 and 48 h

significant for both Curcumin and Propafenone, whereas the production of free radical was significantly inhibited when the concentration $\geq$ 10 μM for both Curcumin and Propafenone. At the concentration $\geq$ 10 μM, the inhibitory effect shows no obvious difference between Curcumin and Propafenone.

At the concentration between 0.1 μM and 10 μM, Propafenone showed a better inhibitory ability than Curcumin. In comparison with the DCF intensity of Aβ_{40} alone, the DCF fluorescence intensity was decreased by 25% and 45% in the presence of 1 μM Curcumin and Propafenone, respectively, when incubated for 36 h. The DCF fluorescence intensity was decreased by 40% and 55% in the presence of 5 μM Curcumin and Propafenone, at 36 h, respectively. Taken together, the results obtained from free radical assays for Curcumin and Propafenone are in agreement with the cell viability and aggregation assays which Propafenone is better than Curcumin on anti-amyloid activity, reduction of free radical production and cytotoxicity induced by Aβ. Furthermore, our results also suggest that the protection of SH-SY5Y cells against Aβ toxicity may be through the reduction of Aβ aggregation and subsequent induced free radical damage for both Propafenone and Curcumin.

5.4 Conclusions

Both theoretical and experimental studies indicated that similar to Curcumin, Propafenone could effectively protect cell against Aβ induced cytotoxicity through the inhibition of Aβ aggregation and reduction of the free radical caused damage. Furthermore, compared to the protective efficacy of Curcumin, Propafenone shows more effective on the prevention of Aβ induced aggregation, free radical production and cytotoxicity. Further new design of anti-amyloid compounds based on the Propafenone will be promising for the future development of effective drugs used on the treatment of AD.

6

Top-Leads from Natural Products for Treatment of Alzheimer's Disease: Docking and Molecular Dynamics Study

6.1 Introduction

In this chapter we have collected 342 compounds derived from Vietnamese plants and studied their binding affinity to full-length Aβ_{1-40} and Aβ_{1-42} peptides and their mature fibrils using Autodock Vina version 1.1 [181] and the MD simulations. For mature fibrils we have considered two-fold symmetry structures derived by Tycko group for hexamer of truncated peptides Aβ_{9-40} (6Aβ_{9-40}) [13, 80] and pentamer of Aβ_{17-42} fragment (5Aβ_{17-42}) by Luhrs group [14]. Top-leads found by the docking technique are further refined by the more accurate MM-PBSA method.

It has been shown that four sets of binding energies to four targets β_{1-40}, Aβ_{1-42}, 6Aβ_{9-40} and 5Aβ_{17-42} are highly correlated with each other. The detailed analysis of nature of ligand binding reveals that together with HB, the electrostatic and vdW interactions also play the important role. Based on the results, obtained by the docking and MM-PBSA methods, we predict that five ligands Dracorubin, Taraxerol, Taraxasterol, Hinokiflavone, and Diosgenin are good candidates for treating AD.

For designing oral drugs for AD it is important to know if they can pass the BBB and be absorbed by human body. We have computed log(BB) and the human intestinal absorption (HIA) [225] using the PreADME software [258]. It was shown that five top-leads fulfill these requirements for AD drugs having high values of log(BB) and HIA. Their toxicity and metabolism are also analyzed.

6.2 Materials and Methods

6.2.1 Set of receptor-ligand complexes

.

We consider four receptors including monomers Aβ_{1-40} and Aβ_{1-42} and protofibrils of their fragments 6Aβ_{9-40} and 5Aβ_{17-42} (first 8 and 16 unstructured amino acids were excluded from mature fibrils). The NMR structures of Aβ_{1-40} (PDB ID: 1BA4 [77]) and Aβ_{1-42} (PDB ID: 1Z0Q [78]) peptides were taken from the PDB. Coordinates of two-fold symmetry 6Aβ_{9-40} were provided by Prof. R. Tycko [80], while the crystal structure of 5Aβ_{17-42} was taken from the PDB (PDB ID: 2BEG [14]). 1BA4 and 2BEG have 10 models while 1Z0Q has 30 models. For docking simulation we have chosen their first model.

The ligands set contains 342 compounds derived from Vietnamese herbs [48] but their chemical structures are known from the Pubchem and Chemspider database (see http://pubchem.ncbi.nlm.nih.gov and http:// http://www.chemspider.com/). The general AMBER force field [195] has been used to generate ligand parameters except for charges, which came from MOPAC using AM1-BCC [198]. This procedure was done by the Ambertools-1.4.

6.2.2 Molecular dynamic simulations

The information of MD simulation using AMBER 10 package [188] is provided in Chapter 3. In particular, nine complexes of 6Aβ_{940}-ligand were placed in a triclinic box of about 9500 water molecules with 0.7 nm distance between the solute and box. The typical initial conformation is shown in Fig. 6.1. 6Aβ_{940} has 2862 atoms, while Dracorubin, Solasodine, Taraxasterol, Amentoflavone, Hinokiflavone, Kulolactone, Hecogenin, Taraxerol, and Diosgenin, respectively, have 61, 74, 81, 58, 58, 79, 73, 81 and 72 atoms (see below). To neutralize systems 6 ions Na^+ were added (Fig. 6.1), except the complex with ligand Solasodine where one adds 5 ions Na^+.

6.2.3 Computational methods and studied quantities

The detail of Autodock Vina is described in Chapter 3. In particular, the exhautiveness was set equal 400 and the center of grids is placed at the center of mass of receptor and grid dimensions were chosen large enough (60x50x50, 70x50x50, 90x70x50 and 80x60x60 $Å^3$ for Aβ_{40}, Aβ_{42}, 6Aβ_{9-40} and 5Aβ_{17-42}, respectively) to cover all parts of receptor.

The binding free energy was computed by MM-PBSA method which has been described in Chapter 3. The BBB and HIA were obtained by the QSAR method.

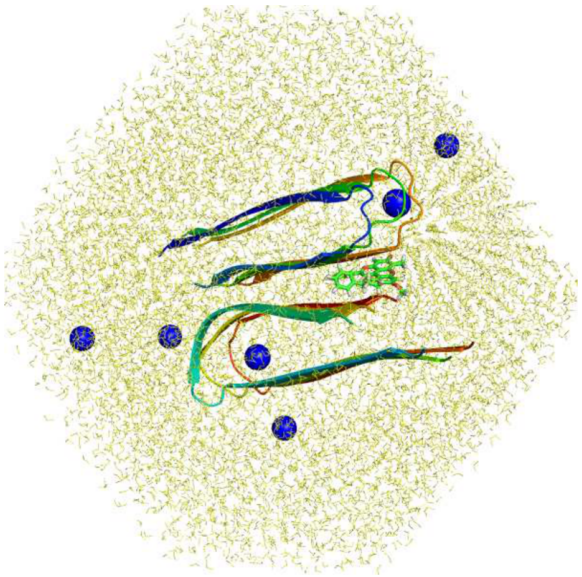

Figure 6.1 Typical initial structure for MD runs of ligand 160270 and 6Aβ_{9-40}. 160270 is colored in green. Blue spheres are ions Na+ added to neutralize the system.

6.3 Results and discussions

6.3.1 Human intestinal absorption.

Having used the PreADME prediction software [224] we have calculated HIA for 342 compounds (Fig. 6.2 and Table S1 [22]). This value varies between 0 and 100% but its average value is very high (81%) implying that most of ligands can be absorbed by human body. Among them 50 compounds have HIA equal 100%, and 227 compounds have HIA>90%. Only 6 ligands are not able to penetrate body having HIA= 0. Curcumin which is a potential drug for treating AD has high HIA of 94%, while other candidates have relatively low absorption ability. For instance, HIA= 65%, 40%, 21%, 40%, and 21% for Ginkgolide A, Ginkgolide B, Ginkgolide C, Ginkgolilde J, and EGCG, respectively (Table S1 [22]). Thus, most of ligands display higher absorption ability compared to leads that are under intensive clinical trial.

6.3.2 Blood-brain barrier.

Since amyloid peptides are located in brain an efficient drug should be able to cross the BBB to interfere their activity. Using the PreADME prediction method we have calculated $\log(BB)$ (Eq. 3.42) which measures a percentage of drug that can permeate brain. The results obtained for all compounds are shown on Table S1 [22].

Experimental values of $\log(BB)$ of drugs published to date cover the range between -2.0 to +1.0 [224]. Compounds with $\log(BB) > 0.3$ can cross the BBB easily, while

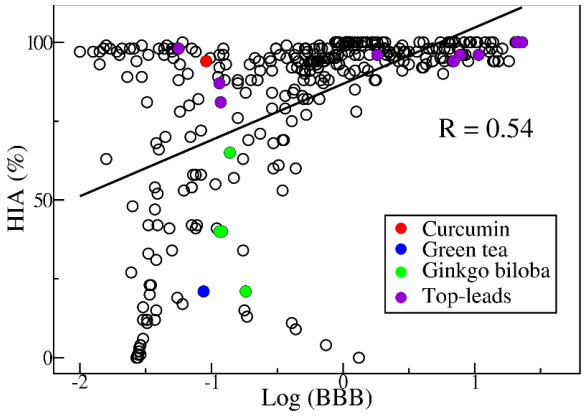

Figure 6.2 Correlation between HIA and BBB for 342 ligands. The correlation level R = 0.54. Violet, red, blue and green refer to top-leads, Curcumin, green tea and gingko biloba, respectively.

compounds with $\log(BB) < -1.0$ are poorly distributed in the brain [224]. As follows from Table S1 [22], the average value of $\log(BB)$ is -0.31. The compound Taraxasterol has the largest penetration ability $\log(BB) = 1.36$, while ligand 10607 has the smallest $\log(BB) = -2.0$. We found 91 compounds with $\log(BB) < -1.0$ and 24 compounds that have $\log(BB)$ larger than 1.00. At least, 227 compounds can pass through the BBB easily. There is weak correlation between HIA and $\log(BB)$ with the correlation level $R = 0.54$ (Fig. 6.2).

6.3.3 Docking results

6.3.3.1 Binding energies: correlation between four sets

Having used the Autodock Vina version 1.1 [181], we performed docking of 342 ligands to Aβ_{1-40}, 6Aβ_{9-40}, Aβ_{1-42}, and 5Aβ_{17-42}. For each receptor $E_{\rm bind}$ obtained from the best mode are listed in Table S1 [22] in SI. The second column refers to ID of ligands according to the Pubchem and Chemspider database (see http://pubchem.ncbi.nlm.nih.gov and http:// http://www.chemspider.com/) The distributions of $E_{\rm bind}$ for four sets are shown in Fig. 6.3. Ligands showing the highest binding affinity to 6Aβ_{9-40} have $-3.1 \leq E_{\rm bind} \leq -9.8$ kcal/mol, while $-3.1 \leq E_{\rm bind} \leq -8.9$, $-2.7 \leq E_{\rm bind} \leq -8.4$, and $-3.4 \leq E_{\rm bind} \leq -8.1$ kcal/mol for Aβ_{1-40}, Aβ_{1-40}, and 5Aβ_{17-42} (Fig. 6.3 and Table S1 [22]), respectively. The average of binding energies of ligands to 6Aβ_{9-40}, 5Aβ_{17-42}, Aβ_{1-40} and A$\beta 1-42$ is -6.6, -6.2, -5.9, and -5.5 kcal/mol, respectively.

Two sets of binding energies to fibril 6Aβ_{9-40} and monomer Aβ_{1-40} display high correlation with the correlation level $R = 0.91$ (Fig. 6.4). In the case of the longer 42-bead peptide, the correlation level drops to $R = 0.78$ for targets Aβ_{1-42} and 5Aβ_{17-42} (Fig. 6.5). For the remaining 4 pairs [6Aβ_{9-40}, 5Aβ_{17-42}], [6Aβ_{9-40}, Aβ_{1-42}], [Aβ_{1-40}, 5Aβ_{17-42}], and [Aβ_{1-40}, Aβ_{1-42}], one has $R = 0.80$, 0.94, 0.74

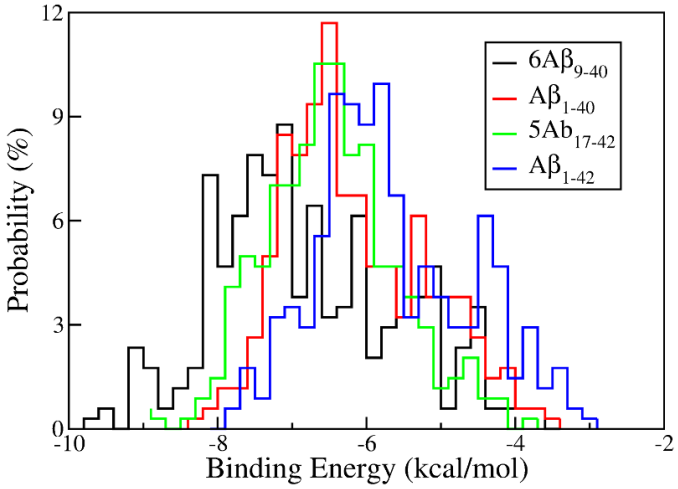

Figure 6.3 Distributions of binding energies of 342 ligands to four receptors. Results were obtained in the best modes of docking by Autodock Vina version 1.1 [181]. The energy bin used for obtaining these distributions is 0.2 kcal/mol. The average values of E_{bind} are -6.6, -5.9, -6.2, and -5.5 kcal/mol for 6Aβ_{9-40} (black), Aβ_{1-40} (red), 5Aβ_{17-42} (green), and Aβ_{1-42} (blue), respectively.

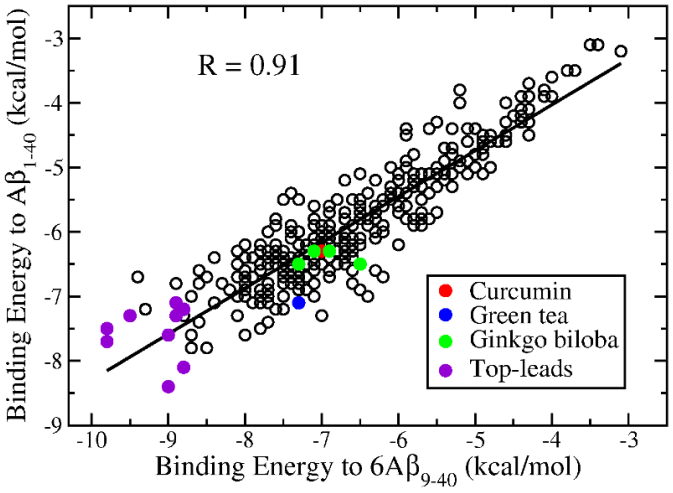

Figure 6.4 Relationship between binding energies to Aβ_{1-40} and 6Aβ_{9-40}. The correlation level $R = 0.91$. Violet, red, blue and green refer to top-leads, Curcumin, green tea and gingko biloba, respectively.

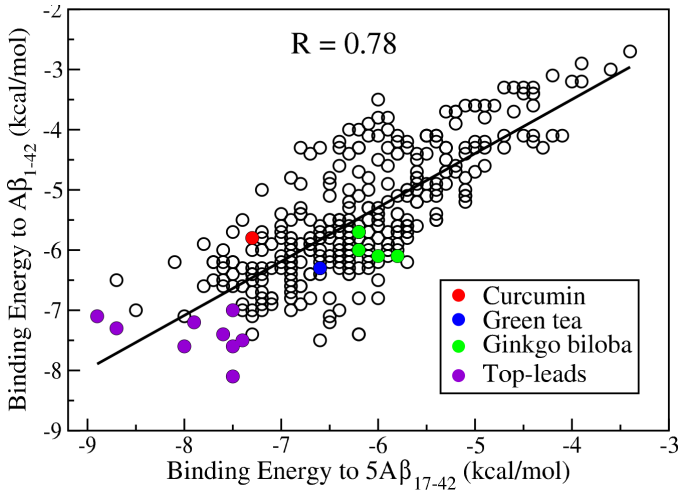

Figure 6.5 Relationship between binding energies to Aβ_{1-42} and 5Aβ_{17-42}. The correlation level R = 0.78. Violet, red, blue and green refer to top-leads, Curcumin, green tea and gingko biloba, respectively.

and 0.92, respectively (Fig. 6.6). Thus, E_{bind} obtained for Aβ_{1-42} show the highest correlation with 6Aβ_{9-40} ($R = 0.94$) but not with 5Aβ_{17-42}.

Overall, the correlation between four sets of E_{bind} is high but this does not mean they provide exactly the same binding affinity ranking. Solasodine and Diosgenin show the highest susceptibility to 6Aβ_{9-40} with $E_{\text{bind}} = -9.8$ kcal/mol (Table S1 [22] in SI) , while Kulolactone has the lowest binding energy $E_{\text{bind}} = -8.9$ kcal/mol to 5Aβ_{17-42} (Table S2 [22]). If one makes ranking by binding energies to Aβ_{1-40} then Dracorubin becomes a top-lead having $E_{\text{bind}} = -8.4$ kcal/mol (Table S3 [22]). Sorting ligands by E_{bind} to monomer Aβ_{1-42}, Amentoflavone occupies the first place with $E_{\text{bind}} = -8.1$ kcal/mol (Table S4 [22]). It should be noted that binding energies are not correlated with either log(BB) or HIA [22].

6.3.3.2 Top-leads revealed by docking results

.

Since we have computed binding energies to four different receptors, there are several possibilities to screen out the best candidates to treat AD. These possibilities will be discussed below.

Top-leads by ranking binding energies to 6Aβ_{9-40}. In search for ligands that can degrade already preformed fibrils of Aβ_{9-40}, one has to use E_{bind} obtained for this receptor. Among 342 compounds we can choose 21 ligands with lowest binding energies from -9.8 to -8.5 kcal/mol (Table S1 [22]). However, Thevetine at position 17 should be excluded not only because it has too low value of HIA (6%) but also low ability to cross the BBB (log(BB) = −1.57). For the latter reason Lactucopicrin

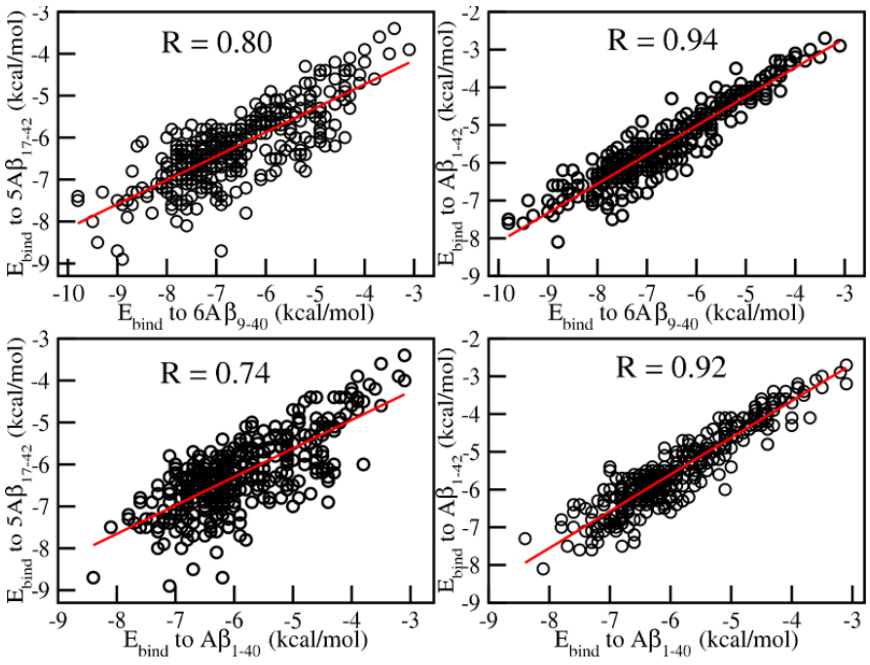

Figure 6.6 Relationship between different sets of binding energies to Aβ_{1-40}, Aβ_{1-42}, 6Aβ_{9-40} and 5Aβ_{17-42}. The correlation levels R = 0.80, 0.94, 0.74 and 0.92 for pairs [6A$\beta_9 - 40$, 5Aβ_{17-42}], [6Aβ_{9-40}, Aβ_{1-42}], [Aβ_{1-40}, 5Aβ_{17-42}], and [Aβ_{1-40}, Aβ_{1-42}], respectively.

(position 15) should be also disregarded. Dracorubin (position 6) has relatively low value of $\log(BB) = -1.25$ but this value is still acceptable if one compares it with other existing drugs [223]. Therefore, for degradation of Aβ_{1-40} aggregates, we recommend the following 19 top-hit compounds:

$$\begin{array}{c} \textit{Solasodine}, \textit{Diosgenin}, \textit{Hinokiflavone}, \textit{Kulactone}, \\ \textit{Sarsasapogenin}, \textit{Dracorubin}, \textit{Taraxasterol}, \textit{Hecogenin}, \\ \textit{Tanshinone}, \textit{Kulolactone}, \textit{Sanguinarine}, \textit{Taraxerol}, \\ \textit{Amentoflavone}, \textit{Limonin}, \textit{Cycloartenol}, \textit{TanshinonII}, \\ \textit{Melianodiol}, \textit{Peiminine}, \textit{Melianol}. \end{array} \tag{6.1}$$

Curcumin (diferulom-rthane), ginkgo biloba (ginkgolide A, B, C, J) and EGCG from the traditional Chinese and Indian medicines have E_{bind} higher than -7.3 kcal/mol and their ranking among 342 compounds is lower than 119 (Table S1 [22]). Thus, based on the virtual screening results, new top 19-leads are more promising than these compounds in treatment of AD.

23 top-leads sorted by binding energies to 5Aβ_{17-42}. Table S2 [22] in SI [22] shows 27 ligands with lowest binding energies to this receptor (-8.9 $\leq E_{\text{bind}} \leq -7.5$ kcal/mol). These ligands are supposed to slow down the Aβ_{1-42} fibril formation better than other compounds. As in the case of 6Aβ_{9-40}, Scillaren A (position 9), Liquiritin (position 11) and Piperine (position 19) in Table S2 [22] should be excluded due to their low ability to cross the BBB. Gomphrenin (position 18) is also skipped having HIA = 11%. Thus we have the following 23 top-leads:

$$\begin{array}{c} \textit{Kulolactone}, \textit{Dracorubin}, \textit{Bixin}, \textit{Kulactone}, \\ \textit{Lobeline}, \textit{Hinokiflavone}, \textit{Adynerin}, \textit{Taraxerol}, \\ \textit{Crocetin}, \textit{Mangostin}, \textit{Glycosminine}, \textit{Hecogenin}, \\ \textit{Cycloartenol}, \textit{Tanshinone}, \textit{Cyclolaudenol}, \textit{Amentoflavone}, \\ \textit{Taraxasterol}, \textit{Solasodine}, \textit{Sanguinarine}, \textit{Conessine}, \\ \textit{Cannabinol}, \textit{Arborine}, \textit{Kaempferide}. \end{array} \tag{6.2}$$

Comparing two sets of top-leads in box 6.1 and box 6.2 one can see that they share 11 common compounds (Solasodine, Hinokiflavone, Kulactone, Dracorubin, Taraxasterol, Tanshinone, Sanguinarine, Taraxerol, Amentoflavone, Cycloartenol, and Hecogenin) which may slow down or prevent the fibril growth of both β_{1-40} and β_{1-42} peptides.

18 top-leads by ranking binding energies to monomer Aβ_{1-40}. On Table S3 in SI [22] we list 21 ligands that have lowest binding energies to this target (-8.4 $\leq E_{\text{bind}} \leq -7.2$ kcal/mol). They are expected to display high propensity to prevent Aβ_{1-40} peptides from aggregation. Excluding Lactucopicrin (position 3), Thevetine (position 11), and Gomphnerin I (position 16) as having low HIA and log(BB), one obtains the following 18 top-leads:

$$\begin{array}{c} \textit{Dracorubin}, \textit{Amentoflavone}, \textit{Peiminine}, \textit{Diosgenin}, \\ \textit{Taraxasterol}, \textit{Rottlerin}, \textit{Limonin}, \textit{Solasodine}, \\ \textit{Tetrandrine}, \textit{Peimine}, \textit{Hinokiflavone}, \textit{Hecogenin}, \\ \textit{Sanguinarine}, \textit{Arnidiol}, \textit{Taraxerol}, \textit{Glochidonol}, \\ \textit{Sarsasapogenin}, \textit{Liriodenine} \end{array} \tag{6.3}$$

No.	ID	Herbs'name	Compound	6Aβ_{9-40}	Aβ_{1-40}	5Aβ_{17-42}	Aβ_{1-42}	Log BB	HIA
1	31342	Solanum xanthocarpum schrad	Solasodine	-9.8	-7.5	-7.5	-7.6	0.84	94%
2	99474	Schizocapsa plantaginea hance	Diosgenin	-9.8	-7.7	-7.4	-7.5	0.89	96%
3	5281627	Thuja orientalis L.	Hinokiflavone	-9.5	-7.3	-8.0	-7.6	-0.94	87%
4	160270	Calamus draco willd	Dracorubin	-9.0	-8.4	-8.7	-7.3	-1.25	98%
5	5270604	Centipeda minima	Taraxasterol	-9.0	-7.6	-7.5	-7.0	1.36	100%
6	5318868	Melia azedarach L.	Kulolactone	-8.9	-7.1	-8.9	-7.1	1.03	96%
7	91453	Agave americana Lin.	Hecogenin	-8.9	-7.3	-7.6	-7.4	0.26	96%
8	92097	Taraxacum officinale	Taraxerol	-8.8	-7.2	-7.9	-7.2	1.32	100%
9	5281600	Selaginella tamariscina	Amentoflavone	-8.8	-8.1	-7.5	-8.1	-0.93	81%

Table 6.1 Nine top-leads revealed by ranking binding energies. They include seven common ligands highlighted in blue in Eq. 6.1- 6.4, Diosgenin from Table S1 [22], and Kulolactone from Table S2 [22]. Second column refers to ID of ligands according to the Pubchem and Chemspider database. Binding energies are measured in kcal/mol.

From boxes 6.1-6.3, it follows that three sets of top-leads share 8 common ligands: Solasodine, Hinokiflavone, Dracorubin, Taraxasterol, Sanguinarine, Taraxerol, Hecogenin, and Amentoflavone.

18 top-leads sorted by binding energies to monomer $A\beta_{1-42}$. As evident from Table S4 [22], 23 ligands have the lowest binding energies in the interval -8.1 $\leq E_{\rm bind} \leq$ -7.0 kcal/mol. After exclusion of Corilagin (position 5), Tomatin (position 8), Tiliroside (position 12), Thevetine (position 15), and Lactucopicin (position 20) which possess low HIA and log(BB), we have the following 18 top-leads:

$$\begin{array}{c} Amentoflavone, Hinokiflavone, Solasodine, Diosgenin, \\ Hecogenin, Sarsasapogenin, Tigogenin, Dracorubin, \\ Taraxerol, Kulolactone, Adynerin, Arnidiol, \\ Kulactone, Taraxasterol, Glochidonol, \\ Chlorogenin, RhodexinA, Glochidiol. \end{array} \tag{6.4}$$

Comparing this set with 8 common ligands obtained for previous 3 sets one can show that they share 7 common ligands which are the best for all four energy sets. They are Solasodine, Hinokiflavone, Dracorubin, Taraxasterol, Taraxerol, Hecogenin, and Amentoflavone.

Universal top-leads by ranking binding energies of all four sets. Seven ligands highlighted in blue in boxes 6.1-6.4 are qualified as universal top-leads by ranking of four energy sets. They are also able to cross the BBB as well as to be absorbed by human

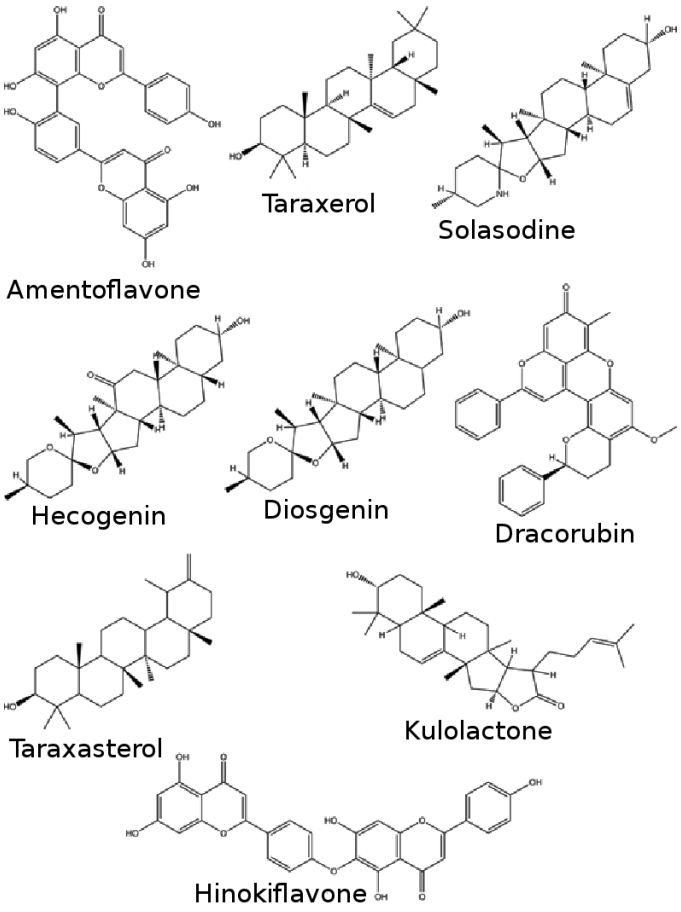

Figure 6.7 Chemical structures of nine top-leads revealed by the herbs method. Their ID are also shown.

body. Because these ligands can bind well to all four receptors 6Aβ_{9-40}, 5Aβ_{17-42}, Aβ_{1-40}, and Aβ_{1-42}, they are supposed to interfere with oligomerization and to degrade mature fibrils of amyloid peptides. Note that the list of 7 common top-leads does not involve Diosgenin (champion of the first set in Table S1 [22]), Kulolactone (champion of the second set in Table S2 [22]). We add these two ligands to the list of universal top-leads. Therefore the full list of top-hits includes 9 ligands and is shown on Table 1, where the names of corresponding plants are also presented. Solasodine, for instance, comes from Solanum xanthocarpum schrad, while Hinokiflavone, Dracorubin, and Taraxerol are derived from Thuja orientalis L., Calamus draco Willd, and Taraxacum officinale, respectively. Chemical structures of top-leads revealed by the docking method are shown in Fig. 6.7.

In term of binding energies 9 top-hit compounds (Table 6.1) are better than existing candidates Curcumin, Ginkgo Biloba and EGCG from green tea in preventing AD. However, the docking approach is not always accurate as it has a number of drawbacks related to omission of receptor dynamics and a limited number of trial positions of ligand. From this prospect, our conclusion that 9 top-leads are superior to other intensively studied natural compounds should be reexamined by more sophisticated approaches. Below this problem will be considered using the MM-PBSA method.

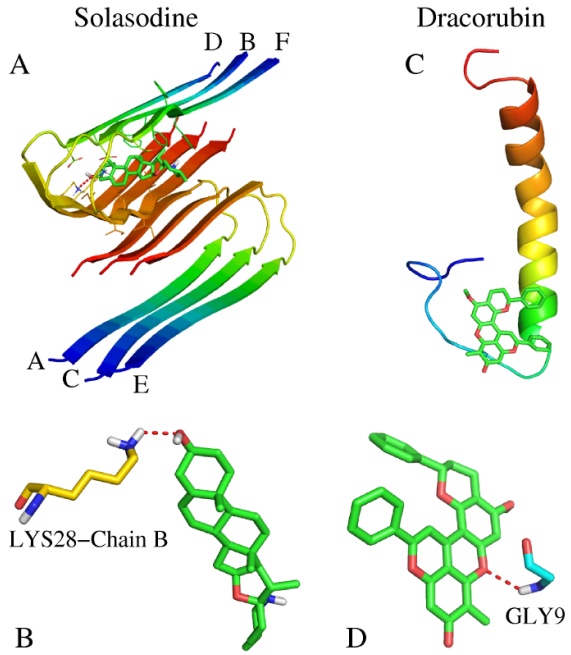

Figure 6.8 The best binding position of Solasodine to 6Aβ_{9-40} (A) and the corresponding HB network (B). (C) and (D) are the same as in (A) and (B) but for Dracorubin-Aβ_{1-40} complex. In both cases only one HB occurs between ligand and target.

6.3.3.3 Hydrogen networks

In this section we focus on the nature of ligand binding to different receptors in the framework of the docking approach. For illustration we consider ligands Solasodine, Dracorubin, Kulolactone, Amentoflavone and Hinokiflavone from 9 top-leads (Table 6.1). The best position of Solasodine in the 6Aβ_{9-40} fibril is shown in Fig. 6.8A. It is in the turn region of upper peptides B, D, and F. Although there exists only one HB between the ligand and Lys28 of receptor (Fig. 6.8B), the corresponding energy remains high ($E_{\text{bind}} = -9.8$ kcal/mol). Since HB energy is 1-5 kcal/mol, other interactions like the Coulomb and vdW interactions also contribute to E_{bind} of Solasodine.

Dracorubin, positioned near the N-terminal of Aβ_{1-40} (Fig. 6.8C), shows the highest binding affinity to this monomer with $E_{\text{bind}} = -8.4$ kcal/mol (Table 6.1). It also forms only one HB with Gly9 of the target (Fig. 6.8D) implying that other contributions are important in complex association. Dracorubin strongly binds to both mature fibrils (see the binding energies on Table 6.1), while their coupling with Aβ_{1-42} is relatively weak.

Among 342 ligands, Kulolactone displays the highest binding affinity to protofibril 5Aβ_{17-42} with $E_{\text{bind}} = -8.9$ kcal/mol. In the best docking mode it locates next to peptide A of the receptor (Fig. 6.9A) but no HB is formed. Thus the binding of this ligand is entirely defined by the Coulomb and vdW interactions.

The hydrogen bonding plays an important role in association of Amentoflavone with monomer Aβ_{1-42} near the N-terminal (Fig. 6.9B) because 4 HBs occur between the

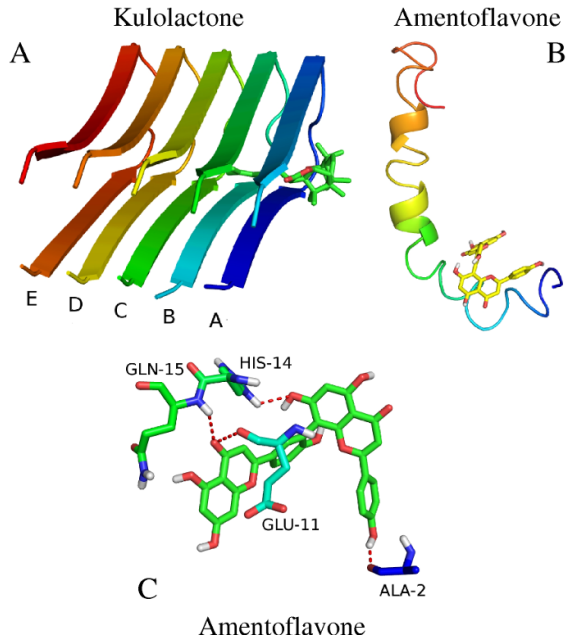

Figure 6.9 (A) The binding place of Kulolactone to the fibril 5Aβ_{17-42}. There is no hydrogen bonding between these two compounds. (B) The docking position of Amentoflavone to monomer Aβ_{1-42} and the corresponding HB network (C). There are four HBs between the ligand and the receptor.

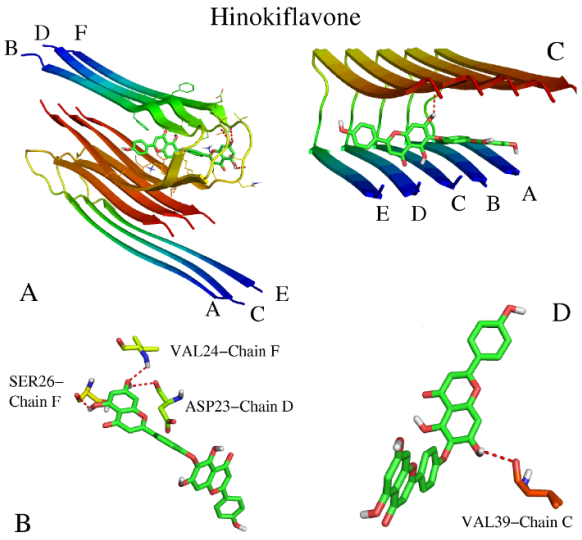

Figure 6.10 (A) The binding place of Hinokiflavone to the fibril 6Aβ_{9-40} (A) and the corresponding HB network (B). HB is formed with Ser26, Val24 and Asp23 from chains F and D of fibril. (C) and (D) are the same as in (A) and (B) but for docking of Hinokiflavone to 5Aβ_{17-42}. There is only one HB between ligand and Val39 of chain C of 5Aβ_{17-42}.

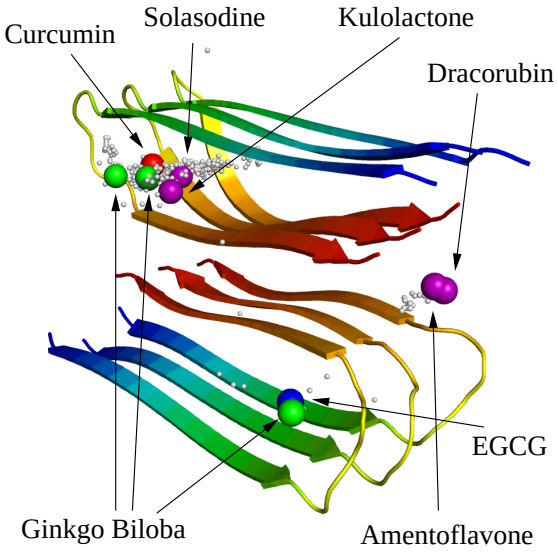

Figure 6.11 Binding positions of different ligands (Curcumin, Gingo Biloba including Ginkgolide A, B, C and J, EGCG, Solasodine, Kulolactone, Dracorubin and Amentoflavone) around the fibril 6Aβ_{9-40}

ligand and amino acids Ala2, Glu11, His 14 and Gln15 of the target. It has the same binding energy $E_{\text{bind}} = -8.1$ kcal/mol to both monomers Aβ_{1-42} and Aβ_{1-40}, but one has only 3 HBs with the latter (results not shown).

To illustrate diversity of hydrogen bonding to different receptors, we consider Hinokiflavone as an example. Similar to Solasodine, this compound is bound to 6Aβ_{9-40} in the turn region inside fibril (Fig. 6.10A). The difference is that Hinokiflavone has 3 HBs with 6Aβ_{9-40} (Fig. 6.10B), whereas Solasodine has only one HB (Fig. 6.8B). This may be associated with the fact that the former has 10 HB acceptors and 5 HB donors, while the latter has 3 HB acceptors and 2 HB donors. Contrary to 6Aβ_{9-40} case, Hinokiflavone locates at the end of peptides of 5Aβ_{17-42} (Fig. 6.10C) having one HB with Val39 of chain C (Fig. 6.10D). In the best docking mode this compound locates near the N-terminal of monomers Aβ_{1-40} and Aβ_{1-42} (Fig. 6.12). It forms 2 HBs with Asp1 and Gln15 of the former and one HB with Glu11 of the latter one (Fig. 6.12).

In short, our analysis reveals that in some cases, for instance binding of Amentoflavone to 5Aβ_{17-42}, hydrogen bonding plays the important role. However, for many complexes (6Aβ_{9-40}-Kulolactone, 5Aβ_{17-42}-Taraxerol, 6Aβ_{9-42}-Taraxerol *etc*) this type of bonding is irrelevant. Such a situation occurs when the number of HB donors and acceptors of ligands is small (Taraxerol has only one HB donor and one HB acceptor). In this case the electrostatic and vdW interactions become dominating.

Diversity of locations of ligands in the best docking mode

Docking positions of representative ligands to receptor 6Aβ_{9-40} are shown in Fig. 6.11. Cleraly, they vary from ligand to ligand. Amentoflavone and Dracorubin from 9 top-leads locate between two layers while, similar to Curcumin, EGCG and Ginkgo biloba, Solasodine and Kulolactone are inside one layer. In the case of 5Aβ_{17-42} Solasodine, Dracorubin and EGCG prefer to be outside of fibril, whereas

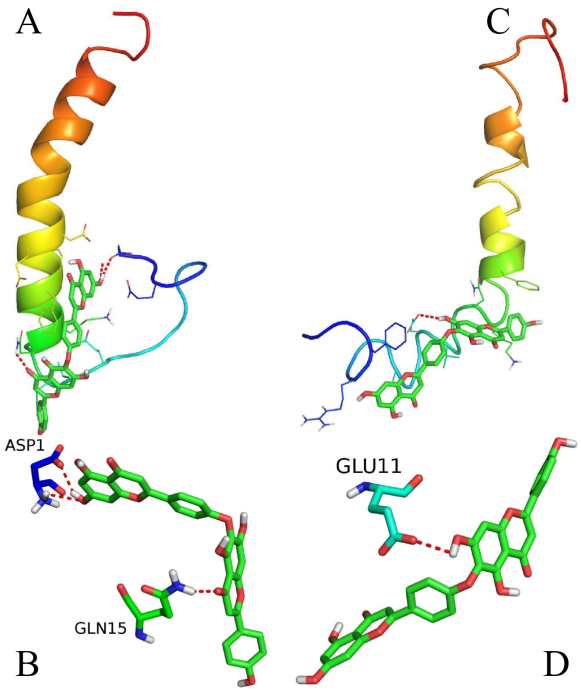

Figure 6.12 (A) The binding place of Hinokiflavone to monomer Aβ_{1-40} (A) and the corresponding HB network (B). (C) and (D) are the same as in (A) and (B) but for docking of Hinokiflavone to Aβ_{1-42}

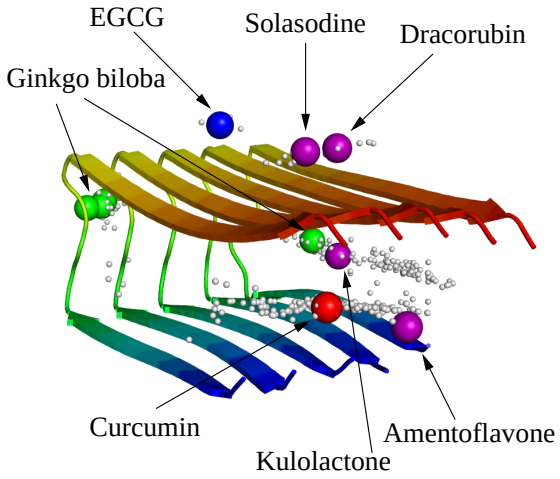

Figure 6.13 The same as in Fig. 6.11 but for 5Aβ_{17-42}.

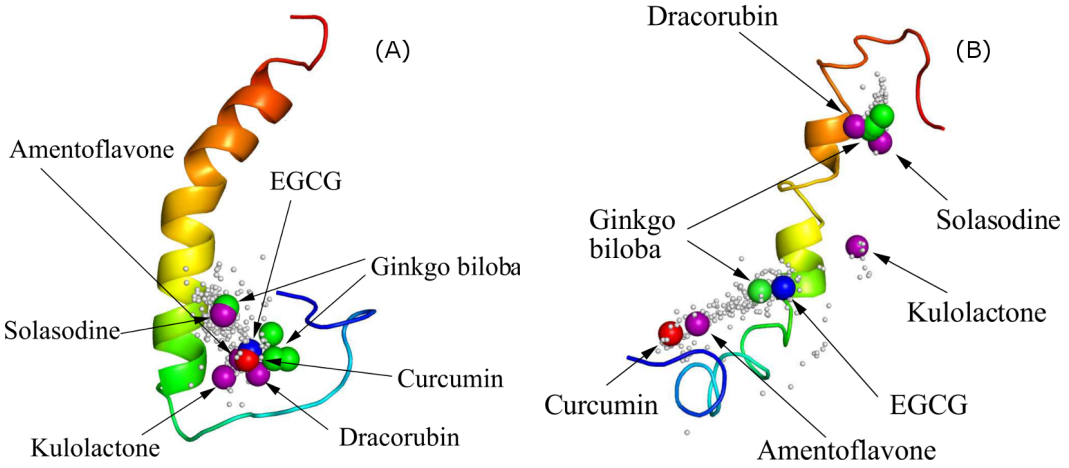

Figure 6.14 (A) Binding positions of different ligands around monomer Aβ_{1-40}. (B) Binding positions of different ligands around monomer Aβ_{1-42}.

No.	ID	Ligand	$-T\Delta S$	ΔE_{vdW}	ΔE_{elec}	ΔG_{PB}	ΔG_{sur}	ΔG_{bind}
1	160270	Dracorubin	21.22	-58.36	-12.06	37.73	-4.12	-15.59
2	92097	Taraxerol	19.04	-41.73	-1.07	12.76	-3.85	-14.85
3	5270604	Taraxasterol	20.25	-50.88	0.03	22.42	-3.95	-12.13
4	5281627	Hinokiflavone	24.16	-55.69	-18.34	42.41	-4.39	-11.85
5	99474	Diosgenin	20.36	-52.25	-4.35	29.61	-4.47	-11.1
6	91453	Hecogenin	19.69	-50.32	-3.07	31.77	-4.21	-6.14
7	5281600	Amentoflavone	21.81	-43.57	0.26	19.88	-3.26	-4.88
8	31342	Solasodine	23.35	-38.60	-118.29	132.4	-3.23	-4.37
9	5318868	Kulolactone	22.68	-45.03	7.39	16.86	-4.30	-2.40

Table 6.2 Binding free energies (in units of kcal/mol) to 6Aβ_{9-40} of nine top-leads revealed by the docking method. Results were obtained by MM-PBSA method.

other compounds stay inside (Fig. 6.13). Thus, only Dracorubin favors to be outside of layer in both cases. As evident from Fig. 6.14 (A), all of considered ligands are located near the N-terminal of monomer Aβ_{1-40}. The situation becomes very different in the Aβ_{1-42} case, where Curcumin, Amentoflavone, EGCG and one of Ginkgo biloba ligands are positioned at the N-end, while Kulolactone prefers to be in the middle (Fig. 6.14 (B)). Other molecules are energetically more favorable to locate at the C-termini.

6.3.4 Refinement of docking results by MM-PBSA method

Since the docking method is not accurate enough for prediction, we refine our finding by calculating the binding free energy of nine top-leads using a more reliable MM-PBSA method. Because docking results obtained for different targets show high correlation, only 6Aβ_{9-40} has been chosen as a receptor for MD simulations.

For each system we have made MD run of 19 ns except 29 ns simulation has been carried out for compound Solasodine. Since all systems behave in a similar way we

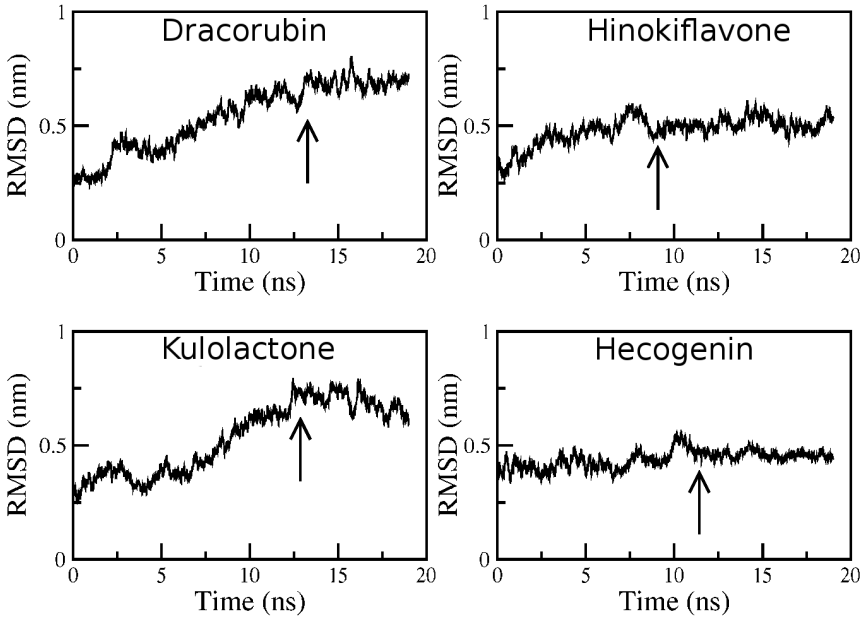

Figure 6.15 Time dependence of RMSD for 4 compounds. Arrow referes to equilibrium time $t_{\rm eq}$ when the system reaches the equilibrium.

show results for four ligands Dracorubin, Hinokiflavone, Kulolactone and Hecogenin that have very different binding free energies (Table 6.2). From the time dependence of backbone RMSD from the initial structures (Fig. 6.15) it is clear that these systems get equilibrium at different time $t_{\rm eq}$ ($t_{\rm eq} \approx 13$, 9, 13 and 11 ns for Dracorubin, Hinokiflavone, Kulolactone and Hecogenin, respectively). Snapshots collected every 10 ps after $t_{\rm eq}$ were used for calculating $\Delta G_{\rm bind}$ by the MM-PBSA method (Materials and Methods) and the results are shown on Table 6.2. The entropic ($T\Delta S$) and nonpolar contribution ($\Delta G_{\rm sur}$) are not sensitive to ligands. For all sytems the vdW interaction dominates over the electrostatic one (Fig. 6.16). The low binding affinity of Kulolactone is mainly associated with repulsion between the receptor and ligand.

In order to understand the nature of ligand binding, we have monitored the time dependence of the number of HBs between the ligand and receptor (Fig. 6.18) and calculated its average value in the equilibrium. Ligand Dracorubin has the higher binding affinity than Hinokiflavone but its HB network is weaker (Fig. 6.18) because the average HB number of the former is equal to 0.33 while for Hinokiflavone one has 1.03. In equilibrium Hecogenin and Kulolactone have almost the same average number of HB (≈ 0.1) but they show different resistance to 6Aβ_{9-40} suggesting that HBs alone do not govern the binding affinity. Using results shown in Fig. 6.19 we obtain the equilibrium average number of SC contacts between receptor and the ligand equal 5.83, 2.87, 2.28 , and 1.04 for Dracorubin, Hinokiflavone, Hecogenin and Kulolactone, respectively. Thus the higher is binding affinity (Table 6.2) the stronger is the SC interaction. The dominance of SC contacts is also illustrated in Fig. 6.17, where the typical conformation of 6Aβ_{9-40}-Hinokiflavone in the equilibrium is shown. Here Hinokiflavone has 3 HBs against 5 SC contacts (not shown) with the target.

The ranking of binding affinity obtained by MM-PBSA method (Table 6.2) is very different from the docking one as the correlation level between two sets of results

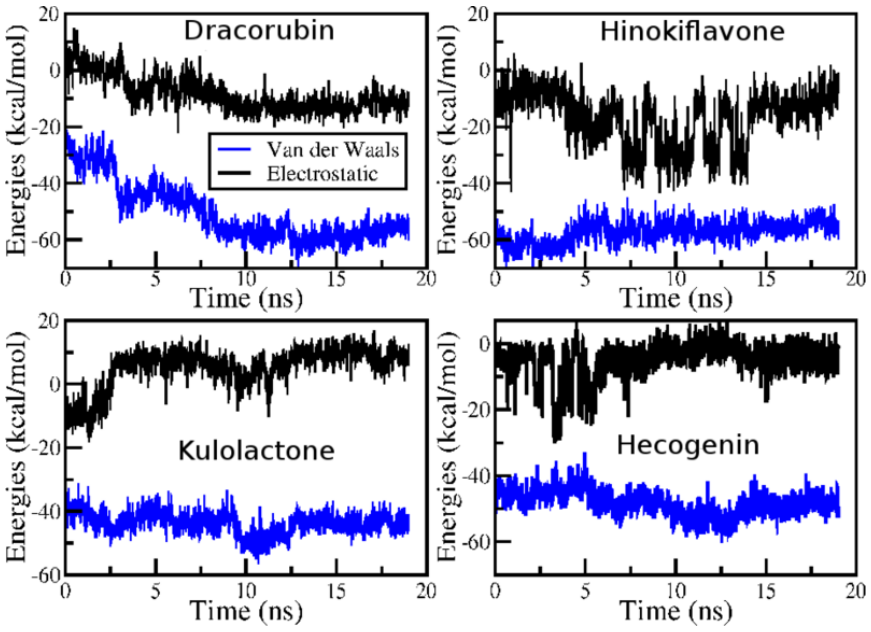

Figure 6.16 Time dependence of vdW (blue) and electrostatic (black) interaction between the ligand and receptor for four leads.

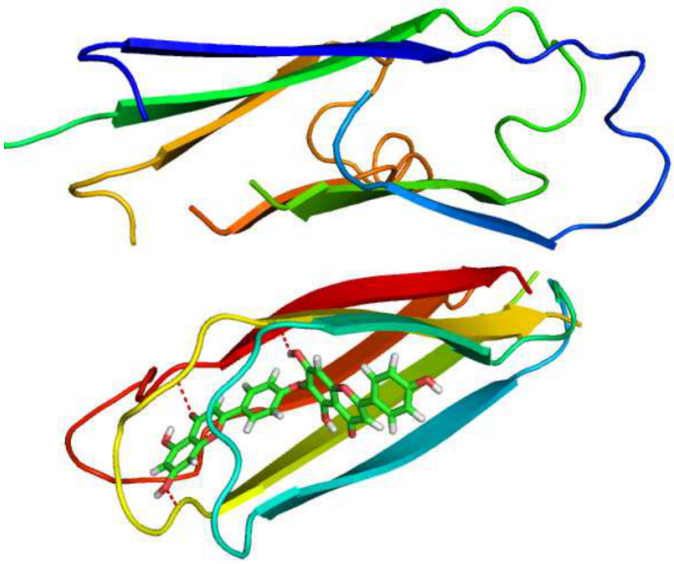

Figure 6.17 Typical snapshot of 6Aβ_{9-40}-Hinokiflavone complex in the equilibrium. Hinokiflavone has 3 HBs (red broken lines) with the target and 5 SC contacts (not shown).

is almost zero. Ligand 160270 ranked fourth by docking (Table 6.1) becomes a champion in MM-PBSA (Table 6.2). Since the latter method is more accurate one should rely on its results. Keeping only ligands that have $\Delta G_{\text{bind}} < -11$ kcal/mol, we predict that Dracorubin, Taraxerol, Taraxasterol, Hinokiflavone and Diosgenin may be good candidates to cope AD. Using the relationship between the binding free energy and inhibition constant K_i ($\Delta G_{\text{bind}} = RT \ln(K_i)$, where the gas constant $R = 1.987 \times 10^{-3}$ kcal/mol) one can show that K_i of five top-leads varies between 8 nM and 4 pM. In other words, they have excellent inhibitory capacity. Having used the MM-PBSA and the same force field and water model we have obtained the binding free energy of Curcumin to 6Aβ_{9-40} $\Delta G_{\text{bind}} \approx -14.3$ kcal/mol (Son Tung Ngo and Mai Suan Li, unpublished results). Using the experimental value $K_i = 0.2$ nM [50], we obtain $\Delta G_{\text{bind}} \approx -13.3$ kcal/mol for binding of Curcumin to Aβ_{9-40} aggregates. Therefore the binding affinity of Dracorubin and Taraxerol to the Aβ fibrils is probably compatible or even higher than Curcumin.

6.3.5 Comparison of pharmacological properties of top leads with Curcumin

Curcumin has HIA of 94% (Table S1 [22]) which is higher than Hinokiflavone (87%) but lower than 4 other top leads (Table 6.1). Thus Taraxerol, Taraxasterol, Diosgenin and Dracorubin may be absorbed by human body better than Curcumin, but all of these compounds have high HIA ($> 85\%$). Taraxerol, Taraxasterol, Diosgenin and Hinokiflavone are supposed to cross the BBB better than Curcumin which has log(BB)=-1.04 (Table 6.1 and Table S1 [22]). Having log(BB)=-1.25 Dracorubin is presumably worse than Curcumin in jumping over BBB.

With the help of PreADME server we have analysed the toxicity of five top-leads and Curcumin (Table S5). Together with Curcumin, Taraxerol and Diosgenin pass the Ames test. The remaining three top compounds may act as a carcinogen (or cause cancer) being positive to this test. Since Taraxerol is positive to both rat and mouse carcinogenicity, it is probably more toxic than Diosgenin and Curcumin. Thus, in term of toxicity our analysis reveals that Diosgenin is likely compatible with Curcumin, while other top-leads are more toxic.

Using software QikProp v3.3 (http://www.schrodinger.com/products/14/17/) we have studied metabolism for 5 top-leads and Curcumin (see page 64 in SI). For Curcumin oxidation of two aromatic OH (the structure of Curcumin is available on position 155 of Table S1 [22]), alpha hydroxylation of carbonyl and ether dealkylation may take place. The aromatic OH oxidation is also possible for Hinokiflavone having 5 aromatic OH atoms (Fig. 6.7) but not for other top-leads. Due to the existence of aromatic OH that can eliminate free radicals Curcumin and Hinokiflavone are supposed to be not highly toxic. However, reactive functional groups (page 64 in SI) in Curcumin and Diosgenin may enhance their toxicity. Similar to Curcumin, the remove of alkyl group from ether likely takes place in Dracorubin. The conversion of benzylic-like H to alcohol can occur only in this compound. A secondary alcohol may be oxidised converting to a ketone in Taraxerol, Diosgenin and Taraxasterol. Alcohole can also be produced from allylic H in these three ligands.

Overall, metabolism pathways are similar for Taraxerol and Diosgenin, while Curcumin share some pathways with Hinokiflavone and Dracorubin. However, one has

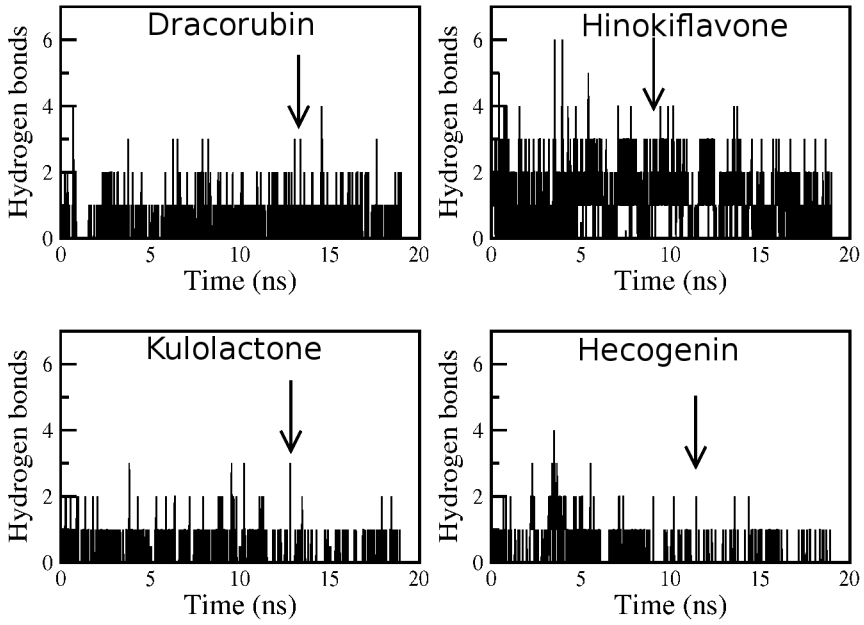

Figure 6.18 The same as in Fig. 6.15 but for the number of HBs between the ligand and receptor. The average number of HBs in equilibrium is 0.33, 1.03, 0.10 and 0.11 for Dracorubin, Hinokiflavone, Hecogenin and Kulolactone, respectively.

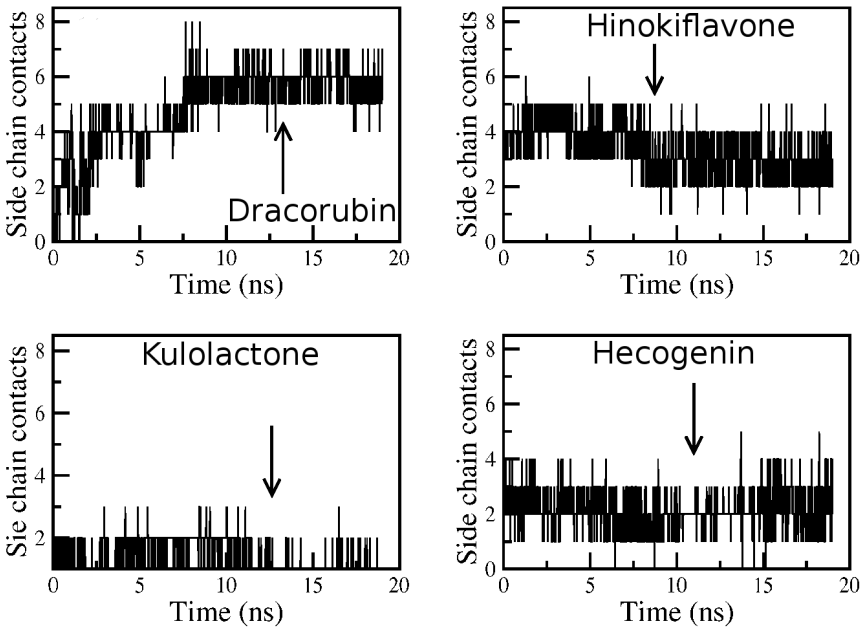

Figure 6.19 The same as in Fig. 6.15 but for the number of contacts between SCs of receptor and ligand. The average number of these contacts in equilibrium is 5.83, 2.87, 2.28 , and 1.04 for Dracorubin, Hinokiflavone, Hecogenin and Kulolactone, respectively.

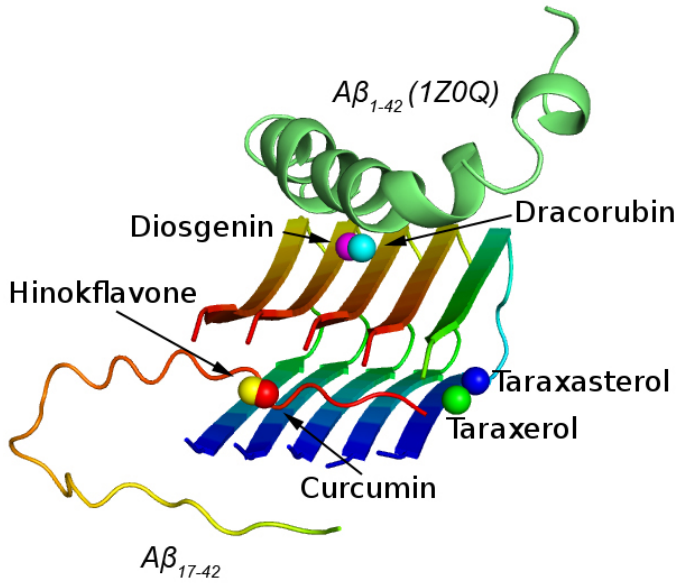

Figure 6.20 Positions of Aβ_{42} (green) and Aβ_{17-42} (red and yellow) in the best docking mode to 5Aβ_{17-42}. The binding energy is equal -204.3 and -318.5 kcal/mol for Aβ_{42} and Aβ_{17-42}, respectively. The result was obtained by the protein-protein docking method. Circles refer to centers of mass of five top-leads and Curcumin in the best docking positions.

to bear in mind that theoretical predictions may be false and further biochemical and pharmacore studies are vital to settle this problem.

6.3.6 Competition between fibril growth and ligand binding

Since the fibril elongation and ligand binding may occur concurrently it is worth to study the competition between these two processes. For this purpose we use the protein docking method [259, 260, 261, 262] implemented in ClusPro server to dock full-length and truncated Aβ peptides to fibrils 5Aβ_{17-42} and 6Aβ_{9-40}. Because the results are quite similar for two targets we focus on the first one. Structure of Aβ_{42} is taken from PDB (PDB ID: 1Z0Q), while the structure of Aβ_{17-42} is extracted from the fibril 5Aβ_{17-42} (PDB ID: 2BEG). The position of Aβ_{42} and Aβ_{17-42} in the best docking mode to 5Aβ_{17-42} is shown in Fig. 6.20 , where five top-leads and Curcumin are also presented. The binding of Aβ_{17-42} is more tight than Aβ_{42} with the binding energy equal to -318.5 and -204.3 kcal/mol, respectively. Aβ_{17-42} forms 56 SC contacts with 5Aβ_{17-42}, while Aβ_{42} has only 9 SC contacts. Since there is no HBs between the target and two peptides, the binding affinity is controlled by SC contacts.

Obviously, Aβ_{42} can interfere with binding of Dracorubin and Diosgenin (Fig. 6.20) as they are close to each other. The truncated peptide Aβ_{17-42} has the docking position different from Aβ_{42} and may interact with Curcumin and Hinokflavone modulating their binding dynamics. Taraxerol and Taraxasterol do not have contacts

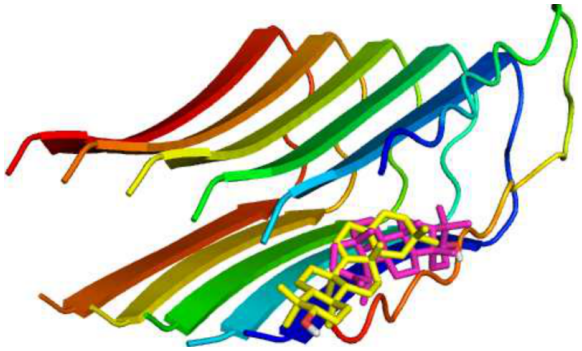

Figure 6.21 The position of Aβ_{17-42} in the third docking mode to 5A$\beta_1$7−42 fibril. The binding energy is -309.2 kcal/mol. Ligands Taraxerol (yellow) and Taraxasterol (pink) are also shown.

with either Aβ_{42} or Aβ_{17-42} in the best docking mode but they may strongly interfere with aggregation because the fibril growth is expected to occur on the fibril edge. Interestingly, in the third docking mode with the binding energy of -309.2 kcal/mol the position Aβ_{17-42} is almost commensurable with the fibril lattice (Fig. 6.21). In this position the docked peptide has the strong interaction with Taraxerol and Taraxasterol.

Thus, the fibril growth may compete with ligand binding. But this scenario follows from the docking simulation and it may change should the real dynamics is taken into account.

6.4 Conclusion

For the first time we have performed the systematic computational study of 342 ligands derived from plants and herbs as potential leads to treat AD. Our main results and remarks are as follows:

1. We have shown that most of compounds can be absorbed by human body, pass through the BBB and have high binding energies to 6Aβ_{9-40}, Aβ_{1-40}, 5Aβ_{17-42}, and Aβ_{1-42}.

2. The role of HB in binding of ligands to four receptors is studied in detail using the docking method. In most of cases together with HBs the electrostatic and vdW interactions make important contribution to E_{bind}. For some complexes the hydrogen bonding is minor and this conclusion is also confirmed by the MM-PBSA method.

3. Locations of ligands in the best docking mode depend not only on ligands themselves but also on receptors (Fig. 6.11, 6.13, 6.12, and 6.14).

4. With the help of the docking and MD simulations we predict that there are 5 top-leads (Table 6.2) that may not only slow down aggregation but also degrade mature fibrils of amyloid peptides. Two of them (Dracorubin and

Taraxerol) are more prominent than Curcumin for treating AD having lower ΔG_{bind}. Five 5 top-leads are derived from plants shown in Fig. S13 of SI [22].

5. Pharmacological characteristics such as HIA, BBB, toxicity and metabolism have been analyzed for top-leads and Curcumin. But our theoretical predictions are just consultative and have to be carefully verified by *in vivo* experiments.

6. We have considered all of 342 compounds with known chemical structures from the book of Prof Do Tat Loi [48]. We believe that more ligands derived from Vietnamese herbs and plants should be available but scattered in different sources. Our next task is to collect them and update our results.

7

In silico and in vitro characterization of anti-amyloidogenic activity of vitamin K3 analogues for Alzheimer's disease

7.1 Introduction

ApoE belongs to apolipoprotein class found in intermediate density lipoprotein (IDLs) and chylomicron that is necessary for regular catabolism of lipoprotein constituents enriched by triglyceride. In the brain, APOE is essentially generated by astrocytes transporting cholesterol to neurons through ApoE receptors. The latter are members of gene family of low-density lipoprotein receptors [53]. ApoE is polymorphic with three major isoforms ApoE2, ApoE3 and ApoE4 which are different from each other just by 1 or 2 residues at position 112 and 158 However this minor differences result in remarkable physiological sequences that ApoE2 and ApoE3 are protective for AD while the overexpression of ApoE4 might become a generic risk factor. Allison was the first who has reported about the possible relationship between vitamin K and AD [54]. Namely, the concentration of this vitamin is lower in blood of persons who have a high level of ApoE4 suggesting that vitamin K supplementation may have impact on treating AD.

In this chapter, we studied the effects of 15 vitamin K3 (VK3) analogues on Aβ_{1-40} aggregation and cellular toxicity. Although many VK3 analogues such as VK3-9, VK3-10, and VK3-6 inhibited the aggregation of Aβ_{1-40}, only VK3-9 was able to protect cells against Aβ_{1-40} induced toxicity. The effective dose of VK3-9 was approximately 0.1 μM, which is as effective as amyloidogenic compounds such as Curcumin [25, 49, 109]. Further simulation analysis revealed that the electrostatic and vdW forces, rather than hydrogen bonding networks, are the key factors governing binding affinities of VK3 analogues to Aβ_{1-40}. The binding energies of Aβ_{1-40}–VK3

analogue complexes displayed a high correlation with the experimental aggregation rates. In conclusion, although most VK3 analogues did not protect cells against Aβ induced toxicity, both simulation and experimental results suggest that VK3-9 is a potent compound for preventing aggregation of amyloid peptides. Other VK3 analogues such as VK3-10 and VK3-6 could be further modified for potential use as therapeutic drugs to treat AD.

7.2 Materials and Methods

7.2.1 Computational methods

Docking of Vitamin K3 analogues to Aβ_{1-40}

The structure of Aβ_{1-40} monomer in water is generated using MD simulations that detail of this information is described in Chapter 4. These structures are initial of molecular docking. Docking information is expressed in Chapter 3. In particular, the exhaustiveness of global search was set to 400 and grid dimensions were 60x40x40 $\AA^3$.

The free binding energy was calculated using the MM-PBSA method (see Chapter 3 for more details).

7.2.2 Synthesis of vitamin K3 analogues

The synthesis procedures of vitamin K3 analogues shown in Fig. 7.5 are described elsewhere [263]. Analogues were kindly provided by Professor C. P. Chen of National Dong Hwa University.

7.2.3 Synthesis and purification of Aβ_{1-40}

Aβ_{1-40} was synthesized in a solid-phase peptide synthesizer (ABI 433A) using standard FMOC protocols with HMP resin. After cleavage from the resin with a mixture of trifluoroacetic acid/H_2O/ethanedithiol thiol anisole/phenol, the peptides were extracted with 1:1 (v:v) ether : H2O containing 0.1peptides were purified using a C18 reverse-phase column with a linear gradient from 0% – 78% acetonitrile. Peptide purity was over 95% as identified by matrix-assisted laser desorption/ionization-time of flight mass spectrometry as shown in Fig. 7.4. One milligram of Aβ_{1-40} peptide was dissolved in 1000 μl trifluoroethanol, and centrifuged (20,000 x g) to sediment the insoluble particles. This Aβ_{1-40} solution was then dried under N_2 gas and resuspended in 1000 μl phosphate buffer, pH 7.4, to provide a stock solution, and stored at -80^{0}C until used.

7.2.4 Free radical assay

The level of free radicals (H_2O_2) induced by Aβ_{1-40} in cell free conditions was analyzed using the DCFH-DA assay [264]. DCF-DA was deacetylated with 50% (v/v)

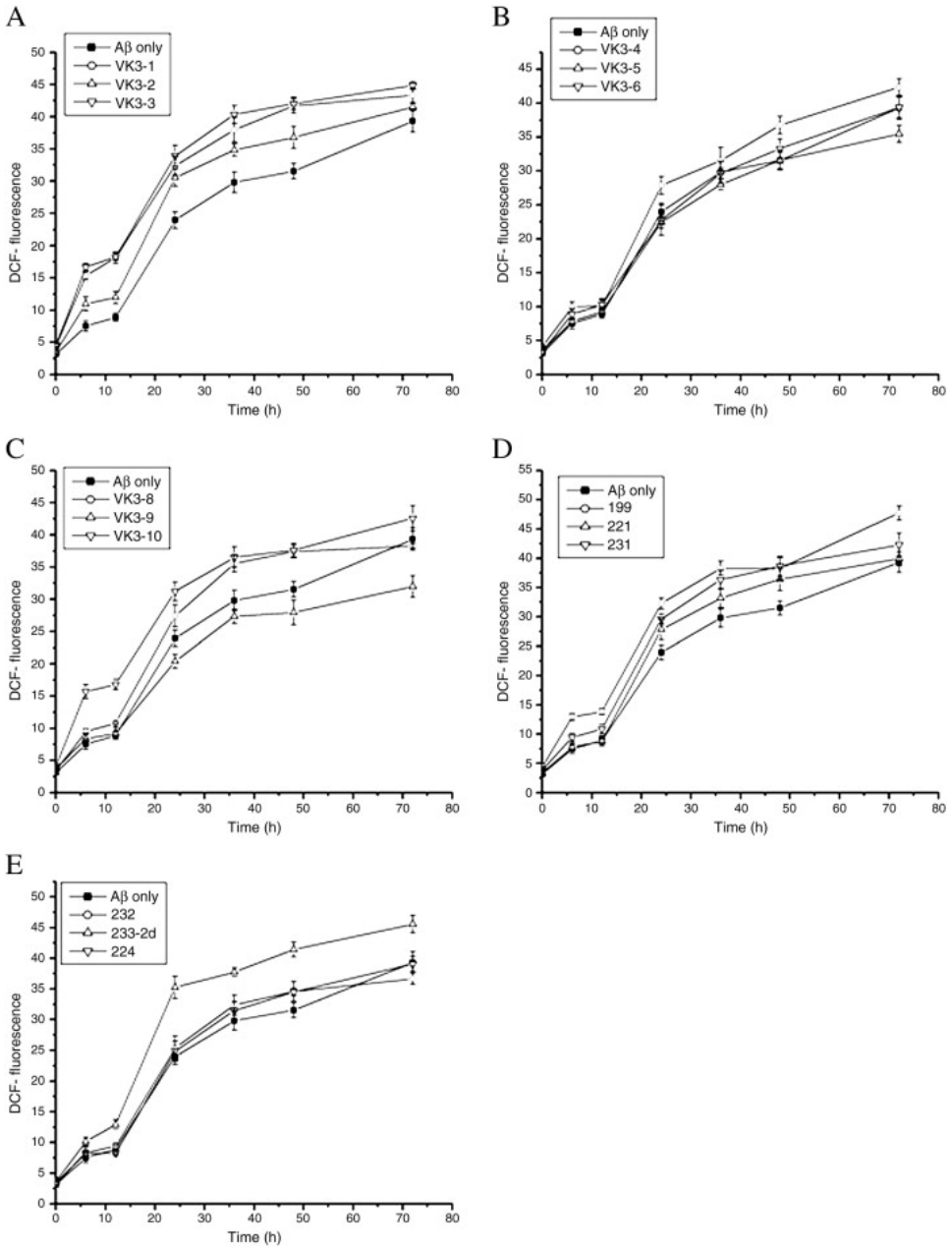

Figure 7.1 Characterization of free radical generation using DCF-fluorescence assay. The 25 μM of Aβ_{1-40} incubated at time-dependent with the 100 ng/ml of VK derivatives. (A) VK3-1, VK3-2 and VK3-3, (B) VK3-4, VK3-5 and VK3-6, (C) VK3-8, VK3-9 and VK3-10, (D) VK3-199, VK3-221 and VK3-231, (E) VK3-232, VK3-233-2d and VK3-224. In (A) to (E), 25 μM of A were used as control.

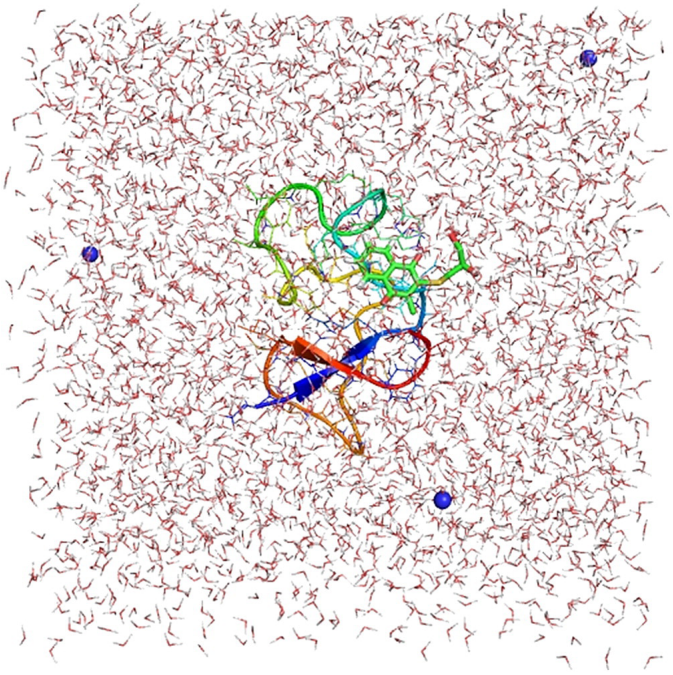

Figure 7.2 Representative snapshot of Aβ_{1-40} (structure 5 from Fig. 7.3) and VK3-9 complex in 5.2x5.2x5.2 nm^3 cubic box which contains about 3700 water molecules. Blue circles refer to three ions Na^+ that have been added to neutralize the system.

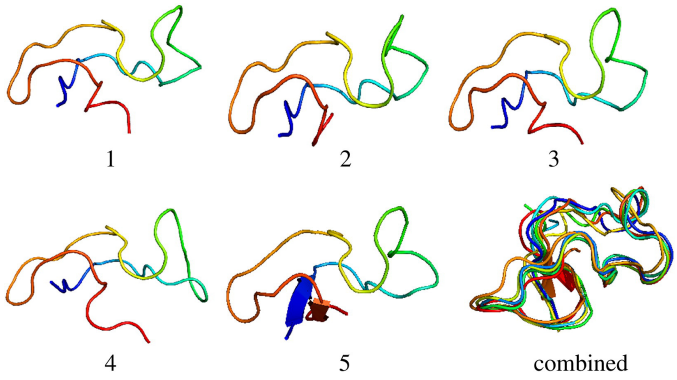

Figure 7.3 Five representative structures of Aβ_{1-40} in water environment generated from 300 ns MD simulations. They were used as structure model for docking of VK3 analogues to Aβ_{1-40}. Models 1-4 are 100% random coil, while model 5 has 17.5%β -structure and 82.5% coil. Structure 5 is the most probable having population of 84%. The superposition of 5 structures is also shown as combined.

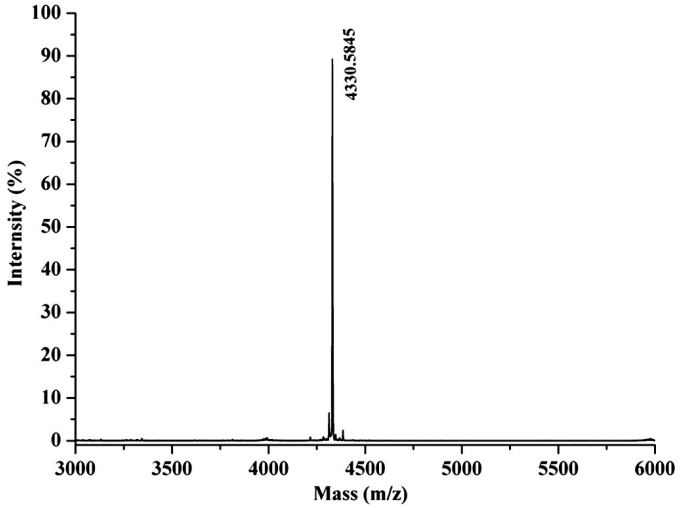

Figure 7.4 The mass spectrum of Aβ40. The theoretic mass of Aβ40 is 4329 Da, while the mass of Aβ_{1-40} shown in mass spectrum is 4330 Da, and the calculated molecular mass of Aβ_{1-40} is 4329 Da.

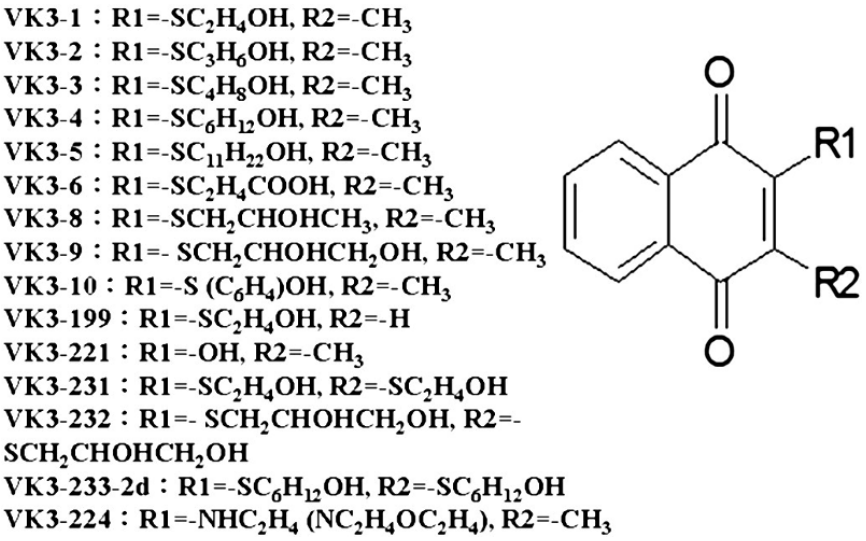

Figure 7.5 Structures of the synthesized VK3 analogues.

0.05 M NaOH for 30 min and neutralized (pH 7.5) to a final concentration of 200 μM as a stock solution. This stock solution was kept on ice in the dark until further use. The reactions were carried out in a 96-well plate (200 μl/well) containing 25 μM of Aβ_{1-40} diluted from the peptide stock solution, 20 μM deacetylated DCF, 5 μM horseradish peroxidase, in Dulbeccos phosphate-buffered saline, pH 7.5. To determine the inhibitory effects of VK3 analogues on inhibition of free radical formation, VK3 analogues with concentrations of 1–1000 ng/ml were added and incubated at 37^0C. Fluorescence readings were recorded on a microplate reader (FlexStation 3, MD) with the excitation wavelength of 485 nm and the emission wavelength of 530 nm. The fluorescence intensity of DCF (H_2O_2 level) was measured every 6 h and from 072 h.

7.2.5 Peptide aggregation assay

Thioflavin-T (ThT) was used to monitor the aggregation state of Aβ_{1-40}. Twenty five μM of Aβ_{1-40} was freshly diluted from peptide stock solution in phosphate buffer, pH 7.4, for peptide aggregation assay. All samples containing a peptide concentration of 25 μM in the absence and presence of 100 ng/ml VK3 analogues and 3 μM ThT were incubated at 37^0C. Samples containing either Aβ peptide only (as a control) or Aβ with VK3 analogues, taken daily from day 0 to day 7, were used to measure the ThT intensity. The fluorescence measurement was performed on a microplate reader (FlexStation 3, MD) at 37^0C. The excitation and emission wavelengths were 440 nm and 485 nm, respectively.

7.2.6 Cell cultures

Human blastoma SH-SY5Y cells were cultured in minimum essential medium supplemented with 10(v/v) antibiotic mixture comprised of penicillin and streptomycin. Cells were kept at 37^0C in a humidified atmosphere of 5% CO_2. SH-SY5Y cells were plated at a density of $1x10^5$ viable cells per well in 96-well plates for further analysis.

7.2.7 Cell viability assay

The cell viability was measured using the WST-1 assay [257]. Five hundred micromoles of Aβ_{1-40} peptide stock solution were initially prepared by dissolving 1 mg of Aβ_{1-40} in 1000 μl trifluoroethanol and centrifuging to sediment the insoluble particles. This peptide solution was dried under N2 gas, redissolved in dimethyl sulfoxide, and incubated at 4^0C for 12 h to provide the final peptide stock solution [265]. For the viability assay, $1x10^5$ cells were incubated in a 96-well microtiter plate containing either 25 μM incubated Aβ peptides only (as a positive control), diluted from the incubated peptide stock solution, or 25 μM incubated Aβ peptides, in the presence of VK3 analogues with concentrations ranging from 1–1000 ng/ml. The reaction was in a total volume of 200 μl per well for 24 h at 37^0C in a humidified atmosphere containing 5% CO_2 before cell viability was assayed. WST-1 solution (10 μl) was added to each well, and the wells were incubated for another 45 h at room temperature. The optical density was determined at 450 nm, using a microplate reader (FlexStation 3, MD).

7.2.8 Fourier-transform infrared (FT-IR) spectroscopy

To investigate the secondary structure of Aβ_{1-40} with or without VK3 analogues, a FT-IR spectrometer (Jasco, FT-IR/4100) equipped with an attenuated total reflection accessory was used to determine the conformation of Aβ_{1-40} during the aggregative process. One hundred microliters of 0.1 mM Aβ solution was coated on ZnSe crystals and dried overnight in a desiccator at room temperature. The spectra were recorded at 1500–1800 cm^{-1} with a 1 cm^{-1} interval. The peak was identified from the first derivation of the IR spectrum in the amide I region, and the secondary structure was analyzed using Original 6.0 software.

7.3 Results

7.3.1 Aβ_{1-40} aggregation in the presence and absence of VK3 analogues

Although VK3 is a well-known neurotoxic compound [266, 267], its structure also contains several features found in some anti-amyloidogenic compounds [150, 268, 269, 270] and in reactive oxygen species (ROS) scavenging compounds [271]. Therefore, 15 VK3 analogues, based on the fine structure of VK3 and shown in Fig. 7.5, were synthesized and used for numerical and experimental studies for their ability to inhibit the aggregation and neurotoxicity of Aβ_{1-40}.

The key hallmark of AD pathogenesis is the formation of toxic Aβ_{1-40} plaques in the brain of AD patients [148, 149]. Therefore, preventing or reducing the aggregation of Aβ has been the primary goal of a number of therapeutic strategies under development or in clinical trials [253, 254, 255]. In the present study, we examined the effects of VK3 analogues on the inhibition of Aβ aggregation using the Th-T fluorescence assay. Fig. 7.6 (A) shows the ratio of Th-T fluorescence intensity of Aβ_{1-40} with VK3 analogues/Aβ_{1-40} alone at day 5. As shown in Figure 7.6 (A), several VK3 analogues, including VK3-2, VK3-6, VK3-8, VK3-9, VK3-10, VK3-199, VK3-221, and VK3-224, were found to inhibit the aggregation of Aβ_{1-40}. Among these VK3 analogues, VK3-10, VK3-6, and VK3-9 were the most effective analogues for the inhibition of Aβ_{1-40} aggregation. In contrast, some VK3 analogues such as VK3-1, VK3-4, VK3-5, and VK3-233-2d, and especially VK3-4 and VK3-5 enhanced the aggregation of Aβ_{1-40}.

7.3.2 Secondary structure of Aβ_{1-40} in the presence and absence of VK3 analogues

In the aggregation process, the conformation of Aβ_{1-40} is converted from either helix or random coil into β-sheet. Results from the aggregation assay showed that several VK3 analogues can inhibit the aggregation of Aβ_{1-40}. Therefore, we examined these VK3 analogues to determine if they could also prevent the conformational change of Aβ_{1-40}. Fig. 7.8 (AD) show the FT-IR spectra for Aβ_{1-40} in the presence of several VK3 analogues at day 1 and day 5. The conformation of Aβ_{1-40} in the presence of

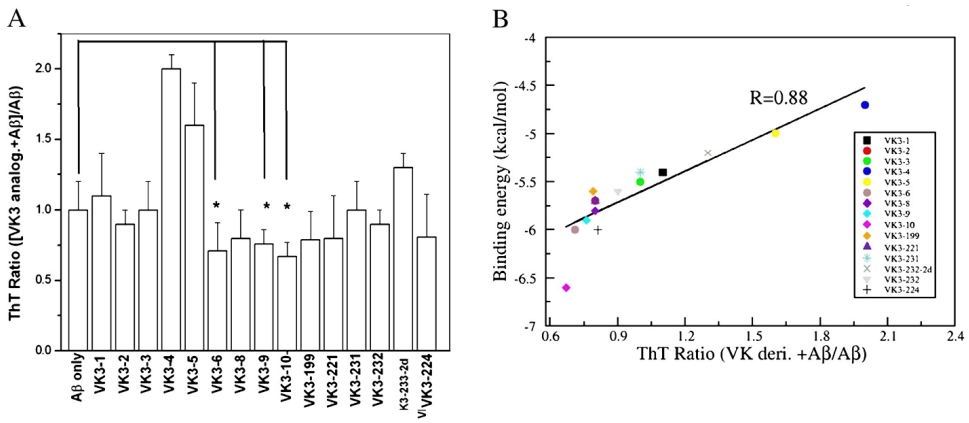

Figure 7.6 Aggregation profile for Aβ_{1-40} in the presence and absence of VK3 analogues. (A) Aggregation of Aβ_{1-40} in the presence and absence of VK3 analogues determined by using the ratio of Th-T fluorescence intensity of (Aβ_{1-40} + VK3 analogues)/(Aβ_{1-40}). The fluorescence intensity ratio presented here was obtained at day 5. VK3-2, VK3-6, VK3-8, VK3-9, VK3-10, VK3-199, VK3-221, VK3-232-2d, and VK3-224 are shown to effectively inhibit Aβ_{1-40} aggregation (*, $P < 0.05$). (B) Plot of correlation between the binding energy and aggregation index ($R = 0.88$).

several VK3 analogues, including VK3-2, VK3-6, VK3-8, VK3-9, VK3-10, VK3-199, VK3-221, and VK3-224, remained largely in a random coil conformation at both day 1 and day 5, as the 1650 cm^{-1} major peak was an indication of random coil. In contrast, the 1650 cm^{-1} peak that appeared in the FT-IR spectra of Aβ_{1-40} alone or in the presence of VK3-1, VK3-3, VK3-5, and VK3-232-2d at day 1 shifted to 1625 cm^{-1} at day 5. This indicated that Aβ_{1-40} converted to an extended β-sheet. These results were consistent with the Th-T aggregation assay, in which VK3-6, VK3-9, VK3-10, VK3-199, and VK3-221 inhibited the conformation change of Aβ_{1-40}.

7.3.3 Cell viability in the presence and absence of VK3 analogues

Since previous results showed that several VK3 analogues can prevent Aβ aggregation and conformation change, their effects on the Aβ induced toxicity were then examined by cell viability assay. Fig. 7.9 (A) shows the related cell viability in the presence of 100 ng/ml of VK3 analogue, incubated for 24 h. Unlike the results obtained in aggregation and secondary structural studies the results of Fig. 7.9 (A) showed that only VK3-9 effectively reduced Aβ induced cell death at concentrations < 100 ng/ml. Further analysis as depicted in Fig. 7.7 showed that, with VK3-9 the cell viability was affected in a dose-dependent manner. Cell survival rate was increased to 50% with 1 ng/ml VK3-9, to 88% with 100 ng/ml VK3-9, and to 92% with 1000 ng/ml VK3-9. For other VK3 analogues, including VK3-1, VK3-2, VK3-3, VK3-8, VK3-4, VK3-5, VK3-6, VK3-10, VK3-119, VK3-221, and VK3-231, the cell survival rate of SH-SY5Y cells was even much lower than in the presence of Aβ_{1-40} alone. The cell viability in the presence of these VK3 analogues were decreased with an increase of VK3 analogue concentration as depicted in Fig. 7.7. For VK3-232,

VK3-233-2d, and VK3-224, the cell viability showed no difference compared to that of 25 μM Aβ_{1-40} alone (as a positive control).

7.3.4 VK3 analogues attenuated Aβ_{1-40} induced free radical formation

For some VK3 analogues such as VK3-10, the results obtained from cell viability assays were consistent with that obtained from aggregation assays. Because the production of ROS by Aβ peptide has been proposed as one of the possible mechanisms causing cell death [148, 149, 257] , the role of VK3 analogues in free radical generation induced by Aβ_{1-40} was studied using the DCF assay. Fig. 7.10 (A) shows the DCF fluorescence intensity of Aβ_{1-40} alone and in the presence of 100 ng/ml VK3 analogues, when incubated for 36 h. In Fig. 7.10 (A), the DCF fluorescence intensity of Aβ_{1-40} in the presence of VK3-9 and VK3-5 was lower than the intensities with Aβ_{1-40} alone or with other VK3 analogues.

In comparison with the DCF intensity of Aβ_{1-40} alone, the DCF fluorescence intensity was decreased by 20% and 15% in the presence of 100 ng/ml VK3-9 and VK3-5, respectively, when incubated for 36 h. The intensity of DCF fluorescence was even further decreased as incubation time increased to 72 h. The DCF fluorescence intensity was further decreased by 25% and 40% for VK3-5 and VK3-9, at 72 h (Fig. 7.1), respectively, indicating that the free radical levels induced by Aβ peptides were effectively lowered by VK3-9 and VK3-5. The results obtained from free radical assays for VK3-9 are in agreement with the cell viability and aggregation assays, suggesting that the protection of SH-SY5Y cells against Aβ toxicity may be through the reduction of Aβ aggregation and subsequent induced free radical damage.

For the other VK3 analogues, the DCF fluorescence intensity of Aβ_{1-40} in the presence of VK3-1, VK3-2, VK3-3, VK3-8, VK3-10, VK3-199, VK3-231, and VK3-232-2d was even more pronounced than that of Aβ_{1-40} alone. This suggests that these VK3 analogues may be able to increase free radical levels. The DCF fluorescence intensity of Aβ_{1-40} in the presence of VK3-4 and VK3-6 was approximately equal to that of Aβ_{1-40} alone. This result could explain why VK3 analogues, such as VK3-10, prevent Aβ aggregation but fail to protect cells from Aβ induced cell toxicity due to the free radicals produced by these VK3 analogues.

7.3.5 Docking of VK3 analogues to Aβ_{1-40}

Experimental studies showed that VK3-9 was the only VK3 analogue capable of protecting SH-SY5Y cells against Aβ induced toxicity. Other VK3 analogues, such as VK3-10 also inhibited Aβ aggregation more effectively than VK3-9. Therefore, we further analyzed the binding affinities of VK3 analogues to Aβ, to determine if additional VK3 analogues could be used as treatments for AD.

For numerical studies, to mimic the conformation of monomeric Aβ, we simulated the monomeric Aβ_{1-40} structure in an aqueous environment (see Fig. 7.3) and used this representative structure as a model for further docking studies of VK3 analogues

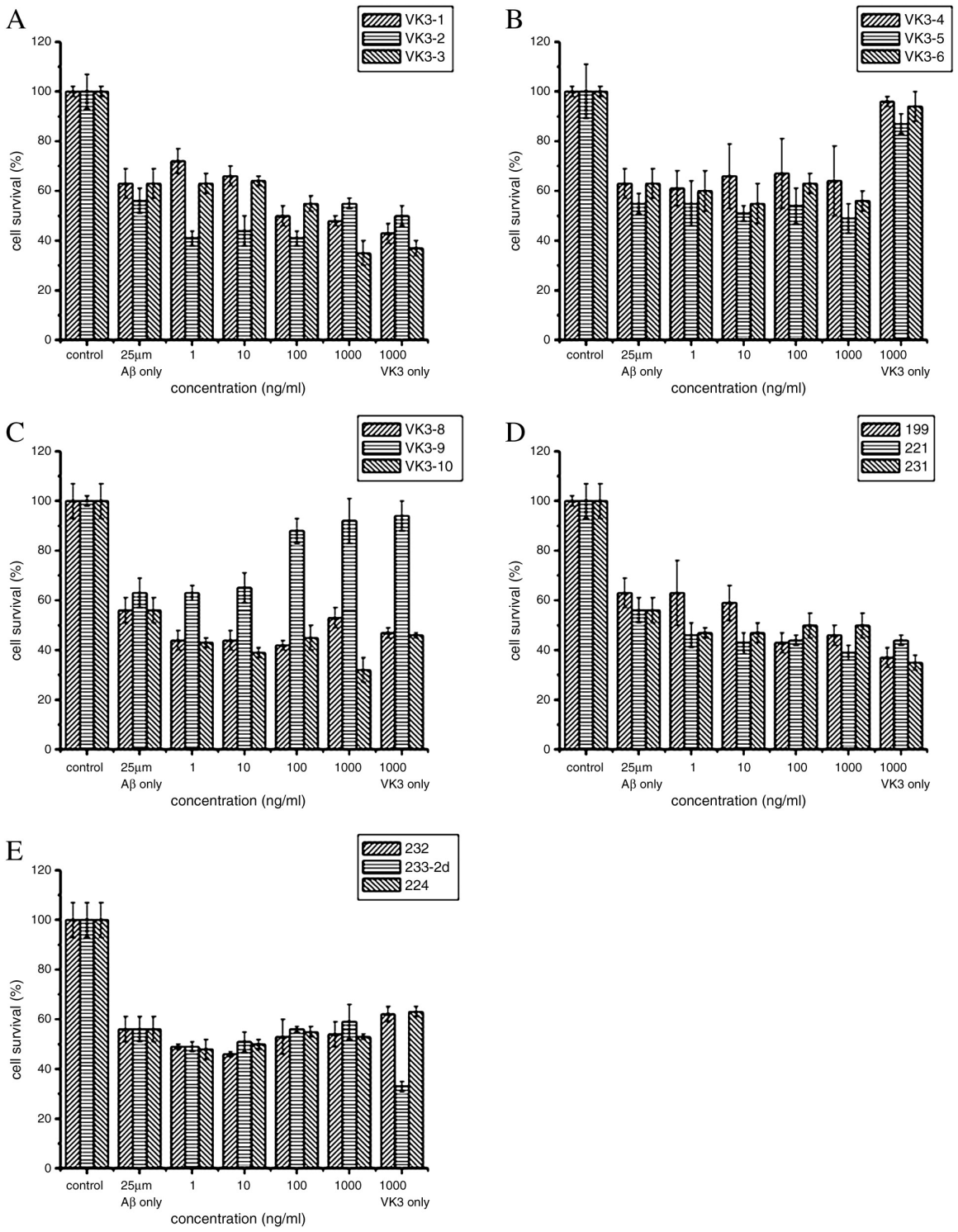

Figure 7.7 Relative cell viability assay assessed by WST-1 assay in different concentration of VK3 analogues. (A) VK3-1, VK3-2 and VK3-3, (B) VK3-4, VK3-5 and VK3-6, (C) VK3-8. VK3-9 and VK3-10, (D) VK3-199, VK3-221 and VK3-231, (E) VK3-232, VK3-233-2d and VK3-224. The first column in (A)-(E) represents the cell viability of cell only. The second column in (A)-(E) represents the cell viability of cell treated with 25 μM Aβ only. The third to sixth column in (A)-(E) represents the cell viability of cell treated with 25 μM Aβ and 1, 10 100 and 1000 ng/mL VK3 analogues. The seventh column represents the cell viability of cell treated with 1000 ng/mL VK3 analogues only.

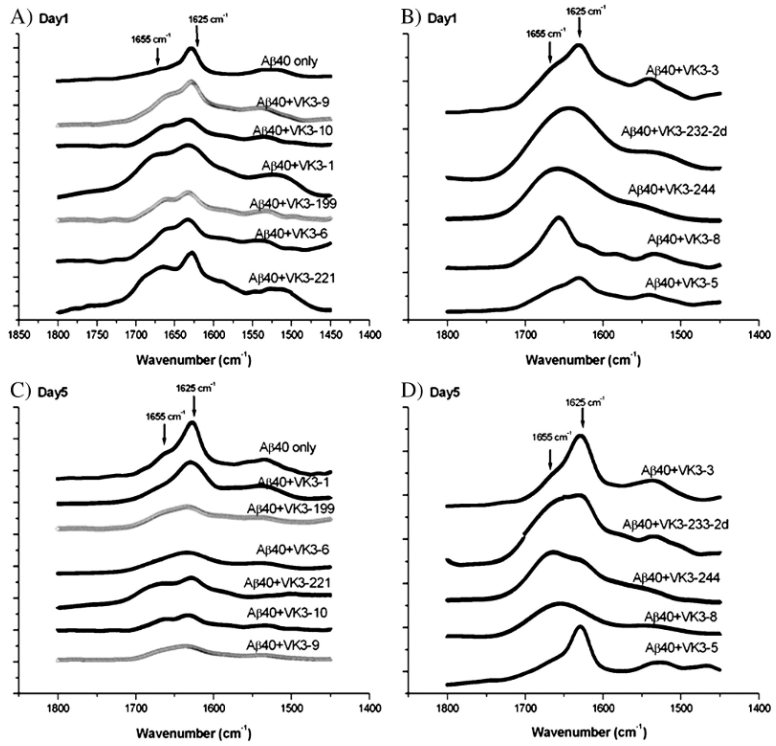

Figure 7.8 FT-IR spectra of 25 μM Aβ_{1-40} in the presence of various VK3 analogues at day 1, (A) and (B), and day 5, (C) and (D). The concentration of VK3 analogues is 100 ng/ml. The peak at 1625 cm^{-1} represents the characteristic of β-sheet conformation

VK3 analogues	ΔG_{bind} (kcal/mol)	Cell survival rate	Free radical generation	Aggregation percentage
VK3-1	-5.4	50	37.5	1.1
VK3-2	-5.7	40	40	0.8
VK3-3	-5.5	55	35	1
VK3-4	-4.7	70	32	2
VK3-5	-5	55	27.5	1.6
VK3-6	-6	65	28	0.71
VK3-8	-5.8	40	35	0.8
VK3-9	-5.9	95	25.5	0.76
VK3-10	-6.6	45	36	0.67
VK3-119	-5.6	40	37.5	0.79
VK3-221	-5.7	42	32.5	0.8
VK3-231	-5.4	50	36	1
VK3-232	-5.6	50	32.5	0.9
VK3-233-2d	-5.2	57	37.5	1.3
VK3-224	-6	55	32	0.81

Table 7.1 Binding free energies (in kcal/mol) of 15 VK3 analogues to Aβ_{1-40} peptide obtained by the docking method. Experimental results on cell survival rate, free radical generation, and aggregation percentages are also shown.

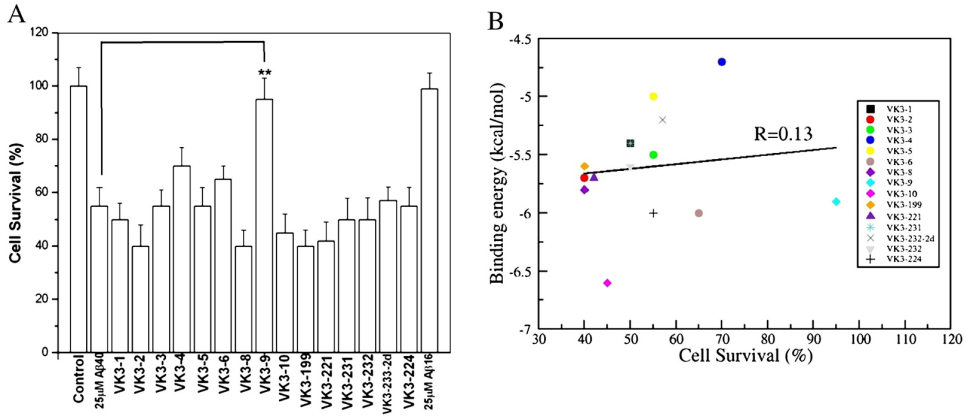

Figure 7.9 Cell viability assay for the toxicity induced by $A\beta_{1-40}$ in the presence and absence of VK3 analogues. (A) Relative cell viability assessed by WST-1 assay in 25 μM of $A\beta_{1-40}$ alone (as positive control) and in 25 μM of $A\beta_{1-40}$ in the presence of 100 ng/ml of VK3 analogues incubated for 24 h. In the last column, $A\beta_{1-16}$ which is not toxic to cells was used as a negative control. Results demonstrate that only VK3-9 effectively protect cells against $A\beta$-induced neurotoxicity (**, $P < 0.01$). (B) The correlation between the binding energy and cell survival rate (R = 0.13).

to $A\beta_{1-40}$. Fig. 7.12 shows the typical structure of $A\beta_{1-40}$ when binding with various VK3 analogues. The related binding energies are summarized in Table 1.

In general, there are two main VK3 binding pockets in $A\beta_{1-40}$. The first VK3 binding pocket is located at the central hydrophobic region around GLU 11–VAL 22, and the second binding pocket is located at the interface of the N- and C-terminus (Fig. 6). The VK3 analogues interacting at the first binding pocket include VK3-1, VK3-2, VK3-3, VK3-4, VK3-8, VK3-199, VK3-231, VK3-224, and VK3-232, whereas VK3-5, VK3-6, VK3-9, VK3-10, and VK3-221 may interact at the second binding pocket. The binding site of VK3-233-2d is close to the second binding site where it interacts with ASP1–PHE4 and ALA30–VAL40. Based on the calculated binding energies, the VK3 analogues located at the second binding pocket interact with $A\beta$ with a higher affinity than the VK3 analogues located at the first binding site.

Furthermore, the VK3 analogues located at the second binding pocket could be divided into two subgroups based on their binding energies. In general, the first subgroup bound to $A\beta$ with a higher affinity than the second group. The first subgroup includes VK3-10, VK3-6, VK3-9, and VK3-221, whereas VK3-5 and VK3-233-2d belong to the second subgroup. Moreover, the binding energy of VK3-10 is the lowest among all VK3 analogues, indicating that this analogue is bound most tightly to $A\beta$. VK3-10 is surrounded by six residues TYR10, GLU11, VAL12, PHE20, VAL36, and VAL40 which are mainly located in the very central hydrophobic region.

Further analysis of hydrogen bonding patterns for the four typical VK3 analogues, VK3-4, VK3-5, VK3-221, and VK3-10, with different binding energies, is shown in Table I. As shown in Fig. 7.15 (A) and (B), VK3-221 has the highest number of HBs, but its binding affinity is lower than that of VK3-10. VK3-4, VK3-5, and VK3-10 have the same number of HBs but their binding affinities are very different,

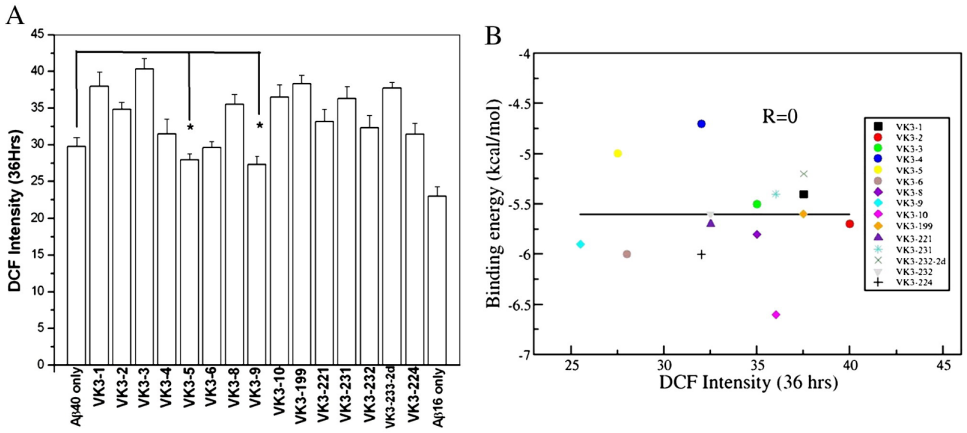

Figure 7.10 Free radical assay for Aβ_{1-40} in the presence and absence of VK3 analogues. (A) Characterization of free radical generation for either 25 μM of Aβ_{1-40} alone or 25 μM of Aβ_{1-40} in the presence of 100 ng/ml of VK3 analogues, assessed by DCF-fluorescence assay. In the last column, A1-16 which can not produce free radicals was used as a negative control. Both VK3-9 and VK3-5 inhibit the free radicals induced by Aβ_{1-40} (* = P $<$ 0.05). (B) The correlation between the binding energy and DCF intensity (R = 0.0).

suggesting that HBs alone are not the key factor governing the binding affinity of the VK3 analogues to Aβ_{1-40}. The fact that hydrogen bonding is not a key factor controlling binding affinity of VK3 analogues to Aβ peptides has been also observed in our previous study of β-sheet disrupting peptides [131].

To gain more insight into the binding affinity mechanisms of VK3 analogues to the aggregated form of Aβ, we performed docking studies of VK3 analogues to fibril forms of Aβ, using the structure previously reported, [272] as shown in Figure S8. As with the monomeric structure (Fig. 6), VK3 analogues have different binding positions in the best docking mode [Fig. 7.11 (A)]. The binding energies also displayed high correlation with the aggregation indices [Fig. 7.11 (B)] with correlation level R = 0.75. VK3-10 has the highest binding affinity, whereas VK3-9 is ranked fifth, suggesting that these compounds associate strongly with Aβ fibrils.

7.3.6 MM-PBSA simulation

To determine the binding properties, we computed the binding free energy ΔG_{bind} using the more accurate MM-PBSA method, which calculates several other energy terms. Because MM-PBSA simulation is very time-consuming, we only choose representative compounds VK3-221, VK3-2, VK3-6, VK3-9, and VK3-10 based on previous docking results, and focused on the last two compounds because VK3-10 has the strongest binding affinity, whereas VK3-9, as shown by our results, is the most promising compound.

MD simulations of various times were performed for VK3-221, VK3-2, VK3-6, VK3-9, and VK3-10. As shown in Figs. S6 and S7, the equilibrium of complexes were reached at different times when the interaction energies between VK3 analogues and

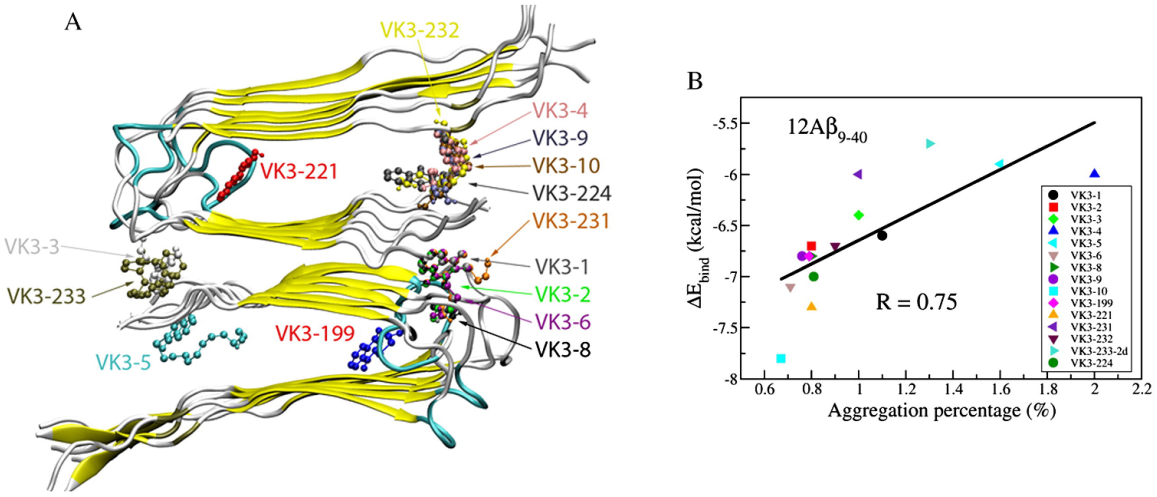

Figure 7.11 (A) The best docking positions of VK3 analogues to fibril A940 (PDB entry code 2LMO) [15]. Note that the first 8 residues of Aβ_{1-40} which are disordered are omitted in fibril construction. (B) The dependence of binding energies of VK3 analogues to fibril Aβ_{9-40} and the aggregation index (correlation level R = 0.75).

Aβ_{1-40} became saturated. As an example, for VK3-9, in trajectory 6 the system reached equilibrium within 22 ns, and the equilibration time was approximately 260 ns for the second trajectory (Fig. 7.13). A similar situation was also observed for VK3-10 (Fig. 7.14) and for other VK3 analogues (data not shown).

Snapshots collected in an equilibrium state were used to estimate ΔG_{bind} by the MM-PBSA method. The final results are shown in Table 2. In agreement with docking and experimental results, VK3-9 and VK3-10 have the lowest ΔG_{bind}, indicating that they have higher binding affinities than VK3-221, VK3-2, and VK3-6. With the exception of VK3-221, the entropic contributions are almost the same for the other VK3 analogues (Table 2). For VK3-6 and VK3-10, the contributions of vdW interactions dominated over that of electrostatic forces, and for VK3-9, VK3-221, and VK3-2, the VdW and electrostatic interactions had almost the same contributions. The nonpolar energies, ΔG_{sur},were not sensitive but this does not apply to the polar energies, ΔG_{PB}.

7.3.7 Correlation of binding energy and experimental properties

The correlation between binding energies and the experimental properties, such as aggregation index, free radical levels, and cell viability are shown in Figures 2 (B), 4 (B) and 5 (B). As shown, only the aggregation indices and binding energies show a good correlation, and there was no correlation between binding energies and free radical levels or cell viability. The correlation index, R value, of aggregation and binding energy was > 0.8, indicating that VK3 analogues bind to Aβ and inhibit aggregation.

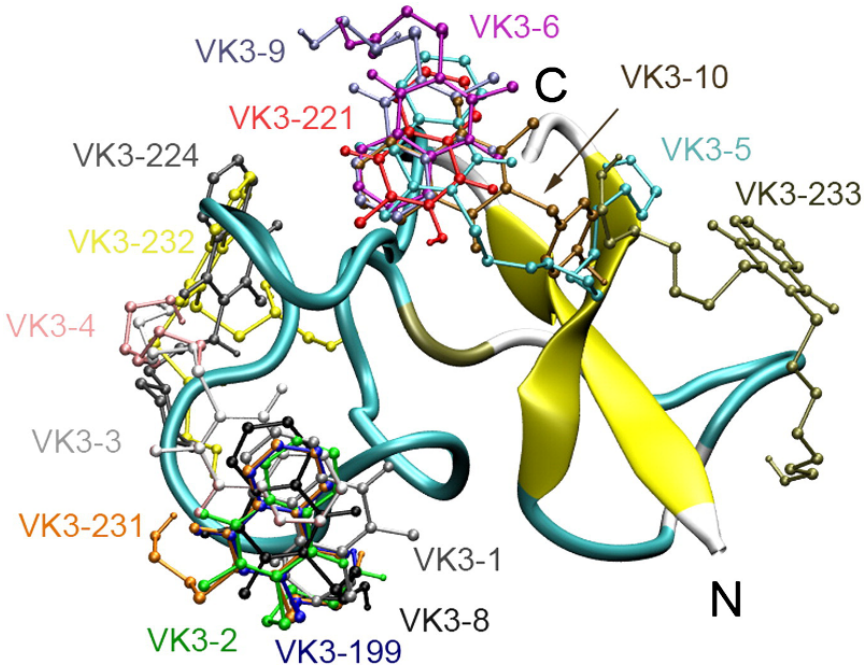

Figure 7.12 The best docking mode of VK3 analogue binding sites obtained using Model-5 of Aβ_{1-40}. The binding site residues which are close to VK3 analogues are listed as follows: VK3-1: GLU11, LEU17, VAL18, PHE19, and PHE20; VK3-2: GLU11, LEU17, VAL18, PHE19, PHE20, and ALA21; VK3-3: GLU11, VAL12, HIS13, HIS14, GLN15, LYS16, PHE19, and PHE20; VK3-4: TYR10, GLU11, VAL12, HIS13, HIS14, GLN15, LYS16, PHE19, and PHE20; VK3-5: TYR10, GLU11, VAL12, HIS13, GLN15, PHE20, VAL36, VAL39, and VAL40; VK3-6: SER8, TYR10, GLU11, VAL12, and HIS13; VK3-8: GLU11, LEU17, VAL18, PHE19, PHE20, and ALA21; VK3-9: SER8, TYR10, GLU11, VAL12, HIS13, and VAL40; VK3-10: TYR10, GLU11, VAL12, PHE20, VAL36, and VAL40; VK3-199: GLU11, LEU17, VAL18, PHE19, and PHE20; VK3-221: TYR10, GLU11,VAL12, HIS13, and PHE20; VK3-224: ASP7, HIS14, LYS16, LEU17, GLU22, ASP23, VAL24, and SER26; VK3-231: GLU11, LYS16, LEU17, VAL18, PHE19, PHE20, and ALA21; VK3-232: ASP7, HIS14, LYS16, LEU17, VAL18, GLU22, ASP23, VAL24, and SER26; VK3-233-2d: ASP1(N), ALA2, PHE4, TYR10, PHE20, ALA30, ILE31, ILE32, VAL36, GLY38, and VAL40

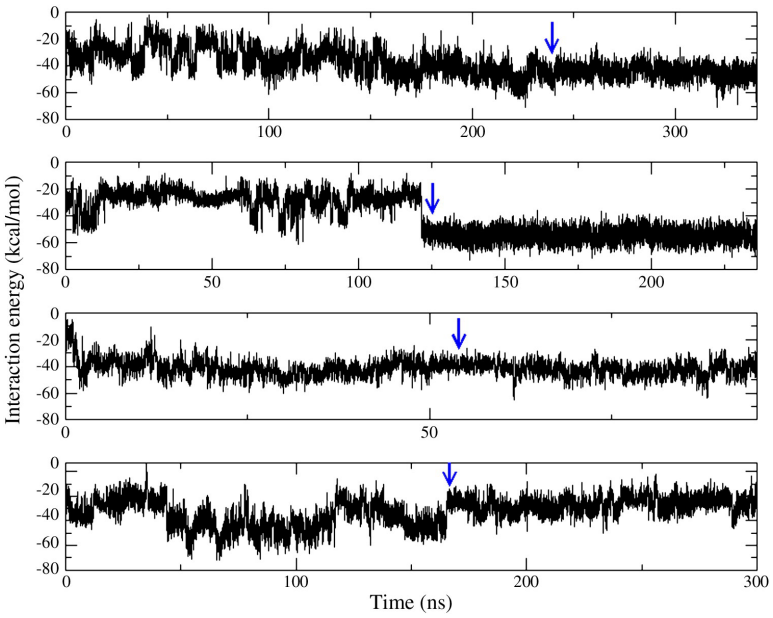

Figure 7.13 Time evolution of the interaction energies of Aβ_{1-40} peptide and VK3-9. Results are obtained for six MD trajectories. Arrows refer to time when the system reaches equilibrium.

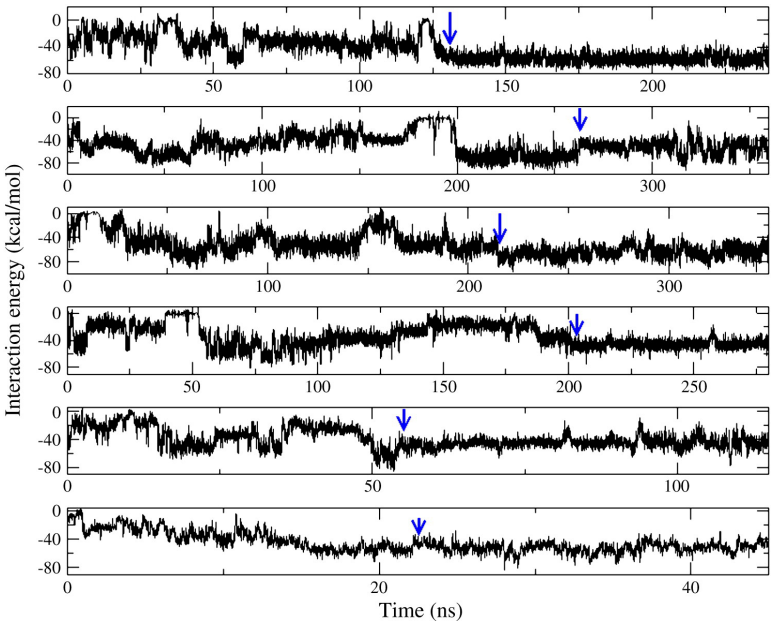

Figure 7.14 Time evolution of the interaction energies of Aβ_{1-40} peptide and VK3-10. Arrows refer to time when the system reaches equilibrium. Results have been obtained for 4 MD trajectories.

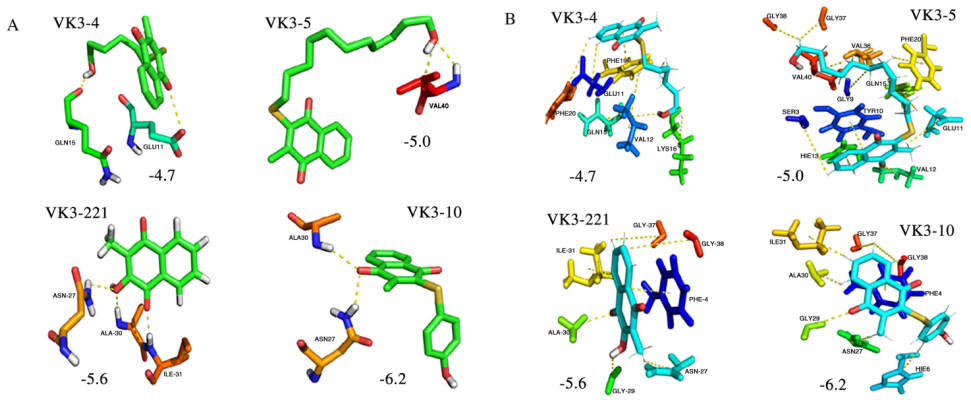

Figure 7.15 Typical HB networks (A) and SC contacts (B) for backbone of VK3-4, VK3-5, VK3-221, and VK3-10. There are 6, 12, 7, and 8 SC contacts for VK3-4, VK3-5, VK3-221, and VK3-10, respectively. Binding energies (in kcal/mol) are shown next to the depictions.

7.4 Discussion

ROS are major toxic species which damage neurons, induce cell death, and which are highly correlated with Aβ aggregation [148, 149, 257]. The development of anti-amyloidogenic and antioxidant agents has been the main target for the therapeutic treatment of AD. Numerous studies have focused on identifying effective compounds which inhibit the aggregation of monomeric Aβ or prevent formation of the ROS generated by Aβ [253, 255].

The deficiency of vitamin K has been demonstrated to be related to pathogenesis of AD [54, 273]. Supplementation of vitamin K may prevent AD [54, 273]. Therefore, based on previous studies [54, 273], we synthesized 15 VK3 analogues and determined their effects on Aβ induced neurotoxicity using numerical and experimental approaches. Our results show that several VK3 analogues such as VK3-10, VK3-9, and VK3-6 can strongly bind to Aβ_{1-40} and inhibit the aggregation of Aβ in vitro, but only VK3-9 has a protective effect by reducing Aβ induced toxicity. MD simulation studies show that VK3-10, VK3-9, and VK3-6 strongly interact with Aβ and possibly inhibit its aggregation.

The reason that most VK3 analogues failed to protect SH-Y5Y cells against Aβ induced neurotoxicity may be because most VK3 analogues can also produce free radicals and cause the death of these cells. It is interesting to note that VK3-4 and VK3-5 promoted the aggregation of Aβ_{1-40}. A possible reason for the effects of VK3-4 and VK3-5 on Aβ aggregation may be similar to that of Congo Red at low concentrations, which can enhance the aggregation of Aβ into fibrils [134]. However, a detailed mechanism will require further investigation.

For VK3-9, 100 ng/ml was sufficient to protect SH-Y5Y cells against Aβ induced toxicity, and cell survival rate was 90capable of inhibiting the free radical generation and aggregation of Aβ. The effective dose of VK3-9 for a 90which was comparable to the IC50 of Curcumin (0.19 0.98 μM) [25, 49, 109, 270]. The simulation of VK3 analogue docking to Aβ monomer suggests that there are two main VK3 binding sites. One is located at the central hydrophobic region, and the other is located at the

VK3 analogues	ΔE_{elec}	ΔE_{vdw}	ΔG_{sur}	ΔG_{PB}	$-T\Delta S$	ΔG_{bind}
VK3-221	-13.77±1.02	-17.05±2.59	-2.09±0.23	20.91±1.87	5.88±0.12	-6.12±3.25
VK3-2	-19.59±8.75	-21.76±5.37	-2.73±0.51	24.41±6.27	10.27±0.47	-9.41±6.30
VK3-6	41.66±22.0	-19.99±5.18	-2.49±0.55	-32.15±24.30	9.60±1.80	-3.37±3.72
VK3-9	-29.06±9.67	-27.75±3.29	-3.35±0.24	31.94±7.85	12.81±0.52	-15.41±3.44
VK3-10	-6.83±2.12	-29.31±6.32	-3.21±0.40	14.91±3.99	12.03±0.48	-12.42±3.87

Table 7.2 Binding free energies (in kcal/mol) of VK3 analogues to Aβ_{1-40} peptide obtained by the MM-PBSA method.

N- and C-terminal interfaces (Fig. 6). The strongest VK3 analogues, such as VK3-10 and VK3-9, interact with Aβ at both the central and C-terminal hydrophobic regions, indicating that the hydrophobic region may play a key role in the aggregation and toxicity of Aβ. In the case of mature fibrils, binding sites are more scattered when compared to the monomeric state (Fig. 7.11). However, VK3-9 and VK3-10 are located at the same position and this is also valid for the monomeric state (Fig. 6). It would be very interesting to verify our prediction on location of binding sites of VK3 analogues by experimental results. It is also important to stress that the simulation provides insights on the binding mechanism, suggesting that the binding of VK3 analogues to Aβ are mainly governed by vdW and electrostatic interactions and not by hydrogen bonding interactions. Knowledge of the contributions of each interaction strategy to binding affinity is very useful for designing new potential lead drugs for successful AD treatment. In this regard, MD simulation is a good complement to experiment tools for drug design.

The structural features of VK3 analogues are similar in configuration to other anti-amyloidogenic compounds such as Curcumin and myricetin, which contain aromatic moieties [23]. Furthermore, the interaction modes of VK3 analogues with Aβ are very similar to that of Curcumin binding to Aβ [134]. Recently, a study of the interaction of Aβ1-42 and Curcumin by solid state nuclear magnetic resonance indicated that Curcumin may interact with residues 12 and 17-21 of Aβ_{1-42} through an aromatic group [23].

The simulation models of VK3-10 and Aβ_{1-40} complexes as shown in Fig. 7.12 (B) also suggest a similar interaction mode as Curcumin and Aβ_{1-42}, in which VK3-9 and VK3-10 may interact with residues of SER8-PHE20 of Aβ_{1-40} and the aromatic carbons adjacent to the methoxy and/or hydroxy group known to form HBs with residues of Aβ_{1-40}.

Further MM-PBSA simulation also indicates that the binding affinities of these VK3 analogues are also comparable to Curcumin. The binding free energies for VK3-9 and VK3-10 are $\Delta G_{\text{bind}} = -15.41 \pm 3.44$ and -12.42 $\pm$ 3.87 kcal/mol (Table 2), respectively. Within error bars, ΔG_{bind} of VK3-9 and VK3-10 are the same as that obtained by MM-PBSA for Curcumin, with $\Delta G_{\text{bind}} = -14.3$ kcal/mol [50]. This value is very close to the experimental estimate $\Delta G_{\text{bind}} = -13.3$ kcal/mol [274]. Taken together, our numerical and experimental results show that VK3-9 and VK3-10 are as potent as Curcumin in preventing aggregation of Aβ, with inhibition constants of approximately a 0.1 μM range [109].

In conclusion, our present study shows that VK3-9 can effectively inhibit the aggregation of Aβ, reduce the free radicals produced by Aβ, and protect cells against Aβ induced toxicity. Although most VK3 analogues do not have protective effects for cells against Aβ induced toxicity, our simulation study indicates that some of the VK3 analogues, such as VK3-10, have a high potential for further development as anti-amyloidogenic drugs for AD treatment.

CONCLUSIONS

We have used Aβ monomer structures generated by MD simulations and fibril structures available in PDB as targets for designing potential candidates for treating AD. Combining the molecular docking, all-atom MD simulations and *in vitro* experiments for estimating binding affinities of small molecules we have made the following predictions:

- Compounds Dracorubin, Taraxerol, Taraxasterol, Hinokiflavone and Diosgenin derived from Vietnamese plants are good candidates for AD treatment because they have high propensity to blocking Aβ aggregation. The QSAR study shows that these compounds possess drug-like properties such as HIA, BBB, toxicity and metabolism.

- Our *in silico* and *in vitro* experiments revealed that vitamin K3 analogues VK3-6, VK3-8, VK3-9, VK3-10, and VK3-224 are good binders to both monomer and protofibril of Aβ peptides. But the most promising drug candidate for AD is VK3-9 which has no cytotoxicity.

- The FEP method in combination with Thioflavin-T fluorescence and TEM technique ascertain that anti-arrhythmic medication Propafenone is a potential drug for AD by inhibiting aggregation of Aβ peptide. Its efficiency is almost the same as Curcumin.

- Curcumin was found to bind to Aβ stronger than Naproxen and Ibuprofen. If the receptor is a monomer then naproxen and ibuprofen are bound to the same place that is different from the binding site of Curcumin. However, all these three compounds presumably have the same binding pocket in fibrils.

- Overall Aβ do not have well-defined binding sites but in the fibril case ligands prefer to locate near the turn region.

- For studied compounds the vdW interaction plays the dominant role in ligand binding except Propafenone for which the contributions of the vdW and electrostatic interactions are equal. Aromatic rings of ligands substantially stabilize protein-ligand complexes.

APPENDIX: List of abbreviations and symbols

Aβ	Amyloid beta
AD	Alzheimer's disease
ADME	Absorption distribution metabolism excretion
AMBER	Assisted Model Building with Energy Refinement
AM1-BCC	Semiempirical-bond charge corrections
ApoE	Apolipoprotein E
APP	Amyloid precursor protein
ATP	Adenosine triphosphate
BBB	Blood-brain barrier
BFGS	Broyden-Fletcher-Goldfarb-Shanno
CHARMM	Chemistry at Harvard macromolecular mechanics
DCF	Dichlorofluorescein
DCFH	Dichlorofluorescein diacetate
DSSP	Define secondary structure of proteins
EGCG	(-)-Epigallocatechin-3-Gallate
FDA	Food and Drug Administration
FEP	Free energy perturbation
HIA	Human intestinal absorption
HB	Hydrogen bond
GROMACS	Groningen machine for chemical simulations
GROMOS	Groningen molecular simulation
LINCS	Linear constraint solver
MD	Molecular dynamics
MOPAC	Molecular orbital package
MM-PBSA	Molecular mechanic-Poisson Boltzmann surface area
MTC	Methylthioninium chloride
NMR	Nuclear magnetic resonance
NPT	Isothermalisobaric ensemble
NSAID	Nonsteroidal anti-inflammatory drugs
NVT	Canonical ensemble
OPLS	Optimized potentials for liquid simulations
PDB	Protein data bank
PME	Particle-Mesh Ewald
REMD	Replica exchange molecular dynamics
RMSD	Root-mean-square deviation
SASA	Solvent accessible surface are
SC	Side chain
SPC	Simple point charge
STRIDE	Structural identification
TEM	Transmission electron microscope
TIP3P	Transferable intermolecular potential 3 point
vdW	van der Waals

Bibliography

[1] Henderson, A. S., and Jorm, A. F. *Definition, and Epidemiology of Dementia: A Review, in Dementia (eds M. Maj and N. Sartorius).* John Wiley & Sons, Ltd, Chichester, UK, 2002.

[2] Alzheimer's_association. Alzheimer's disease facts and figures 2014.

[3] Greene, J. D. W., Baddeley, A. D., and Hodges, J. R. Analysis of the episodic memory deficit in early Alzheimer's disease: Evidence from the doors and people test. *Neuropsychologia 34*, 6 (1996), 537–551.

[4] Price, B. H., Gurvit, H., Weintraub, S., Geula, C., Leimkuhler, E., and Mesulam, M. Neuropsychological patterns and language deficits in 20 consecutive cases of autopsy-confirmed Alzheimer's disease. *Arch. Neuro. 50*, 9 (1993), 931–937.

[5] Esteban-Santillan, C., Praditsuwan, R., Ueda, H., and Geldmacher, D. S. Clock drawing test in very mild Alzheimer's disease. *J. Am. Geriatr. Soc. 46*, 10 (1998), 1266–1269.

[6] Herrup, K. The case for rejecting the amyloid cascade hypothesis. *Nat. Neuro. 18*, 6 (2015), 794–799.

[7] Hardy, J., and Selkoe, D. J. The amyloid hypothesis of Alzheimer's disease: Progress and problems on the road to therapeutics. *Science 297*, 5580 (2002), 353–356.

[8] Alonso, A., Zaidi, T., Novak, M., Grundke-Iqbal, I., and Iqbal, K. Hyperphosphorylation induces self-assembly of tau into tangles of paired helical filaments/straight filaments. *Proc. Natl. Acad. Sci. 98*, 12 (2001), 6923–6928.

[9] Citron, M. Strategies for disease modification in Alzheimer's disease. *Nat. Rev. Neurosci. 5* (2004), 677–685.

[10] Aguzzi, A., and O'Connor, T. Protein aggregation diseases: pathogenicity and therapeutic perspectives. *Nat. Rev. Dru. 9* (2010), 237–248.

[11] Eanes, E. D., and Glenner, G. G. X-ray diffraction studies on amyloid filaments. *J. Histochem. Cytochem. 16* (1968), 673–677.

[12] Kirschner, D. A., Abraham, C., and Selkoe, D. J. X-ray-diffraction from intraneuronal paired helical filaments and extraneuronal amyloid fibers in Alzheimers-disease indicates cross-beta conformation. *Proc. Natl. Acad. Sci. USA 83* (1986), 503–507.

[13] Petkova, A. T., Ishii, Y., Balbach, J., Antzutkin, O., Leapman, R., Delaglio, F., and Tycko, R. A structural model for Alzheimer's beta-amyloid fibrils based on experimental constraints from solid state nmr. *Proc. Natl. Acad. Sci. USA 99* (2002), 16742–16747.

[14] Luhrs, T., Ritter, C., Adrian, M., Riek-Loher, D., Bohrmann, B., Doeli, H., Schubert, D., and Riek, R. 3d structure of Alzheimer's amyloid-beta(1-42) fibrils. *Proc. Natl. Acad. Sci. USA 102* (2005), 17342–17347.

[15] Kayed, R., Head, E., Thompson, J. L., McIntire, T. M., Milton, S. C., Cotman, C. W., and Glabe, C. G. Common structure of soluble amyloid oligomers implies common mechanism of pathogenesis. *Science 300* (2003), 486–489.

[16] Caughey, B., and Lansbury, P. T. Protofibrils, pores, fibrils, and neurodegeneration: Separating the responsible protein aggregates from the innocent bystanders. *Annu. Rev. Neurosci. 26* (2003), 267–298.

[17] Chiti, F., and Dobson, C. M. Protein misfolding, functional amyloid, and human disease. *Annual Rev. Biochemistry 75* (2006), 333–366.

[18] Nasica-Labouze, J., Nguyen, P. H., Sterpone, F., Berthoumieu, O., Buchete, N.-V., CotÃl', S., De Simone, A., Doig, A. J., Faller, P., Garcia, A., Laio, A., Li, M. S., Melchionna, S., Mousseau, N., Mu, Y., Paravastu, A., Pasquali, S., Rosenman, D. J., Strodel, B., Tarus, B., Viles, J. H., Zhang, T., Wang, C., and Derreumaux, P. Amyloid β protein and Alzheimer's disease: When computer simulations complement experimental studies. *Chem. Rev. 115*, 9 (2015), 3518–3563.

[19] Li, H. Y., Monien, M. B., Lomakin, A., Zemel, R., Fradinger, E. A., Tan, M. A., Spring, S. M., Urbanc, B., Xie, C. W., Benedek, G. B., and Bitan, G. Mechanistic investigation of the inhibition of a beta 42 assembly and neurotoxicity by a beta 42 c-terminal. *Biochemistry 49* (2010), 6358–6364.

[20] Wu, C., Murray, M. M., Summer, S. L. B. L., Condron, M. M., Bitan, G., Shea, J. E., and Bowers, M. T. The structure of a beta 42 c-terminal fragments probed by a combined experimental and theoretical study. *J. Mol. Biol. 387* (2009), 492–501.

[21] Tjerngber, L. O., Naslund, J., Lindqvist, F., Jahannson, J., Karlstrom, A. R., Thyberg, J., Terenius, L., and Nordstedt, C. Arrest of beta-amyloid beta-peptide fibril formation by a pentapeptide. *J. Biol. Chem. 271* (1996), 8545–8548.

[22] Ngo, S. T., and Li, M. S. Top-leads from natural products for treatment of Alzheimer's disease: docking and molecular dynamics study. *Molecular Simulation 39* (2013), 279–291.

[23] Ngo, S. T., and Li, M. S. Curcumin binds to aβ_{1-40} peptides and fibrils stronger than ibuprofen and naproxen. *J. Phys. Chem. B 116*, 34 (2012), 10165–10175.

[24] Viet, M. H., Chen, C.-Y., Hu, C.-K., Chen, Y.-R., and Li, M. S. Discovery of dihydrochalcone as potential lead for Alzheimer's disease: *in silico* and *in vitro* study. *PLoS ONE 8*, 11 (11 2013), e79151.

[25] Yang, F. S., Lim, G. P., Begum, A. N., Ubeda, O. J., Simmons, M. R., Ambegaokar, S. S., Chen, P. P., Kayed, R., Glabe, C. G., Frautschy, S. A., and Cole, G. M. Curcumin inhibits formation of amyloid beta oligomers and fibrils, binds plaques, and reduces amyloid in vivo. *J. Biol. Chem. 280*, 7 (2005), 5892–5901.

[26] Bastianetto, S., Yao, Z. X., Papadopoulos, V., and Quirion, R. Neuroprotective effects of green and black teas and their catechin gallate esters against beta-amyloid-induced toxicity. *Eur J Neurosci 23* (2006), 55–64.

[27] DeKosky, S. T. Ginkgo biloba prevention trial in order individuals. Tech. rep., National Center for Complementary and Alternative Medicine, http://www.clinicaltrials.gov/ct2/show/NCT00010803, 2010.

[28] Yatin, S. M., Yatin, M., Varadarajan, S., Ain, K.B., and Butterfield, D.A. Role of spermine in amyloid beta-peptide-associated free radical-induced neurotoxicity. *J. Neurosci Res. 63*, 5 (2001), 395–401.

[29] Dolphin, G. T., Chierici, S., Ouberai, M., Dumy, P., and Garcia, J. A multimeric quinacrine conjugate as a potential inhibitor of Alzheimer's beta-amyloid fibril formation. *Chembiochem 9*, 6 (2008), 952–963.

[30] Bush, A. I. Metal complexing agents as therapies for Alzheimer's disease. *Neurobiol. Aging 23* (2002), 1031–1038.

[31] Evans, C. G., Wisen, S., and Gestwicki, J. E. Heat shock proteins 70 and 90 inhibit early stages of amyloid beta aggregation in vitro. *J. Biol. Chem. 281*, 44 (2006), 33182–33191.

[32] Schenk, D., Barbour, R., Dunn, W., Gordon, G., Grajeda, H., Guido, T., Hu, K., Huang, J., Johnson-Wood, K., Khan, K., Kholodenko, D., Lee, M., Liao, Z., Lieberburg, I., Motter, R., Mutter, L., Soriano, F., Shopp, G., Vasquez, N., Vandevert, C., Walker, S., Wogulis, M., Yednock, T., Games, D., and Seubert, P. Immunization with amyloid-beta attenuates Alzheimer-disease-like pathology in the pdapp mouse. *Nature 400*, 6740 (1999), 173–177.

[33] Svennerholm, L. Gangliosides-a new therapeutic agent against stroke and Alzheimer's disease. *Life Sci. 55* (1994), 2125–2134.

[34] Castillo, G. M., Ngo, C., Cummings, J., Wight, T. N., and Snow, A. D. Perleacan binds to the beta-amyloid proteins (aβ) of Alzheimer's disease, accelerate abeta fibril formation, and maintains abeta fibril stability. *J. Neurochem. 69* (1997), 2452–2465.

[35] Nitz, M., Fenili, D., Darabie, A., Wu, L., Cousins, J., and McLaurin, J. Modulation of amyloid-beta aggregation and toxicity by inosose stereoisomers. *FEBS J. 275* (2008), 1663–1674.

[36] Takahashi, T., Tada, K., and Mihara, H. Rna aptamers selected against amyloid beta-peptide (abeta) inhibit the aggregation of abeta. *Molecular Biosystems 5* (2009), 986–991.

[37] Coskuner, O., and Murray, I. V. J. Adenosine triphosphate (atp) reduces amyloid-beta protein misfolding in vitro. *J Alzheimers Dis 41* (2014), 561–574.

[38] Wang, J., Ono, K., Dickstein, D. L., Arrieta-Cruz, I., Zhao, W., Qian, X., Lamparello, A., Subnani, R., Ferruzzi, M., Pavlides, C., Ho, L., Hof, P. R., Teplow, D. B., and Pasinetti, G. M. Carvedilol as a potential novel agent for the treatment of Alzheimer's disease. *Neurobiol Aging 32*, 12 (2011), 2321.e1 – 2321.e12.

[39] Paris, D., Quadros, A., Humphrey, J., Patel, N., Crescentini, R., and Fiona. Nilvadipine antagonizes both abeta vasoactivity in isolated arteries, and the reduced cerebral blood flow in {APPsw} transgenic mice. *Brain Res. 999*, 1 (2004), 53 – 61.

[40] Grover, S., Apushkin, M., and Fishman, G. Topical dorzolamide for the treatment of cystoid macular edema in patients with retinitis pigmentosa. *Am. J. Ophthalmol. 141*, 5 (2006), 850–858.

[41] von Itzstein, M., Wu, W.-Y., Kok, G. B., Pegg, M. S., Dyason, J. C., Jin, B., Phan, T. V., Smythe, M. L., White, H. F., Oliver, S. W., Colman, P. M., Varghese, J. N., Ryan, D. M., Woods, J. M., Bethell, R. C., Hotham, V. J., Cameron, J. M., and Penn, C. R. Rational design of potent sialidase-based inhibitors of influenza virus replication. *Nature 363*, 6428 (1993), 418–423.

[42] Boolell, M., Allen, M. J., Ballard, S. A., Gepi-Attee, S., Muirhead, G. J., Osterloh, I. H., and Gingell, C. Sildenafil: an orally active type 5 cyclic gmp-specific phosphodiesterase inhibitor for the treatment of penile erectile dysfunction. *Int. J. Impot. Res. 8*, 2 (1996), 47–52.

[43] Shen, C.-H., Wang, Y.-F., Kovalevsky, A. Y., Harrison, R. W., and Weber, I. T. Amprenavir complexes with hiv-1 protease and its drug-resistant mutants altering hydrophobic clusters. *FEBS Journal 277*, 18 (2010), 3699–3714.

[44] Madrid, P. B., Chopra, S., Manger, I. D., Gilfillan, L., Keepers, T. R., Shurtleff, A. C., Green, C. E., Iyer, L. V., Dilks, H. H., Davey, R. A., Kolokoltsov, A. A., Carrion, Jr, R., Patterson,

J. L., Bavari, S., Panchal, R. G., Warren, T. K., Wells, J. B., Moos, W. H., Burke, R. L., and Tanga, M. J. A systematic screen of fda-approved drugs for inhibitors of biological threat agents. *PLoS ONE 8*, 4 (04 2013), e60579.

[45] Sara Varea. Atp in Alzheimer disease. in: Clinicaltrials.gov [internet]. bethesda (md): National library of medicine (us). 2000- [cited 2015 mar 04], 2014. NLM Identifier: NCT02279511.

[46] Johns Hopkins University and Icahn School of Medicine at Mount Sinai. Trial of carvedilol in Alzheimer's disease. in: Clinicaltrials.gov [internet]. bethesda (md): National library of medicine (us). 2000- [cited 2015 mar 04]): National library of medicine (us). 2000- [cited 2015 mar 04], 2014. NLM Identifier: NCT01354444.

[47] Lawlor, B. A phase iii trial of nilvadipine to treat Alzheimer's disease (nilvad). in: Clinicaltrials.gov [internet]. bethesda (md): National library of medicine (us). 2000- [cited 2015 mar 04]. NLM Identifier: NCT02017340.

[48] Loi, D. T. *Medical plants and medicines of Vietnam (in Vietnamese).* Medicine Publisher, Ha Noi, 2004.

[49] Porat, Y., Abramowitz, A., and Gazit, E. Inhibition of amyloid fibril formation by polyphenols: Structural similarity and aromatic interactions as a common inhibition mechanism. *Chem. Biol. Drug Des. 67*, 1 (2006), 27–37.

[50] Ryu, E. K., Choe, Y. S., Lee, K. H., Choi, Y., and Kim, B. T. Curcumin and dehydrozingerone derivatives: Synthesis, radiolabeling, and evaluation for beta-amyloid plaque imaging. *J. Med. Chem. 49* (2006), 6111–6119.

[51] Schrodinger, L. Small-molecule drug discovery suite 2010: Qikprop version 3.3, 2010. New York, NY.

[52] Ngo, S. T., Fang, S. T., Huang, S. H., Chou, C. L., Li, M. S., and Chen, Y. C. Anti-arrhythmic medication Propafenone is potential drug for Alzheimers disease by inhibiting aggregation of amyloid beta peptide: *in silico* and *in vitro* studies. *Sci. Rep.* (2015), *submitted*.

[53] Liu, Chia-Chan and Kanekiyo, Takahisa and Xu, Huaxi and Bu, G. Apolipoprotein E and Alzheimer disease: risk, mechanisms and therapy. NATURE REVIEWS NEUROLOGY, 9 (2013), 106-118.

[54] Allison, A. The possible role of vitamin k deficiency in the pathogenesis of Alzheimer's disease and in augmenting brain damage associated with cardiovascular disease. *Med. Hypotheses 57*, 2 (2001), 151 – 155.

[55] Ringman, J. M., Frautschy, S. A., Cole, G. M., Masterman, D. L., and Cummings, J. L. A potential role of the curry spice curcumin in Alzheimer's disease. *Curr Alzheimer Res 2* (2005), 131–136.

[56] Cole, G. M., and Frautschy, S. A. Mechanisms of action of non-steroidal anti-inflammatory drugs for the prevention of Alzheimer's disease. *CNS Neuro Disord Drug Targets 9* (2010), 140–148.

[57] Raman, E. P., Takeda, T., and Klimov, D. K. Molecular dynamics simulations of ibuprofen binding to a beta peptides. *Biophys. J. 97* (2009), 2070–2079.

[58] Kim, S., Chang, W. E., Kumar, R., and Klimov, D. K. Naproxen interferes with the assembly of a beta oligomers implicated in Alzheimer's disease. *Biophys. J 100* (2011), 2024–2032.

[59] Agdeppa, E. D., Kepe, V., Petric, A., Satyamurthy, N., Liu, J., Huang, S. C., Small, G. W., Coled, G. M., and Barrio, J. R. In vitro detection of (s)-naproxen and ibuprofen binding to plaques in the Alzheimer's brain using the position emission tomography molecular imaging probe 2-(1-6-[(2-[18F]fluoroethyl)(methyl)amino]-2-naphthylethylidene)malononitrile. *Neuroscience 117* (2003), 723–730.

[60] Cummings, J. L. Alzheimer's disease. *N. Engl J. of Med. 351* (2004), 56–67.

[61] Galasko, D., Bennett, D., Sano, M., Ernesto, C., Thomas, R., Grundman, M., and Ferris, S. An inventory to assess activities of daily living for clinical trials in Alzheimer's disease. the Alzheimer's disease cooperative study. *Alzheimer Dis Assoc Disord. 11* (1997).

[62] Selkoe, D. J. Alzheimer's disease is a synaptic failure. *Science 298*, 5594 (2002), 789–791.

[63] Masliah, E., Mallory, M., Alford, M., DeTeresa, R., Hansen, L., McKeel, W., and Morris, J. Altered expression of synaptic proteins occurs early during progression of Alzheimer's disease. *Neurology 56* (2001).

[64] DeKosky, S. T. and Scheff, S. W. Synapse loss in frontal cortex biopsies in Alzheimer's disease: correlation with cognitive severity. *Ann. Neurol. 27* (1990).

[65] Terry, R., Masliah, E., Salmon, D., Butters, N., DeTerasa, R., Hill, R., Hansen, L., and Katzman, R. Physical basis of cognitive alterations in Alzheimer's disease: synapse loss is the major correlate of cognitive impairment. *Ann. Neurol. 30* (1991).

[66] Davies, C., Mann, D., Sumpter, P., and Yates, P. A quantitative morphometric analysis of the neuronal and synaptic content of the frontal and temporal cortex in patients with Alzheimer's disease. *J. Neuro. Sci. 78*, 2 (1987), 151–164.

[67] Masliah, E., Crews, L., and Hansen, L. Synaptic remodeling during aging and in Alzheimer's disease. *J. Alzheimers Dis 9* (2006), 91–99.

[68] Bulic, B., Pickhardt, M., Schmidt, B., Mandelkow, E.-M., Waldmann, H., and Mandelkow, E. Development of tau aggregation inhibitors for Alzheimer's disease. *Angew. Chem. Int. Ed. 48*, 10 (2009), 1740–1752.

[69] Khlistunova, I., Biernat, J., Wang, Y., Pickhardt, M., von Bergen, M., Gazova, Z., Mandelkow, E., and Mandelkow, E.-M.

Inducible expression of tau repeat domain in cell models of tauopathy: Aggregation is toxic to cells but can be reversed by inhibitor drugs. *J. Biol. Chem. 281*, 2 (2006), 1205–1214.

[70] SantaCruz, K., Lewis, J., Spires, T., Paulson, J., Kotilinek, L., Ingelsson, M., Guimaraes, A., DeTure, M., Ramsden, M., McGowan, E., Forster, C., Yue, M., Orne, J., Janus, C., Mariash, A., Kuskowski, M., Hyman, B., Hutton, M., and Ashe, K. H. Tau suppression in a neurodegenerative mouse model improves memory function. *Science 309*, 5733 (2005), 476–481.

[71] Querfurth, H. W., and Laferla, F. M. Mechanisms of disease Alzheimer's disease. *N. Eng J. Med 362* (2010), 329–344.

[72] Rapoport, M., Dawson, H. N., Binder, L. I., Vitek, M. P., and Ferreira, A. Tau is essential to beta-amyloid-induced neurotoxicity. *Proc. Natl. Acad. Sci. USA 99*, 9 (2002), 6364–6369.

[73] Hardy, J. and Allsop, D. Amyloid deposition as the central event in the aetiology of Alzheimer's disease. *Trends. Pharmacol. Sci. 12*, 10 (1991), 383–388.

[74] Walsh, D. M., and Selkoe, D. J. A beta oligomers a decade of discovery. *J. Neurochem. 101*, 5 (2007), 1172–1184.

[75] Bernstein, S. L., Dupuis, N. F., Lazo, N. D., Wyttenbach, T., Condron, M. M., Bitan, G., Teplow, D. B., Shea, J.-E., Ruotolo, B. T., Robinson, C. V., and Bowers, M. T. Amyloid-beta protein oligomerization and the importance of tetramers and dodecamers in the aetiology of Alzheimer's disease. *Nat. Chem. 1*, 4 (2009), 326–331.

[76] Priller, C., Bauer, T., Mitteregger, G., Krebs, B., Kretzschmar, H., and Herms, J. Synapse formation and function is modulated by the amyloid precursor protein. *J. Neurosci. 26*, 27 (2006), 7212–7221.

[77] Coles, M., Bicknell, W., Watson, A. A., Fairlie, D. P., and Craik, D. J. Solution structure of amyloid beta-peptide(1-40) in a water-micelle environment. is the membrane-spanning domain where we think it is? *Biochemistry 37* (1998), 11064–11077.

[78] Tomaselli, S., Esposito, V., Vangone, P., van Nuland, N. A., Bonvin, A. M., Guerrini, R., Tancredi, T., Temussi, P. A., and Picone, D. The alpha-to-beta conformational transition of Alzheimer's abeta-(1-42) peptide in aqueous media is reversible: a step by step conformational analysis suggests the location of beta conformation seeding. *ChemBiochem 7* (2006), 257–267.

[79] Yang, M., and Teplow, D. B. Amyloid β-protein monomer folding: free energy surfaces reveal alloform-specific differences. *J. Mol. Biol. 384* (2008), 450–464.

[80] Petkova, A. T., Yau, W. M., and Tycko, R. Experimental constraints on quaternary structure in Alzheimer's β-amyloid fibrils. *Biochemistry 45* (2006), 498–512.

[81] Paravastu, A. K., Leapman, R. D., Yau, W. M., and Tycko, R. Molecular structural basis for polymorphism in Alzheimer's β-amyloid fibrils. *Proc. Natl. Acad. Sci. USA 105* (2008), 18349–18354.

[82] Lu, J., Qiang, W., Yau, W., Schwieters, C., Meredith, S., and R., T. Molecular structure of β-amyloid fibrils in Alzheimer's disease brain tissue. *Cell 154*, 6 (2013), 1257–1268.

[83] Xiao, Y., Ma, B., McElheny, D., Parthasarathy, S., Long, F., Hoshi, M., Nussinov, R., and Ishii, Y. Aβ(1-42) fibril structure illuminates self-recognition and replication of amyloid in Alzheimer's disease. *Nat. Struct. Mol. Biol. 22*, 6 (Jun 2015), 499–505.

[84] National Institute on Aging. Alzheimer's disease medications: fact sheet, 2014.

[85] Wischik, C. M., Harrington, C. R., and Storey, J. M. Tau-aggregation inhibitor therapy for Alzheimer's disease. *Biochem. Pharmacol. 88*, 4 (2014), 529–539.

[86] Harrington, C., Horsley, D., Rickard, J., and Wischik, C. Materials and methods relating to protein aggregation in neurodegenerative disease, Nov. 21 2002. WO Patent App. PCT/GB2002/000,153.

[87] Wischik, C. M., Bentham, P., Wischik, D. J., and Seng, K. M. Tau aggregation inhibitor (TAI) therapy with remberTM arrests disease progression in mild and moderate Alzheimer's disease over 50 weeks. *Alzheimers Dement. 4*, 4 (2008), T167.

[88] Pickhardt, M., Gazova, Z., von Bergen, M., Khlistunova, I., Wang, Y., Hascher, A., Mandelkow, E.-M., Biernat, J., and Mandelkow, E. Anthraquinones inhibit tau aggregation and dissolve Alzheimer's paired helical filaments in vitro and in cells. *J. Bio. Chem. 280*, 5 (2005), 3628–3635.

[89] Bulic, B., Pickhardt, M., and Mandelkow, E. Progress and developments in tau aggregation inhibitors for Alzheimer disease. *J. Med. Chem. 56*, 11 (2013), 4135–4155.

[90] Carlson, E., May, J., and Kiessling, L. Chemical probes of udp-galactopyranose mutase. *Chem. Bio. 13*, 8 (2006), 825–837.

[91] Pickhardt, M., Larbig, G., Khlistunova, I., Coksezen, A., Meyer, B., Mandelkow, E.-M., Schmidt, B., and Mandelkow, E. Phenylthiazolyl-hydrazide and its derivatives are potent inhibitors of tau aggregation and toxicity in vitro and in cells. *Biochemistry 46*, 35 (2007), 10016–10023.

[92] Pickhardt, M., Biernat, J., Khilistunova, I., Wang, Y.-P., Gazova, Z., Mandelkow, E.-M., and Mandelkow, E. NPhenylamine Derivatives as Aggregation Inhibitors in Cell Models of Tauopathy *Curr. Alzh. Res. 4*, 4 (2007), 397–402.

[93] Necula, M., Chirita, C. N., and Kuret, J. Cyanine Dye N744 Inhibits Tau Fibrillization by Blocking Filament Extension: Implications for the Treatment of Tauopathic Neurodegenerative Diseases. *Biochemistry 44*, 30 (2005), 10227–10237.

[94] Taniguchi, S., Suzuki, N., Masuda, M., Hisanaga, S.-i., Iwatsubo, T., Goedert, M., and Hasegawa, M. Inhibition of heparin-induced tau filament formation by phenothiazines, polyphenols, and porphyrins. *J. Bio. Chem. 280*, 9 (2005), 7614–7623.

[95] Knowles, J. R. Enzyme-catalyzed phosphoryl transfer reactions. *Annu. Rev. Biochem. 49*, 1 (1980), 877–919. PMID: 6250450.

[96] Ross, J. Energy transfer from adenosine triphosphate. *J. Phys. Chem. B 110*, 13 (2006), 6987–6990. PMID: 16571012.

[97] Vincent, I. J., and Davies, P. Atp-induced loss of alz-50 immunoreactivity with the a68 proteins from Alzheimer brain is mediated by ubiquitin. *Proc. Natl. Acad. Sci. USA 87*, 12 (1990), 4840–4844.

[98] Marczynski, T. J. {GABAergic} deafferentation hypothesis of brain aging and Alzheimer's disease revisited. *Brain Res. Bull. 45*, 4 (1998), 341–379.

[99] de la Torre, J. C. Cerebral hypoperfusion, capillary degeneration, and development of Alzheimer's disease. *Alzheimer Dis. Assoc. Disord. 14* (2000), S72–S81.

[100] Zhu, X., Smith, M. A., Perry, G., and Aliev, G. Mitochondrial failures in Alzheimer's disease. *Am. J. Alzheimers Dis. Other Demen. 19*, 6 (2004), 345–352.

[101] Exley, C., and Korchazhkina, O. V. Promotion of formation of amyloid fibrils by aluminium adenosine triphosphate (alatp). *J. Inorg. Biochem. 84*, 34 (2001), 215 – 224.

[102] Eggertsen, R., Sivertsson, R., Andren, L., and Hansson, L. Haemodynamic effects of carvedilol, a new beta-adrenoceptor blocker and precapillary vasodilator in essential hypertension. *J. Hypertens 2* (1984), 529–534.

[103] Food and Drug Administration, USA FDA approves first generic versions of coreg. FDA news release [cited 2015 mar 04], 2007.

[104] Howlett, D. R., George, A. R., Owen, D. E., Ward, R. V., and Markwell, R. E. Common structural features determine the effectiveness of carvedilol, daunomycin and rolitetracycline as inhibitors of Alzheimer beta-amyloid fibril formation. *Biochem. J. 343* (1999), 419–423.

[105] Pasinetti, G., Rosen, Z., Rosenberg, P., and Wang, J. Carvedilol as a potential novel disease modifying agent for the treatment of Alzheimer's disease. *Alzheimer Dem. 5*, 4, Supplement (2009), e27–e28.

[106] Macedo, B., Magalhães, J., Batista, A. R., and Saraiva, M. J. Carvedilol treatment reduces transthyretin deposition in a familial amyloidotic polyneuropathy mouse model. *Pharmacol. Res. 62*, 6 (2010), 514–522.

[107] Kim, D. S., Park, S.-Y., and Kim, J.-Y. Curcuminoids from curcuma longa l. (zingiberaceae) that protect {PC12} rat pheochromocytoma and normal human umbilical vein endothelial cells from aβ_{142} insult. *Neurosci. Lett. 303*, 1 (2001), 57–61.

[108] Lim, G. P., Chu, T., Yang, F., Beech, W., Frautschy, S. A., and Cole, G. M. The curry spice curcumin reduces oxidative damage and amyloid pathology in an Alzheimer transgenic mouse. *J. Neurosci. 21* (2001), 8370–8377.

[109] Ono, K., Hasegawa, K., Naiki, H., and Yamada, M. Curcumin has potent anti-amyloidogenic effects for Alzheimer's beta-amyloid fibrils in vitro. *J. Neurosci. Res. 75*, 6 (2004), 742–750.

[110] Sanghamitra, N. J. M., Varghese, N., and Rao, C. N. R. Effect of curcumin and cu2+/zn2+ ions on the fibrillar aggregates formed by the amyloid peptide and other peptides at the organic-aqueous interface. *Chem. Phys. Lett. 496*, 1-3 (2010), 104–108.

[111] Zhao, L. N., Chiu, S.-W., Benoit, J., Chew, L. Y., and Mu, Y. The effect of curcumin on the stability of abeta dimers. *J. Phys. Chem. B 116*, 25 (2012), 7428–7435.

[112] Department of Veterans Affairs. Curcumin and yoga therapy for those at risk for Alzheimer's disease. in: Clinicaltrials.gov [internet]. bethesda (md): National library of medicine (us). 2000- [cited 2015 mar 04], 2014. NLM Identifier: NCT01811381.

[113] Taguchi, H., Yanagisawa, D., Morikawa, S., Hirao, K., Shirai, N., and Tooyama, I. Synthesis and tautomerism of curcumin derivatives and related compounds. *Australian J. Chem. 68* (2015), 224–229.

[114] Endo, H., Nikaido, Y., Nakadate, M., Ise, S., and Konno, H. Structure activity relationship study of curcumin analogues toward the amyloid-beta aggregation inhibitor. *Bioorg. Med. Chem. Lett. 24*, 24 (2014), 5621 – 5626.

[115] Zhang, X., Tian, Y., Yuan, P., Li, Y., Yaseen, M. A., Grutzendler, J., Moore, A., and Ran, C. A bifunctional curcumin analogue for two-photon imaging and inhibiting crosslinking of amyloid beta in Alzheimer's disease. *Chem. Commun. 50* (2014), 11550–11553.

[116] Drugbank. Nilvadipine information [cited 2015 mar 04]. Available from: http://www.drugbank.ca/drugs/DB06712.

[117] Cho, H., Ueda, M., Shima, K., Mizuno, A., Hayashimatsu, M., Ohnaka, Y., Takeuchi, Y., Hamaguchi, M., and Aisaka, K. a. Dihydropyrimidines: novel calcium antagonists with potent and long-lasting vasodilative and anti-hypertensive activity. *J. Med. Chem. 32*, 10 (1989), 2399–2406.

[118] Matsuda, H., Araki, N., Kuji, I., Ohkubo, T., Imabayashi, E., and Shimazu, K. Effect of nilvadipine on regional cerebral blood flow in a patient with early Alzheimer disease. *Clin. Med. Chem. 33* (2008), 34–35.

[119] Hanyu, H., Hirao, K., Shimizu, S., Sato, T., Kiuchi, A., and Iwamoto, T. Nilvadipine prevents cognitive decline of patients with mild cognitive impairment. *Int. J. Geriatr. Psychiatry. 22*, 12 (2007), 1264–1266.

[120] Paris, D., Bachmeier, C., Patel, N., Quadros, A., Volmar, C., Laporte, V., Ganey, J., Beaulieu-Abdelahad, D., Ait-Ghezala, G., Crawford, F., and Mullan, M. Selective antihypertensive dihydropyridines lower abeta accumulation by targeting both the production and the clearance of abeta across the blood-brain barrier. *Mol. Med. 17* (2011), 149–162.

[121] Iwasaki, K., Egashira, N., Takagaki, Y., Yoshimitsu, Y., Hatip-Al-Khatib, I., Mishima, K., and Fujiwara, M. Nilvadipine prevents the impairment of spatial memory induced by cerebral ischemia combined with beta-amyloid in rats. *Biol. Pharm. Bull. 30*, 4 (2007), 698–701.

[122] Bachmeier, C., Beaulieu-Abdelahad, D., Mullan, M., and Paris, D. Selective dihydropyiridine compounds facilitate the clearance of beta-amyloid across the bloodbrain barrier. *Eur. J. Pharmacol. 659*, 23 (2011), 124–129.

[123] Hirata, K., Yamaguchi, H., Takamura, Y., Takagi, A., Fukushima, T., Iwakami, N., Saitoh, A., Nakagawa, M., and Yamada, T. A novel neurotrophic agent, t-817ma [1-{3-[2-(1-Benzothiophen-5-yl) Ethoxy] Propyl}-3-azetidinol maleate], attenuates amyloid-beta-induced neurotoxicity and promotes neurite outgrowth in rat cultured central nervous system neurons. *J. Pharmacol. Exp. Ther. 314*, 1 (2005), 252–259.

[124] Nguyen, P. T. H., Kimura, T., Ho, S. A., Tran, A. H., Ono, T., and Nishijo, H. Ameliorative effects of a neuroprotective agent, t-817ma, on place learning deficits induced by continuous infusion of amyloid-beta peptide (140) in rats. *Hippocampus 17*, 6 (2007), 443–455.

[125] Kimura, T., Hong Nguyen, P. T., Ho, S. A., Tran, A. H., Ono, T., and Nishijo, H. T-817MA, a neurotrophic agent, ameliorates the deficits in adult neurogenesis and spatial memory in rats infused i.c.v. with amyloid-beta peptide. *Br. J. Pharmacol. 157*, 3 (2009), 451–463.

[126] Kawasaki, T., Ago, Y., Kitao, T., Nashida, T., Takagi, A., Takuma, K., and Matsuda, T. A neuroprotective agent, t-817ma (1-{3-[2-(1-benzothiophen-5-yl)ethoxy]propyl} azetidin-3-ol maleate), prevents 1-methyl-4-phenyl-1,2,3,6-tetrahydropyridine-induced neurotoxicity in mice. *Neuropharmacology 55*, 5 (2008), 654–660.

[127] Moreno, H., Choi, S., Yu, E., Brusco, J., Avila, J., Moreira, J., Sugimori, M., and Llinas, R. R. Blocking effects of human tau on squid giant synapse transmission and its prevention by t-817MA. *Front. Synaptic Neurosci. 3*, 3 (2011), doi: 10.3389fnsyn.2011.00003.

[128] Takamura, Y., Ono, K., Matsumoto, J., Yamada, M., and Nishijo, H. Effects of the neurotrophic agent t-817MA on oligomeric amyloid-β induced deficits in long-term potentiation in the hippocampal {CA1} subfield. *Neurobiol. Aging 35*, 3 (2014), 532–536.

[129] Toyama Chemical Co., L. Efficacy and safety of t-817ma in patients with mild to moderate Alzheimer's disease (us202). in: Clinicaltrials.gov [internet]. bethesda (md): National library of medicine (us). 2000- [cited 2015 mar 04], 2014. NLM Identifier: NCT02079909.

[130] Liu, T., Lin, Y., Wen, X., Jorissen, R. N., and Gilson, M. K. Bindingdb: a web-accessible database of experimentally determined proteinligand binding affinities. *Nucleic Acids Res. 35*, suppl 1 (2007), D198–D201.

[131] Viet, M. H., Ngo, S. T., Lam, N. S., and Li, M. S. Inhibition of aggregation of amyloid peptides by beta-sheet breaker peptides and their binding affinity. *J. Phys. Chem. B 115* (2011), 7433–7446.

[132] Huy, P. D. Q., Yu, Y.-C., Ngo, S. T., Thao, T. V., piao Chen, C., Li, M. S., and Chen, Y.-C. In silico and in vitro characterization of anti-amyloidogenic activity of vitamin k3 analogues for Alzheimer's disease. *BBA - Gen. Sub. 1830*, 4 (2013), 2960–2969.

[133] Miyata, M., Sato, T., Kugimiya, M., Sho, M., Nakamura, T., Ikemizu, S., Chirifu, M., Mizuguchi, M., Nabeshima, Y., Suwa, Y., Morioka, H., Arimori, T., Suico, M. A., Shuto, T., Sako, Y., Momohara, M., Koga, T., Morino-Koga, S., Yamagata, Y., and Kai, H. The crystal structure of the green tea polyphenol ()epigallocatechin gallate-transthyretin complex reveals a novel binding site distinct from the thyroxine binding site. *Biochem. 49*, 29 (2010), 6104–6114.

[134] Kim, Y.-S., Randolph, T. W., Manning, M. C., Stevens, F. J., and Carpenter, J. F. Congo red populates partially unfolded states of an amyloidogenic protein to enhance aggregation and amyloid fibril formation. *J. Biol. Chem. 278*, 12 (2003), 10842–10850.

[135] Conte, A., Pellegrini, S., and Tagliazucchi, D. Synergistic protection of {PC12} cells from β-amyloid toxicity by resveratrol and catechin. *Brain Res. Bull. 62*, 1 (2003), 29–38.

[136] Choi, Y.-T., Jung, C.-H., Lee, S.-R., Bae, J.-H., Baek, W.-K., Suh, M.-H., Park, J., Park, C.-W., and Suh, S.-I. The green tea polyphenol ()epigallocatechin gallate attenuates β-amyloid-induced neurotoxicity in cultured hippocampal neurons. *Life Sci. 70*, 5 (2001), 603–614.

[137] Weggen, S., Eriksen, J. L., Das, P., Sagi, S. A., Wang, R., Pietrzik, C. U., Findlay, K. A., Smith, T. E., Murphy, M. P., Butler, T.,

Kang, D. E., Marquez-Sterling, N., Golde, T. E., and Koo, E. H. A subset of nsaids lower amyloidogenic a beta 42 independently of cyclooxygenase activity. *Nature 414* (2001), 212–216.

[138] Yao, Z.-X., Han, Z., Drieu, K., and Papadopoulos, V. Ginkgo biloba extract (egb 761) inhibits β-amyloid production by lowering free cholesterol levels. *J. Nutr. Biochem. 15*, 12 (2004), 749–756.

[139] JANSSEN Alzheimer Immunotherapy Research & Development, L. Randomized safety, tolerability and pilot efficacy of an-1792 in Alzheimer's disease. in: Clinicaltrials.gov [internet]. bethesda (md): National library of medicine (us). 2000- [cited 2015 mar 04], 2001. NLM Identifier: NCT00021723.

[140] JANSSEN Alzheimer Immunotherapy Research & Development, L. Study evaluating acc-001 in subjects with mild to moderate Alzheimer's disease. in: Clinicaltrials.gov [internet]. bethesda (md): National library of medicine (us). 2000- [cited 2015 mar 04], 2007. NCT00498602.

[141] Novartis. Safety and tolerability study in patients with mild to moderate Alzheimer's disease (ad). in: Clinicaltrials.gov [internet]. bethesda (md): National library of medicine (us). 2000- [cited 2015 mar 04], 2006. NCT00411580.

[142] Corp., M. S. . D. A study of v950 in people with Alzheimer disease (v950-001 am7). in: Clinicaltrials.gov [internet]. bethesda (md): National library of medicine (us). 2000- [cited 2015 mar 04], 2007. NCT00464334.

[143] JANSSEN Alzheimer Immunotherapy Research & Development, L. Bapineuzumab in patients with mild to moderate Alzheimer's disease (apoe4 carrier) . in: Clinicaltrials.gov [internet]. bethesda (md): National library of medicine (us). 2000- [cited 2015 mar 04], 2007. NCT00575055.

[144] JANSSEN Alzheimer Immunotherapy Research & Development, L. Effects of ly2062430 in subjects with mild-to-moderate Alzheimer's disease and in healthy volunteers. in: Clinicaltrials.gov [internet]. bethesda (md): National library of medicine (us). 2000- [cited 2015 mar 04], 2006. NCT00329082.

[145] Asien, P., Vellas, B., and Hampel, H. Moving towards early clinical trials for amyloid-targeted therapy in Alzheimer's disease. *Nat. Rev. Drug. Discov. 12* (2013), 324.

[146] Mullard, A. Sting of Alzheimer's failures offset by upcoming prevention trials. *Nat. Rev. Drug. Discov. 11* (2012), 657–660.

[147] Pratico, D. and Delanty, N. Oxidative injury in diseases of the central nervous system: focus on Alzheimer's disease. *Am. J. Med. 109* 7 (2000), 577–585.

[148] Butterfield, D. A., Reed, T., Newman, S. F., and Sultana, R. Roles of amyloid beta-peptide-associated oxidative stress and brain protein modifications in the pathogenesis of Alzheimer's disease and mild cognitive impairment. *Free Radic. Biol. Med. 43*, 5 (2007), 658–677.

[149] Yatin, S., Varadarajan, S., Link, C., and Butterfield, D. In vitro and in vivo oxidative stress associated with Alzheimer's amyloid β-peptide (1-42). *Neurobiol. Aging 20*, 3 (1999), 325–330.

[150] Ono, K., Yoshiike, Y., Takashima, A., Hasegawa, K., Naiki, H., and Yamada, M. Vitamin A exhibits potent antiamyloidogenic and fibril-destabilizing effects in vitro. *Experimental Neurology 189*, 2 (2004), 380–392.

[151] Yamin, G., Ono, K., Inayathullah, M., and Teplow, D. B. Amyloid β-protein assembly as therapeutic target of Alzheimer's disease. *Curr. Phar. Design 14*, 30 (2008), 3231–3246.

[152] Fosgerau, K., and Hoffmann, T. Peptide therapeutics: current status and future directions. *Drug. Discov. Today 20*, 1 (2015), 122–128.

[153] Tjernberg, A., Edlund P. O., and Noren, B. Screening of eltanolone metabolites in dog urine by anion-exchange/reversed-phase liquid chromatography and mass spectrometry. *J. Chromatorgr B. Biomed. Sci. App. 715* (1998), 395–407.

[154] Soto, C. M., Kindy, S., Baumann, M., and Frangione, B. Inhibition of Alzheimer's amyloidosis by peptides that prevent β-sheet conformation. *Biochem. Biophys. Res. Commun. 226* (1996), 672–680.

[155] Gordon, D. J., Sciarretta, K. L., and Meredith, S. C. Inhibition of beta-amyloid(40) fibrillogenesis and disassembly of beta-amyloid(40) fibrils by short beta-amyloid congeners containing n-methyl amino acids at alternate residues. *Biochemistry 40*, 28 (2001), 8237–8245.

[156] Viet, M. H., Siposova, K., Bednarikova, Z., Antosova, A., Nguyen, T. T., Gazova, Z., and Li, M. S. *In silico* and *in vitro* study of binding affinity of tripeptides to amyloid β fibrils: Implications for Alzheimer's disease. *J. Phys. Chem. B 119*, 16 (2015), 5145–5155.

[157] Varadarajan, S., Yatin, S., and Butterfield, D. Alzheimer's amyloid beta peptide (1-42) fibrils are not always neurotoxic. *Alz. rep. 3*, 2 (2000), 71–76.

[158] Cherny, R., Atwood, C., Xilinas, M., Gray, D., Jones, W., McLean, C., Barnham, K., Volitakis, I., Fraser, F., Kim, Y., Huang, X., Goldstein, L., Moir, R., Lim, J., Beyreuther, K., Zheng, H., Tanzi, R., Masters, C., and Bush, A. Treatment with a copper-zinc chelator markedly and rapidly inhibits beta-amyloid accumulation in Alzheimer's disease transgenic mice. *Neuron. 30*, 3 (2001), 665–676.

[159] Lee, C.-W., Zhuang, Z.-P., Kung, M.-P., Plossl, K., Skovronsky, D., Gur, T., Hou, C., Trojanowski, J. Q., Lee, V. M.-Y., and Kung, H. F. Isomerization of (z,z) to (e,e)1-bromo-2,5-bis-(3-hydroxycarbonyl-4-hydroxy)styrylbenzene in strong base: probes for amyloid plaques in the brain. *J. Med. Chem. 44*, 14 (2001), 2270–2275.

[160] Ono, M., Kawashima, H., Nonaka, A., Kawai, T., Haratake, M., Mori, H., Kung, M.-P., Kung, H. F., Saji, H., and Nakayama, M. Novel benzofuran derivatives for pet imaging of beta-amyloid plaques in Alzheimer's disease brains. *J. Med. Chem. 49*, 9 (2006), 2725–2730.

[161] Yung-Chi, C., and Prusoff, W. H. Relationship between the inhibition constant (Ki) and the concentration of inhibitor which causes 50 per cent inhibition (IC50) of an enzymatic reaction. *Biochem. Pharmacol. 22*, 23 (1973), 3099–3108.

[162] Dadashpour, S., Tuylu Kucukkilinc, T., Unsal Tan, O., Ozadali, K., Irannejad, H., and Emami, S. Design, synthesis and in vitro study of 5,6-diaryl-1,2,4-triazine-3-ylthioacetate derivatives as cox-2 and beta-amyloid aggregation inhibitors. *Archiv. der Pharmazie. 348*, 3 (2015), 179–187.

[163] Huang, M., Xie, S.-S., Jiang, N., Lan, J.-S., Kong, L.-Y., and Wang, X.-B. Multifunctional coumarin derivatives: Monoamine oxidase b (mao-b) inhibition, anti-beta-amyloid (Aβ) aggregation and metal chelation properties against Alzheimer's disease. *Bioorg. Med. Chem. Lett. 25*, 3 (2015), 508–513.

[164] Du, W., Guo, J., Gao, M., Hu, S., Dong, X., Han, Y., Liu, F., and Jiang, S nd Sun, Y. Brazilin inhibits amyloid beta-protein fibrillogenesis, remodels amyloid fibrils and reduces amyloid cytotoxicity. *Sci. Rep. 5*, 7992 (2015), doi: 10.1038srep07992

[165] Wang, J., Shi, Z., Zhang, M., Xin, G., Pang, T., Zhou, P., Chen, J., Qi, L., Yang, H., Xu, X., and Li, P. Camptothecin and its analogs reduce amyloid-beta production and amyloid-beta42-induced il-1beta production. *J. Alzheimers Dis. 43* (2015), 465–477.

[166] Zhang, T., Zhang, J., Derreumaux, P., and Mu, Y. Molecular mechanism of the inhibition of egcg on the Alzheimer aβ_{1-42} dimer. *J. Phys. Chem. B. 117* (2013), 3993–4002.

[167] Liu, F., Du, W., Sun, Y., Zheng, J., and Dong, X. Atomistic characterization of binding modes and affinity of peptide inhibitors to amyloid-beta protein. *Front. Chem. Sci. Eng. 8*, 4 (2014), 433–444.

[168] Hess, B., Kutzner, C., van der Spoel, D., and Lindahl, E. Gromacs 4: Algorithms for highly efficient, load-balanced, and scalable molecular simulation. *J. Chem. Theory Comput. 4* (2008), 435–447.

[169] Wang, Y., Li, L., Chen, T., Chen, W., and Xu, Y. Microsecond molecular dynamics simulation of Aβ_{42} and identification of a novel dual inhibitor of abeta42 aggregation and bace1 activity. *Acta Pharmacol. Sin. 34* (2013), 1243–1250.

[170] Chen, C. Y.-C. TCM database@taiwan: The world's largest traditional chinese medicine database for drug screening *in silico*. *PLoS ONE 6*, 1 (2011), e15939.

[171] Huy, P. D. Q., and Li, M. S. Binding of fullerenes to amyloid beta fibrils: size matters. *Phys. Chem. Chem. Phys. 16*, 37 (2014), 20030–20040.

[172] Xie, L., Luo, Y., Lin, D., Xi, W., Yang, X., and Wei, G. The molecular mechanism of fullerene-inhibited aggregation of Alzheimer's [small beta]-amyloid peptide fragment. *Nanoscale 6* (2014), 9752–9762.

[173] Sugita, Y., and Okamoto, Y. Replica-exchange molecular dynamics method for protein folding. *Chem. l Phys. Lett. 314*, 12 (1999), 141–151.

[174] Chang, W. L. E., Takeda, T., Raman, E. P., and Klimov, D. K. Molecular dynamics simulations of anti-aggregation effect of ibuprofen. *Biphys. J. 98* (2010), 2662–2670.

[175] OBrien, E. P., Okamoto, Y., Straub, J. E., Brooks, B. R., and Thirumalai, D. Thermodynamic perspective on the docklock growth mechanism of amyloid fibrils. *J. Phys. Chem. B 113*, 43 (2009), 14421–14430.

[176] Takeda, T., Kumar, R., Raman, E. P., and Klimov, D. K. Nonsteroidal anti-inflammatory drug naproxen destabilizes a beta amyloid fibrils: A molecular dynamics investigation. *J. Phys. Chem. B 114* (2010), 15394–15402.

[177] Tarus, B., Nguyen, P. H., Berthoumieu, O., Faller, P., Doig, A. J., and Derreumaux, P. Molecular structure of the NQTrp inhibitor with the Alzheimer A beta 128 monomer. *Eur. J. Med. Chem. 91*, SI (2015), 43–50.

[178] Zhang, T., Xu, W., Mu, Y., and Derreumaux, P. Atomic and Dynamic Insights into the Beneficial Effect of the 1,4-Naphthoquinon-2-yl-L-tryptophan Inhibitor on Alzheimer's A beta 1-42 Dimer in Terms of Aggregation and Toxicity. *ACS Chem. Neuro. 5*, 2 (2014), 148–159.

[179] Chebaro, Y., Jiang, P., Zang, T., Mu, Y., Nguyen, P. H., Mousseau, N., and Derreumaux, P. Structures of A beta 17-42 Trimers in Isolation and with Five Small-Molecule Drugs Using a Hierarchical Computational Procedure. *J. Phys. Chem. B 116*, 29, SI (2012), 8412–8422.

[180] Huang, S.-Y., Grinter, S. Z., and Zou, X. Scoring functions and their evaluation methods for protein-ligand docking: recent advances and future directions. *Phys. Chem. Chem. Phys. 12* (2010), 12899–12908.

[181] Trott, O., and Olson, A. J. Improving the speed and accuracy of docking with a new scoring function, efficient optimization, and multithreading. *J. Comput. Chem. 31* (2010), 455–461.

[182] Sanner, M. F. Python: A programming language for software intergration and development. *J. Mol. Graphics Mod. 17* (1999), 57–61.

[183] Morris, G. M., Godsell, D. S., Halliday, R. S., Huey, R., Hart, W. E., Belew, R. K., and Olson, A. J. Automated docking using a lamarckian genetic algorithm and an empirical binding free energy function. *J. Comput. Chem. 19* (1998), 1639–1662.

[184] Morris, G. M., Goodsell, D. S., Huey, R., and Olson, A. J. Distributed automated docking of flexible ligands to proteins: Parallel applications of autodock 2.4. *J. Comput-Aided. Mol. Des. 10* (1996), 293–304.

[185] Shanno, D. F. Conditioning of quasi-newton methods for function minimization. *Math. Comp. 24*, 111 (1970), 647–656.

[186] Alder, B. J., and Wainwright, T. E. Studies in molecular dynamics. I. general method. *J. Chem. Phys 31*, 459 (1959).

[187] Rhahman, A. Correlations in the motion of atoms in liquid argon. *Phys. Rev. 136* (1964).

[188] Case, D., Darden, T., Cheatham, T., Simmerling, C., Wang, J., Duke, R., Luo, R., Crowley, M., R.C.Walker, Zhang, W., Merz, K., B.Wang, Hayik, S., Roitberg, A., Seabra, G., Kolossváry, I., K.F.Wong, Paesani, F., Vanicek, J., X.Wu, Brozell, S., Steinbrecher, T., Gohlke, H., Yang, L., Tan, C., Mongan, J., Hornak, V., Cui, G., Mathews, D., Seetin, M., Sagui, C., Babin, V., , and Kollman, P. Amber 10. Tech. rep., University of California, San Francisco, 2008.

[189] van Gunsteren, W., Billeter, S. R., Eising, A. A., Hünenberger, P. H., Krüger, P., Mark, A. E., Scott, W., and Tironi, I. *Biomolecular Simulation: The GROMOS96 Manual and User Guide.* Vdf Hochschulverlag AG an der ETH, Zurich, 1996.

[190] Scott, W. R. P., Hunenberger, P. H., Tironi, I. G., Mark, A. E., Billeter, S. R., Fennen, J., e. Torda, A., Huber, T., Kruger, P., and van Gunsteren, W. F. The gromos biomolecular simulation program package. *J. Phys. Chem. A 103* (1999), 3596–3607.

[191] Hornak, V., Abel, R., Okur, A., Strockbine, B., Roitberg, A., and Simmerling, C. Comparison of multiple amber force fields and development of improved protein backbone parameters. *Proteins 65*, 3 (2006), 712–725.

[192] Kaminski, G. A., and Friesner, R. A. Evaluation and reparametrization of the opsl-aa force field for proteins via comparison with accurate quantum chemical calculations on peptides. *J. Phys. Chem. B. 105* (2001), 6474–6487.

[193] Vanommeslaeghe, K., Hatcher, E., Acharya, C., Kundu, S., Zhong, S., Shim, J., Darian, E., Guvench, O., Lopes, P., Vorobyov, I., and Mackerell, A. D. Charmm general force field: A force field for drug-like molecules compatible with the charmm all-atom additive biological force fields. *J. Comput. Chem. 31*, 4 (2010), 671–690.

[194] Hockney, R. W., Goel, S. P., and Eastwood, J. Quit high resolution computer models of plasma. *J. Comp. Phys. 14*, 2 (1974), 148–158.

[195] Wang, J. M., Wolf, R. M., Caldwell, J. W., Kollman, P. A., and Case, D. A. Development and testing of a general amber force field. *J. Comput. Chem. 25*, 9 (2004), 1157–1174.

[196] Stewart, J. Mopac 2002. *Fujitsu Limited, Tokyo* (1999).

[197] Jakalian, A., Bush, B. L., and Jack, D. B. Fast, efficient generation of high-quality atomic charges. am1-bcc model: I. method. *J. Comput. Chem. 21* (2000), 132–146.

[198] Jakalian, A., Jack, D. B., and Bayly, C. I. Fast, efficient generation of high-quality atomic charges. am1-bcc model: II. parameterization and validation. *J. Comput. Chem. 23*, 16 (2002), 1623–1641.

[199] Jorgensen, W. L., Chandrasekhar, J., Madura, J. D., Impey, R. W., and Klein, M. L. Comparison of simple potential functions for simulating liquid water. *J. Chem. Phys. 779* (1983), 926–935.

[200] Darden, T., York, D., and Pedersen, L. Particle mesh Ewald: An nlog(n) method for Ewald sums in large systems. *J. Chem. Phys. 98*, 12 (1993), 10089–10092.

[201] Uberuaga, B. P., Anghel, M., and Voter, A. F. Synchronization of trajectories in canonical molecular-dynamics simulations: Observation, explanation, and exploitation. *J. Chem. Phys. 120* (2004), 6363–6374.

[202] Sindhikara, D. J., Kim, S., Voter, A. F., and Roitberg, A. E. Bad seeds sprout perilous dynamics: Stochastic thermostat induced trajectory synchronization in biomolecules. *J. Chem. Theory Comput. 5* (2009), 1624–1631.

[203] Hess, B., Bekker, H., Berendsen, H. J. C., and Fraaije, J. G. E. M. LINCS: A linear constraint solver for molecular simulations. *J. Comp. Chem. 18*, 12 (1997), 1463–1472.

[204] Berendsen, H. J. C., Postma, J. P. M., van Gunsteren, W. F., Dinola, A., and Haak, J. R. Molecular-dynamics with coupling to an external bath. *J. Chem. Phys. 81*, 8 (1984), 3684–3690.

[205] Parrinello, M., and Rahman, A. Polymorphic transitions in single crystals: A new molecular dynamics method. *J. Appl. Phys. 52* (1981), 7182–7190.

[206] Berendsen, H. J. C., Postma, J. P. M., van Gunsteren, W. F., , and Hermans, J. *Intermolecular Forces*. Reidel, Dordrecht, 1981.

[207] Schuttelkopf, A. W., and van Aalten, D. M. F. Prodrg - a tool for high-throughput crystallography of protein-ligand complexes. *Acta Crystallogr. D60* (2004), 1355–1363.

[208] Lemkul, J., Allen, W., and Bevan, D. Practical considerations for building gromos-compatible small-molecular topologies. *J. Chem. Inf. Model. 50* (2010), 2221–2235.

[209] Mulliken, R. Electronic population analysis on lcaoxmo molecular wave functions. i. *J. Chem. Phys. 23* (1955), 1833.

[210] van Gunsteren, W. F., and Berendsen, H. J. C. A leap-frog algorithm for stochastic dynamics. *Mol. Sim. 1* (1988), 173–185.

[211] Reddy, M., and Erion, M. *Free energy calculations in rational drug design*. Springer ISBN-13: 978-0-306-46676-2, 2001.

[212] Sharp, K. A., and Honig, B. Electrostatic interactions in macromolecules: theory and applications. Annu. Rev. Biophys. *Biophys. Chem. 19* (1990), 301–332.

[213] Shrake, A., and Rupley, J. A. Environment and exposure to solvent of protein atoms-lysozyme and insulin. *J. Mol. Biol. 79*, 2 (1973), 351–371.

[214] Sitkoff, D., Sharp, K. A., and Honig, B. Accurate calculation of hydration free energies using macroscopic solvent models. *J. Phys. Chem. 97*, 7 (1994), 1978–1988.

[215] McQuarrie, D. A. *Statistical Thermodynamics*, 2 ed. Harper and Row, New York, 1973.

[216] Yang, J., and Chen, J. Neurodegenerative Diseases (2013)

[217] Ngo, S. T., Mai, B. K., Hiep, D. M., and Li, M. S. Estimation of the binding free energy of AC1NX476 to hiv-1 protease wild type and mutations using free energy perturbation method. *Chem. Biol. Drug Des.* (2015), doi: 10.1111cbdd.12518.

[218] Jayachandran, G., Shirts, M. R., Park, S., and Pande, V. S. Parallelized-over-parts computation of absolute binding free energy with docking and molecular dynamics. *J. Chem. Phys. 125* (2006), 084901.

[219] Fujitani, H., Tanida, Y., Ito, M., Jayachandran, G., and Snow, C. D. Direct calculation of the binding free energies of fkbp ligands. *J. Chem. Phys. 123* (2005), 084108.

[220] Bennett, C. H. Efficient estimation of free energy differences from monte carlo data. *J. Comput. Phys. 22* (1976), 245–268.

[221] Garg, P., and Verma, J. In silico prediction of blood brain barrier permeability: An artificial neural network model. *J. Chem. Inf. Model. 46* (2006), 289–297.

[222] Crivori, P., Cruciani, G., Carrupt, P., and Testa, B. Predicting blood-brain barrier permeation from three-dimensional molecular structure. *J. Med. Chem. 43* (1998), 2204–2216.

[223] Rose, K., and Hal, L. H. Modeling blood-brain barrier partitioning using the electrotopological state. *J. Chem. Inf. Comput. Sci. 42* (2002), 651–666.

[224] Clark, D. E. R. Calculation of polar molecular surface area and its application to the prediction of transport phenomena. 2. prediction of blood-brain barrier penetration. *J. Pharm Sci. 88* (1999), 815–821.

[225] Wessel, M. D., Jurs, P. C., Tolan, J. W., and Muskal, S. M. Prediction of human intestinal absorption of drug compounds from molecular structure. *J. Chem. Inf. Comput. Sci. 38* (1998), 726–735.

[226] Lipinski, C. A., Lombardo, F., and Dominy, B. W. Experimental and computational approaches to estimate solubility and permeability in drug discovery and development settings. *Adv. Drug. Deliv. Rev. 23* (1997), 3–25.

[227] Zhao, Y. H., Le, J., Abraham, M. H., Hersey, A., Eddershaw, P. J., Luscombe, C. N., Boutina, D., Beck, G., Sherborne, B., Cooper, I., and Platts, J. A. Evaluation of human intestinal absorption data and subsequent derivation of a quantitative structure-activity relationship (qsar) with the abraham descriptors. *J. Pharm Sci. 90* (2001), 749–784.

[228] Raevsky, O. A., Schaper, K.-J., Artursson, P., and McFarland, J. W. A novel approach for prediction of intestinal absorption of drugs in humans based on hydrogen bond descriptors and structural similarity. *Quant. Struct. -Act. Relat. 20* (2002), 402–413.

[229] Joosten, R. P., te Beek, T. A., Krieger, E., Hekkelman, M. L., Hooft, R. W., Schneider, R., Sander, C., and Vriend, G. A series of pdb related databases for everyday needs. *Nucleic. Acids Res. 39*, suppl 1 (2011), D411–D419.

[230] Kabsch, W., and Sander, C. Dictionary of protein secondary structure: Pattern recognition of hydrogen-bonded and geometrical features. *Biopolymers 22*, 12 (1983), 2577–2637.

[231] Holliday, J. D., Ranade, S. S., and Willett, P. A fast algorithm for selecting sets of dissimilar molecules from large chemical databases. *Quant. Struct.-Act. Rel. 14*, 6 (1995), 501–506.

[232] Barreiro, G., Guimar, C. R. W., Tubert-Brohman, I., Lyons, T. M., Tirado-Rives, J., and Jorgensen, W. L. Search for non-nucleoside inhibitors of hiv-1 reverse transcriptase using chemical similarity, molecular docking, and mm-gb/sa scoring. *J. Chem. Inf. Model. 47*, 6 (2007), 2416–2428. PMID: 17949071.

[233] Imbimbo, B. An update on the efficacy of non-steroidal anti-inflammatory drugs in Alzheimer's disease. *Expert Opin. Investig. Drug 18* (2009), 1147–1168.

[234] Vlad, S. C., Miller, D. R., Kowall, N. W., and Felson, D. T. Protective effects of nsaids on the development of Alzheimer's disease. *Neurology 70* (2008), 1672–1677.

[235] Takeda, T., Chang, W. L. E., Raman, E. P., and Klimov, D. K. Binding of nonsteroidal anti-inflammatory drugs to a beta fibril. *Proteins 78*, 13 (2010), 2849–2860.

[236] Bolton, E. E., Wang, Y., Thiessen, P. A., and Bryant, S. H. Chapter 12 pubchem: Integrated platform of small molecules and biological activities. vol. 4 of *Annu. Rep. Comput. Chem.*. Elsevier, 2008, pp. 217–241.

[237] Sticht, H., Bayer, P., Willbold, D., Dames, S., Hilbich, C., Beyreuther, K., Frank, R. W., and Rosch, P. Structure of amyloid a4-(1-40)-peptide of Alzheimer's disease. *Eur. J. Biochem. 233* (1995), 293–298.

[238] Xu, X. P., and Case, D. A. Automated prediction of ^{15}N, $^{13}C_\alpha$, $^{13}C_\beta$ and ^{13}C' chemical shifts in proteins using a density functional database. *J. Biomol. NMR. 21*, (2001), 321–333.

[239] Xu, X. P., and Case, D. A. Probing multiple effects on ^{15}N, $^{13}C_\alpha$, $^{13}C_\beta$ and ^{13}C' chemical shifts in peptides using density functional theory. *Biopolymers 65*, (2002), 408–423.

[240] Hou, L., Shao, H., Zhang, Y., Li, H., Menon, N. K., Neuhaus, E. B., Brewer, J. M., Byeon, I.-J. L., Ray, D. G., Vitek, M. P., Iwashita, T., Makula, R. A., Przybyla, A. B., and Zagorski, M. G. Solution nmr studies of the Aβ_{1-40} and Aβ_{1-42} peptides establish that the met35 oxidation state affects the mechanism of amyloid formation. *J. Am. Chem. Soc 126*, 7 (2004), 1992–2005.

[241] Viet, M. H., and Li, M. S. Amyloid peptide aβ_{40} inhibits aggregation of aβ_{42}: evidence from molecular dynamics simulations. *J. Chem. Phys. 136* (2012), 245105.

[242] Wishart, D. S., Bigam, C. G., Holm, A., Hodges, R. S., and Sykes, B. D. H-1, c-13 and n-15 random coil nmr chemical-shifts of the common amino acids. 1. investigation of nearest neighbor effects. *J. Biomolecular NMR 5*, 1 (1995), 67–81.

[243] Daura, X., Gademann, K., Jaun, B., Seebach, D., van Gunsteren, W., and Mark, A. Peptide folding: When simulation meets experiment. *Angew. Chem. Int. Ed. 38* (1999), 236–240.

[244] Sgourakis, N. G., Yan, Y. L., McCallum, S. A., Wang, C. Y., and Garcia, A. E. The Alzheimer's peptides a beta 40 and 42 adopt distinct conformations in water: A combined md/nmr study. *J. Mol. Biol 368*, 5 (2007), 1448–1457.

[245] Srinivasan, J., III, T. C., Cieplak, P., Kollman, P., and Case., D. Continuum solvent studies of the stability of DNA, RNA, and Phosphoramidate-DNA helices. *J. Am. Chem. Soc. 120*, 37 (1998), 9401–9409.

[246] Kollman, P., Massova, I., Reyes, C., Kuhn, B., Huo, S., Chong, L., Lee, M., Lee, T., Duan, Y., Wang, W., Donini, O., Cieplak, P., Srinivasan, J., Case, D., and T.E. Cheatham, I. Calculating structures and free energies of complex molecules: combining molecular mechanics and continuum models. *Acc. Chem. Res. 33*, 12 (2000), 889–897.

[247] Nguyen, T. T., Mai, B. K., and Li, M. S. Study of tamiflu sensitivity to variants of a/h5n1 virus using different force fields. *J. Chem. Info. Model. 51* (2011), 2266–2276.

[248] Yan, Y. L., and Wang, C. Y. A beta 40 protects non-toxic a beta 42 monomer from aggregation. *J. Mol. Biol 369*, 4 (2007), 909–916.

[249] Wang, Y., Xiao, J., Suzek, T. O., Zhang, J., Wang, J., Zhou, Z., Han, L., Karapetyan, K., Dracheva, S., Shoemaker, B. A., Bolton,

E., Gindulyte, A., and Bryant, S. H. Pubchem's bioassay database. *Nucleic Acids Res. 40*, D1 (2012), D400–D412.

[250] Opazo, C., Huang, X., Cherny, R. A., Moir, R. D., Roher, A. E., White, A. R., Cappai, R., Masters, C. L., Tanzi, R. E., Inestrosa, N. C., and Bush, A. I. Metalloenzyme-like activity of Alzheimer's disease beta-amyloid: Cu-dependent catalytic convesion of dopamine, cholesterol, and biological reducing agents to neurotoxic h2o2. *J. Biol. Chem. 277*, 43 (2002), 40302–40308.

[251] Willett, P., Barnard, J. M., and Downs, G. M. Chemical similarity searching. *J. Chem. Inf. Comput. Sci. 38*, 6 (1998), 983–996.

[252] Hamelberg, D., and McCammon, J. A. Standard free energy of releasing a localized water molecule from the binding pockets of proteins: double-decoupling method. *J. Am. Chem. Soc. 126*, 24 (2004), 7683–7689.

[253] Lee, V. M.-Y. Amyloid binding ligands as Alzheimer's disease therapies. *Neurobiol. Aging 23*, 6 (2002), 1039 – 1042.

[254] Nie, Q., Du, X., and Geng, M. Small molecule inhibitors of amyloid beta peptide aggregation as a potential therapeutic strategy for Alzheimer's disease. *Acta Pharmacol. Sin. 32* (2011), 545–551.

[255] Kolstoe, S., and Wood, S. Drug targets for amyloidosis. *Biochem. Soc. Trans. 38* (2010), 466–470.

[256] Wang, J., Zhang, Y., and Du, S. The protective effect of curcumin on abeta induced aberrant cell cycle reentry on primary cultured rat cortical neurons. *Eur. Rev. Med. Pharmacol. Sci. 16*, 4 (2012), 445 – 454.

[257] Liao, M., Tzeng, Y., Chang, L. Y., Huang, H., Lin, T., Chyan, C., and Chen, Y. The correlation between neurotoxicity, aggregative ability and secondary structure studied by sequence truncated abeta peptides. {*FEBS*} *Lett. 581*, 6 (2007), 1161–1165.

[258] Lee, S. K., Lee, I. H., Kim, H. J., Chang, G. S., Chung, J. E. and No, K. T.. The preadme approach: Web-based program for rapid prediction of physico-chemical, drug absorption and drug-like properties. *EuroQSAR 2002 Designing Drugs and Crop Protectants: processes, problems and solutions, Blackwell Publishing, Massachusetts, USA* (2003), 418–420.

[259] Kozakov, D., Brenke, R., Comeau, S. R., and Vajda, S. An fft-based protein docking program with pairwise potentials. *Proteins 65*, 2 (2006), 392–406.

[260] Kozakov, D., Hall, D. R., Beglov, D., Brenke, R., Comeau, S. R., Shen, Y., Li, K., Zheng, J., Vakili, P., Paschalidis, I. C., and Vajda, S. Achieving reliability and high accuracy in automated protein docking: Cluspro, piper, sdu, and stability analysis in capri rounds. *Proteins 78*, 15 (2010), 3124–3130.

[261] Comeau, S. R., Gatchell, D. W., Vajda, S., and Camacho, C. J. Cluspro: a fully automated algorithm for protein-protein docking. *Nucl. Acids Res. 32* (2004), W96–W99.

[262] Comeau, S. R., Gatchell, D. W., Vajda, S., and Camacho, C. J. Cluspro: an automated docking and discrimination method for the prediction of protein complexes. *Bioinfor. 20*, 1 (2004), 45–50.

[263] Chen, C., Liu, Y.-Z., Shia, K.-S., and Tseng, H.-Y. Synthesis and anticancer evaluation of vitamin {K3} analogues. *Bioor. Med. Chem. Lett. 12*, 19 (2002), 2729–2732.

[264] Rota, C., Fann, Y. C., and Mason, R. P. Phenoxyl free radical formation during the oxidation of the fluorescent dye 2',7'-dichlorofluorescein by horseradish peroxidase: Possible consequences for oxidative stress measurements. *J. Biol. Chem. 274*, 40 (1999), 28161–28168.

[265] LeVine, H. III Alzheimer's beta-peptide oligomer formation at physiologic concentrations. *Anal. Biochem. 335*, 1 (2004), 81–90.

[266] Loor, G., Kondapalli, J., Schriewer, J. M., Chandel, N. S., Hoek, T. L. V., and Schumacker, P. T. Menadione triggers cell death through ros-dependent mechanisms involving {PARP} activation without requiring apoptosis. *Free Radic. Biol. Med. 49*, 12 (2010), 1925–1936.

[267] Sasaki, R., Suzuki, Y., Yonezawa, Y., Ota, Y., Okamoto, Y., Demizu, Y., Huang, P., Yoshida, H., Sugimura, K., and Mizushina, Y. DNA polymerase gamma inhibition by vitamin k3 induces mitochondria-mediated cytotoxicity in human cancer cells. *Cancer Science 99*, 5 (2008), 1040–1048.

[268] Re, F., Airoldi, C., Zona, C., Masserini, M., La Ferla, B., Quattrocchi, N., and Nicotra, F. Beta amyloid aggregation inhibitors: small molecules as candidate drugs for therapy of Alzheimer's disease. *Curr. Med. Chem. 17* (2010), 2990–3006.

[269] Hirohata, M., Ono, K., Naiki, H., and Yamada, M. Non-steroidal anti-inflammatory drugs have anti-amyloidogenic effects for Alzheimer's beta-amyloid fibrils in vitro. *Neuropharmacol. 49*, 7 (2005), 1088–1099.

[270] Ono, K., Hasegawa, K., Naiki, H., and Yamada, M. Anti-parkinsonian agents have anti-amyloidogenic activity for Alzheimer's beta-amyloid fibrils in vitro. *Neurochem. Int. 48*, 4 (2006), 275–285.

[271] Lamson, D., and Plaza, S. The anticancer effects of vitamin kl. *Altern. Med. Rev. 8* (2003), 303–318.

[272] Petkova, A. T., Leapman, R. D., Guo, Z., Yau, W.-M., Mattson, M. P., and Tycko, R. Selfpropagating, molecular-level polymorphism in Alzheimer's β-amyloid fibrils. *Science 307*, 5707 (2005), 262–265.

[273] Presse, N., Shatenstein, B., Kergoat, M.-J., and Ferland, G. Low vitamin k intakes in community-dwelling elders at an early stage of Alzheimer's disease. *J. Am. Diet. Assoc. 108*, 12 (2008), 2095–2099.

[274] Masuda, Y., Fukuchi, M., Yatagawa, T., Tada, M., Takeda, K., Irie, K., ichi Akagi, K., Monobe, Y., Imazawa, T., and Takegoshi, K. Solid-state {NMR} analysis of interaction sites of curcumin and 42-residue amyloid beta-protein fibrils. *Bioor. Med. l Chem. 19*, 20 (2011), 5967–5974.